Western University

Scholarship@Western

5-3-2017 12:00 AM

Developing and Testing a Model of Site Amplification for Southern Ontario

Sebastian Braganza, *Western University*

Supervisor: Dr. Gail Atkinson, *The University of Western Ontario*
A thesis submitted in partial fulfillment of the requirements for the Master of Science degree in Geophysics

Recommended Citation

Abstract

Commonly-applied methods to estimate ground-motion amplification for earthquake hazard applications in southern Ontario are highly generalized. Site amplification effects have typically been estimated by a parameter that is not well-known in the region, the time-averaged shear-wave velocity in the top 30 metres of soil; V_{S30}. Moreover, V_{S30} is not well correlated with site amplification in this region. This study develops a model that can better estimate ground motions and shaking intensities in southern Ontario based on readily-available information. The model is based on a site's peak response frequency (f_{peak}), which can be estimated from depth-to-bedrock. This f_{peak}-based model estimates ground motions differently compared to a V_{S30}-based model, as given by the National Building Code of Canada (NBCC). Field surveys show that the estimate of f_{peak} is stable over a distance of 1 km. The developed model can be used to estimate site response for building code and ShakeMap applications.

Keywords

Co-Authorship Statement

This thesis is prepared in integrated-article format and includes the following manuscripts written by Sebastian Braganza and the co-authors. Sebastian is the first author on studies of site amplification in southern Ontario. Sebastian performed the analyses described in this thesis and authored these reports with assistance from the co-authors.

1) Braganza, S., Atkinson, G.M., Ghofrani, H., Hassani, B., Chouinard, L., Rosset, P., Motazedian, D., Hunter, J. (2016). Modeling Site Amplification in Eastern Canada on a Regional Scale, manuscript published in Seismological Research Letters.

2) Braganza, S., Atkinson, G.M. (2017). A Model for Estimating Amplification Effects on Seismic Hazards and Scenario Ground Motions in Southern Ontario, manuscript accepted for publication in the Canadian Journal of Civil Engineering.

3) Braganza, S., Atkinson, G.M., Molnar, S. (2017). Assessment of the Spatial Variability of Site Response in Southern Ontario, manuscript submitted to Seismological Research Letters.

The thesis and composed articles were completed under the supervision of Dr. Gail M. Atkinson.

Acknowledgments

First and foremost, I would like to express my utmost gratitude to my supervisor, Dr. Gail Atkinson, for providing me with the opportunity to work in the engineering seismology group over the past few years. Under her guidance, I was able to grow as a geoscientist and successfully complete the three papers related to my thesis. The skills that I learned and developed as her student are skills that I will undoubtedly use for the rest of my life.

I would also like to thank everyone in the engineering seismology group at Western, especially Dr. Karen Assatourians, Dr. Hadi Ghofrani, Dr. Behzad Hassani and Dr. Sheri Molnar. Their help, teachings and suggestions greatly improved the quality of this research.

Last, but not least, I would like to thank my parents. Their love, support and encouragement have helped me to persevere and are what have made all of my academic achievements possible.

Table of Contents

List of Tables

List of Figures

List of Appendices

List of Abbreviations

ENA	Eastern North America
OGS	Ontario Geological Survey
GMICE	Ground-motion-to-intensity conversion equation
NEHRP	National Earthquake Hazards Reduction Program
NBCC	National Building Code of Canada
MMI	Modified Mercalli Intensity
GMPE	Ground-motion prediction equation
PSA	Pseudo-spectral acceleration
PGV	Peak ground velocity
PGA	Peak ground acceleration
PGA_{ref}	Expected PGA for a reference site class C
PGA_r	PGA as estimated by GMPE from Boore et al. (2014)
UHS	Uniform hazard spectrum
SEED	Standard for the Exchange of Earthquake Data
H/V	Horizontal-to-vertical spectral ratio
$(H/V)_{EQ}$	Earthquake horizontal-to-vertical spectral ratio
$(H/V)_{MT}$	Microtremor horizontal-to-vertical spectral ratio
V_S	Shear-wave velocity
V_{S30}	Shear-wave velocity in the top 30 metres of soil

Vs_{av}	Time-averaged shear-wave velocity
F_{nl}	Linear component of site amplification
F_{lin}	Nonlinear component of site amplification
F_s	Total site amplification
f_{peak}	Peak frequency of response
A_{peak}	Peak amplitude of response
A	Amplification factor
g	Acceleration due to gravity (9.81 m/s^2)
D	Depth-to-bedrock
T	Fundamental site period
n	Number of felt intensity reports
$\mathbf{M}$	Moment magnitude
$\Delta\sigma$	Stress drop, sometimes also called stress parameter

Chapter 1

1   Introduction

1.1   Motivation for this Research

The amplification of seismic waves in soft, surficial sediment layers is referred to as site amplification or site response. This physical phenomenon has been observed throughout the world and for many different earthquakes. Its occurrence is due to a simple principle related to the conservation of energy: as shear waves from deeper layers travel to the surface of the earth, they will enter layers that are typically softer and less dense, and as a result, the shear-wave velocity will decrease; thus, the amplitude of the waves will increase. Since shear waves refract toward the vertical as they enter softer layers of sediment and since their direction of particle motion is perpendicular to the direction of propagation, the amplification of these waves occurs primarily in the horizontal direction. It is this horizontal shaking that is associated with felt shaking and increased damage that is observed during earthquakes (e.g., Trifunac and Todorovska, 1997).

An excellent illustration of site amplification is the 1985 Michoacan (Mexico City) earthquake. The moment magnitude (**M**) 8.0 earthquake resulted in only moderate damage near the epicenter where rock is prominent, but extensive structural damage was observed ~350 km away in Mexico City, which is dominated by soft clay sediments (Kramer, 1996). Even within Mexico City, strong-motion instruments recorded vastly different horizontal ground accelerations, depending on whether the instrument was on rock or soft clay. **Figure 1-1** shows an example of contrasting horizontal acceleration records from two different sites for this earthquake; strong-motion station UNAM was situated on basaltic rock, while station SCT was located on soft soil. The record from SCT shows much higher ground accelerations.
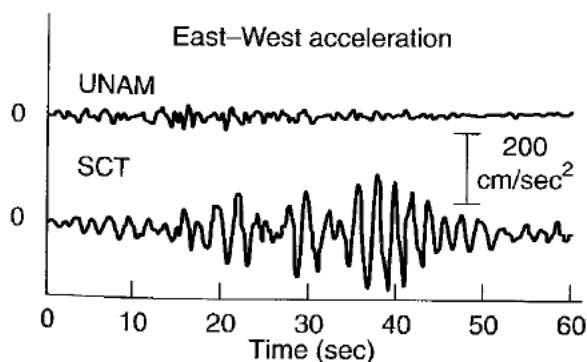
Figure 1-1: Horizontal (east-west) acceleration time histories from two strong motion stations in Mexico City during the M8.0 Michoacan earthquake. Station UNAM was situated on basaltic rock, while SCT was located on soft soil (from Kramer, 1996).

While the site amplification example of Mexico City is a fairly extreme one, the phenomenon will exist to some extent for any region that is home to varying surficial soil types. In this study, the focus is on predicting site response in Canada's most densely-populated region: southern Ontario.

1.2   Seismicity in Southern Ontario

Southern Ontario is a fairly stable seismic region when compared to active regions such as California or Japan. The region does not frequently experience damaging earthquakes, as it is located in the middle of the North American Plate. However, small-to-moderate earthquakes of **M**3 to 5 (with **M** ≈ 4.5 being the damage threshold) occur frequently throughout the region, with larger events occurring less frequently. Many of these earthquakes originate in the Western Quebec Seismic Zone, which extends more than 500 km from the Timiskaming region of Quebec, through the Ottawa-Montreal corridor, to the Adirondack Highlands of New York (Ma and Eaton, 2007; Basham et al., 1979). The Southern Great Lakes Seismic Zone is also host to earthquakes of **M**3 to 5, although they occur infrequently here. It has been hypothesized that earthquakes occurring in the region below Lake Ontario can be attributed to fluids, which alter the pore pressures and stress regime within the rocks (Mereu et al., 2002). **Figure 1-2** shows

the distribution of earthquakes in southern Ontario during the time period from 1991 to 2013 (Assatourians et al., 2013).
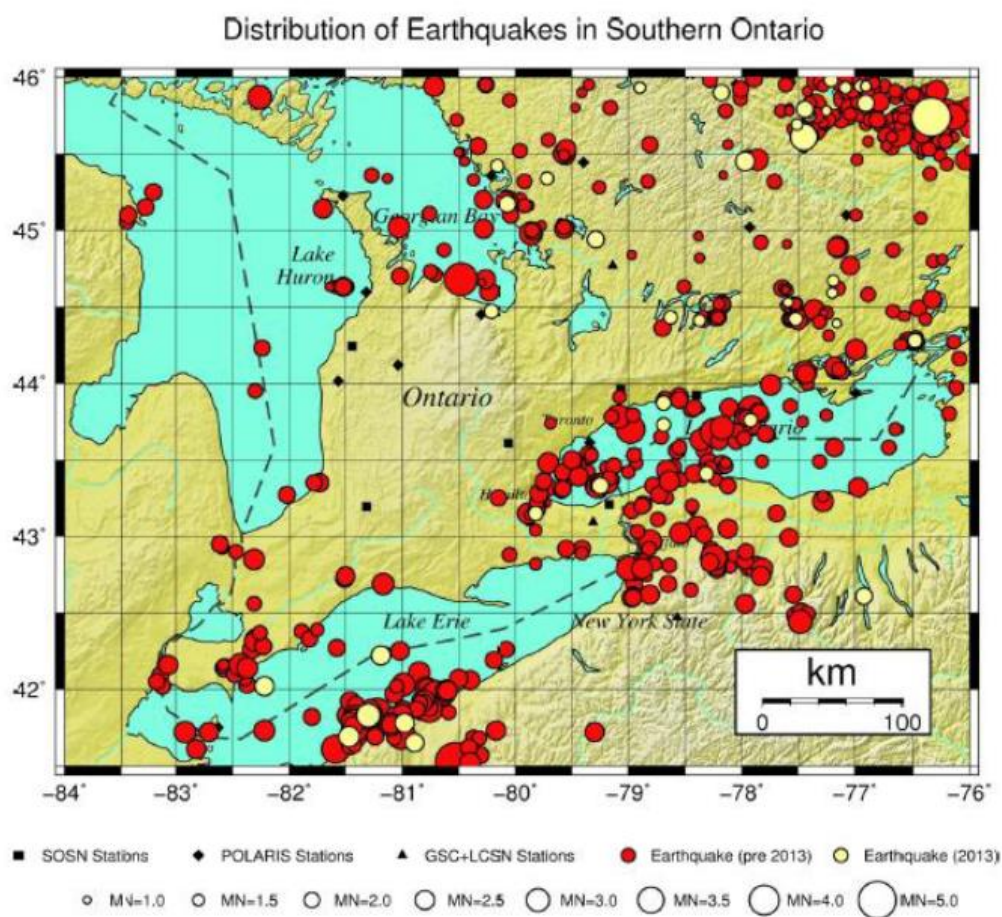
Figure 1-2: Seismicity in southern Ontario (1991 to 2013). Earthquake symbol sizes are scaled by their magnitudes (based on the Nuttli magnitude scale, MN). The cluster of events in the northeast corner of the map originate from the Western Quebec Seismic Zone (from Assatourians et al., 2013).

A few notable twenty-first century earthquakes to be felt in the region are the 2002 **M**5.0 Au Sable Forks, New York (Atkinson and Sonley, 2003), 2010 **M**5.0 Val-des-Bois, Quebec (Atkinson and Assatourians, 2010), and 2013 **M**4.5 Ladysmith, Quebec (Atkinson et al., 2014), earthquakes. Thus, even though southern Ontario has relatively low levels of seismic activity, the region still periodically experiences earthquakes that are widely felt, and there is the potential for damaging motions. The seismic risk is

considered moderate, despite the relatively-low activity levels, due to the region's high population density. Assessments on how seismicity and site amplification impacts the region are therefore important.

1.3   Review of Studies on Site Response Parameters

Ground-motion prediction equations (GMPEs) are a common way to describe expected earthquake motions, accounting for average earthquake source, path and site effects. The site term in the GMPE commonly uses shear-wave velocity in the top 30 metres of soil (V_{S30}) as the descriptive variable. Denser/stiffer soil materials are associated with higher V_{S30} values. In many applications, V_{S30} is estimated based on correlations with topographic slope (Wald and Allen, 2007). The shortfall with this proxy method is that it does not work well in regions like southern Ontario that have subdued topographic relief. However, using site-specific studies to obtain more accurate V_{S30} values can be an expensive and time-consuming procedure. Moreover, many seismograph stations in southern Ontario only have inferred or assumed values of V_{S30}, making the degree of correlation between V_{S30} and site amplification difficult to assess. Using alternative approaches to estimate site response in southern Ontario is therefore appealing.

Alternative methods for estimating site response include the horizontal-to-vertical (H/V) ratio method, which uses spectral ratios of ground motions to estimate a site's peak frequency of response (f_{peak}), in addition to other parameters, such as a site's surficial geology. The f_{peak} of a site is typically within a narrow frequency bandwidth, within which the H/V ratio is at a maximum; this is related to the site's subsurface properties (e.g., sediment thickness). The benefit of using f_{peak} as a site response variable is that it is relatively easy to obtain and it provides information for sites that are deeper than 30 m. Moreover, characterizing shallow sites (< 30 m) can be problematic when using V_{S30} if there is an intrusion of high-velocity bedrock in the top 30 m (e.g., McPherson and Hall, 2013).

A number of recent studies have examined the use of f_{peak} as a site response parameter in various regions of the world. As an example, in Italy, Di Alessandro et al.

(2012) used site periods from H/V spectral ratios as a means for site classification and found that the H/V ratio method reduced the standard deviation from GMPEs and better captured the long and short period resonance from deep and shallow soil sites, respectively. In Japan, Zhao and Xu (2013) and Ghofrani and Atkinson (2014) similarly found that f_{peak} or site period from H/V ratios was a better predictive site variable than V_{S30} for longer period (or deeper) sites. Moreover, larger and more distinct peaks in amplification spectra are expected in regions like Japan where there exists a soft sediment layer overlying hard bedrock (Class I regions), providing conditions for a strong impedance contrast (Aki and Richards, 2002; Ghofrani and Atkinson, 2014). This differs from regions like California (Class II), which are characterized by a gradational soil profile, resulting in broader amplification spectra, lower spectral peak amplitudes, and peaks at lower frequencies. **Figure 1-3** shows examples of H/V spectra from Class I and II regions. Since southern Ontario is characterized by a range of soil types overlying very hard, glaciated bedrock (shear-wave velocity or $V_S \approx 2800$ m/s; Boore and Joyner, 1997), it is expected that H/V spectra in the region will resemble that of Class I regions, such as Japan; thus, the argument for f_{peak} being a more applicable site response variable than V_{S30} likely also applies to southern Ontario.
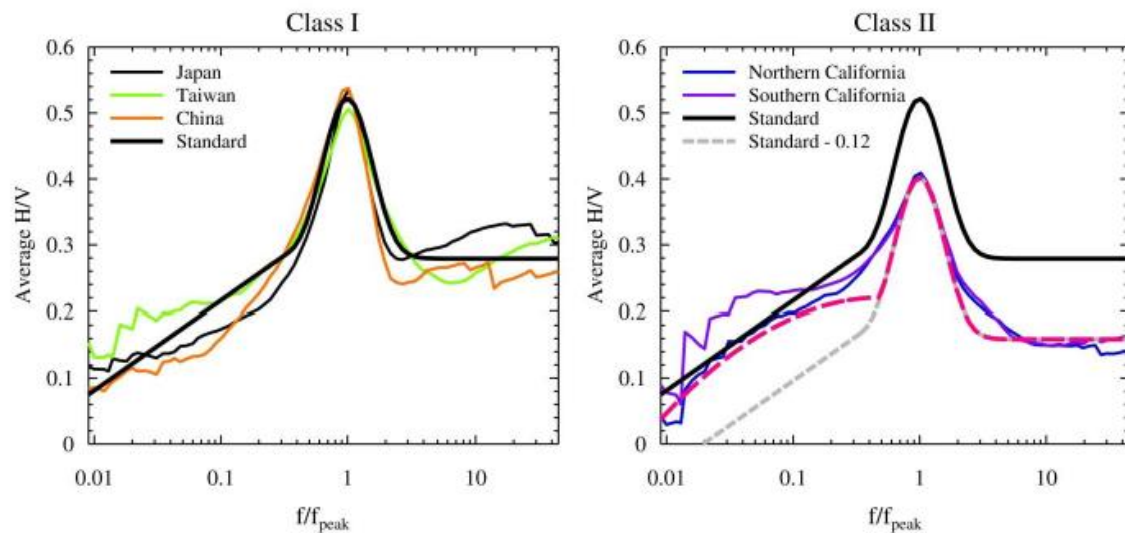
Figure 1-3: Examples of H/V spectra from Class I (left) and Class II (right) regions. H/V spectra in Class I regions are typically more distinct and have greater peak

amplitudes. Note that the H/V is in base 10 log units. A standard Gaussian curve, derived from empirical data from Japan, is superimposed on both plots (from Ghofrani and Atkinson, 2014).

1.4   Organization of Work

In chapter 2, we use H/V spectral ratios from earthquake records in southern Ontario in order to characterize site response in the region. We show that site response can be modeled using a couple of variables that are readily obtainable: f_{peak} (determined from the H/V ratio or sediment depth) and surficial geology or sediment type. These variables are used to create a preliminary model of site amplification that can be used with GMPEs for the region, as well as for predicting ground motions or shaking intensity on a regional scale. Chapter 2 has been published as *Modeling Site Amplification in Eastern Canada on a Regional Scale* in Seismological Research Letters.

In chapter 3, the site amplification model based on f_{peak} is compared to one based on V_{S30}, as given by the 2015 National Building Code of Canada (NBCC). Earthquakes and scenario events are used to estimate ground motions and shaking intensities. It is shown that both models generally predict similar felt intensities but show significant differences in their predicted amplification of ground motions as a function of frequency. The results of this chapter support the use of f_{peak} as a site response variable for estimating amplification effects in southern Ontario. Chapter 3 has been accepted for publication as *A Model for Estimating Amplification Effects on Seismic Hazards and Scenario Ground Motions in Southern Ontario* in the Canadian Journal of Civil Engineering.

In chapter 4, we measure the spatial variability of f_{peak} within 1 km distance of 10 seismograph stations in southern Ontario. Establishing spatial variability of f_{peak} is useful for assessment of regional site response and its uncertainty: we can estimate site response if f_{peak} is known, and thus it is important to know to what distances the value of f_{peak} is spatially stable. We find that, on average, $\log_{10}(f_{peak})$ as measured by microtremor survey observations is within 0.13 units of the value recorded at the seismograph station (using

H/V from earthquake records), for survey sites within 1 km of the station. Chapter 4 has been submitted for publication as *Assessment of the Spatial Variability of Site Response in Southern Ontario* in Seismological Research Letters.

Finally, a summary of all findings is provided in chapter 5, in addition to suggestions for future work.

References

Aki, K and Richards, P.G. (2002). Quantitative Seismology, 2nd edition. University Science Books. Sausalito, California. 700.

Assatourians, K., Atkinson, G.M., Dunn, B. and Li, M. (2013). The Southern Ontario Seismograph Network Activity Report for Ontario Power Generation. Department of Earth Sciences, The University of Western Ontario. 165.

Atkinson, G.M. and Sonley, E. (2003). Ground Motions from the 2002 Au Sable Forks **M**5.0 Earthquake. *Seismological Research Letters*, **74**, no. 3, 399–349.

Atkinson, G.M. and Assatourians, K. (2010). Attenuation and Source Characteristics of the 23 June 2010 M 5.0 Val-des-Bois, Quebec, Earthquake. *Seismological Research Letters*, **81**, 849–860.

Atkinson, G.M., Assatourians, K. and Lamontagne, M. (2014). Characteristics of the 17 May 2013 M 4.5 Ladysmith, Quebec, Earthquake. *Seismological Research Letters*, **85**, no. 3, 755–762.

Basham, D.M., Weichert, D.H., and Berry, M.J. (1979). Regional assessment of seismic risk in eastern Canada. *Bulletin of the Seismological Society of America*, **11**, 1567–1602.

Boore, D.M., and Joyner, W.B. (1997). Site Amplifications for Generic Rock Sites, *Bulletin of the Seismological Society of America,* **87**, no. 2, 327–341.

Di Alessandro, C., Bonilla, L.F., Boore, D.M., Rovelli, A. and Scotti, O. (2012). Predominant-Period Site Classification for Response Spectra Prediction Equations in Italy. *Bulletin of the Seismological Society of Am*erica, **102,** no. 2, 680–695.

Ghofrani, H. and Atkinson, G.M. (2014). Site Condition Evaluation Using Horizontal-to-

Vertical Response Spectral Ratios of Earthquakes in the NGA-West 2 and Japanese Databases. *Bulletin of Soil Dynamics and Earthquake Engineering*, **67**, 30–43.

Kramer, S.L. (1996). Geotechnical Earthquake Engineering. Prentice-Hall, Inc. Upper Saddle River, New Jersey. 653.

Ma, S. and Eaton, D. (2007). Western Quebec seismic zone (Canada): Clustered, mid-crustal seismicity along a Mesozoic hot spot track. *Journal of Geophysical Research*, **17**, 16.

McPherson, A. and Hall, L. (2013). Site Classification for Earthquake Hazard and Risk Assessment in Australia. *Bulletin of the Seismological Society of Am*erica, **103**, no. 2A, 1085–1102.

Mereu, R.F., Asmis, H.W., Dunn, B., Brunet, J., Eaton, D., Dineva, S. and Yapp, A. (2002). The Seismicity of the Western Lake Ontario Area: Results from the Southern Ontario Seismic Network (SOSN), 1992-2001. *Seismological Research Letters*, **73**, no. 4, 534–551.

Trifunac, M.D. and Todorovska, M.I. (1997). Northridge, California, Earthquake of 1994: density and red-tagged buildings versus peak horizontal velocity and intensity of shaking. *Soil Dynamics and Earthquake Engineering*, **16**, no. 3, 209–222.

Wald, D.J. and Allen, T.I. (2007). Topographic Slope as a Proxy for Seismic Site Conditions and Amplification. *Bulletin of the Seismological Society of America*, **97**, 5, 1379–1395.

Zhao, J.X. and Xu, H. (2013). A Comparison of VS30 and Site Period as Site Effect Parameters in Response Spectral Ground-Motion Prediction Equations. *Bulletin of the Seismological Society of America*, **103**, no. 1, 1–18.

Chapter 2

2 Modeling Site Amplification in Eastern Canada on a Regional Scale

2.1 Introduction

Eastern North America (ENA) has relatively low levels of seismic activity, but earthquakes nevertheless pose a moderate risk due to densely-populated urban centers and critical infrastructure. Moreover, sediments in many parts of ENA tend to strongly amplify ground motions from moderate earthquakes. A good example of this is the moment magnitude (**M**) 5.0 Val-des-Bois earthquake, which had a felt area of approximately 3 million km^2 and produced the strongest shaking ever felt in Canada's capital city of Ottawa, more than 60 km away (Atkinson and Assatourians, 2010); the shaking in Ottawa was particularly strong on soil sites (Pal and Atkinson, 2012). The sediments in ENA are comprised of postglacial sands, clays and tills of variable stiffness and thickness, which often overlie very hard glaciated bedrock, providing a sharp contrast in shear wave velocity. This produces strong and highly variable site amplification within the region. Proper modeling of these amplification effects is critical in the interpretation of recorded ground motions and the evaluation of hazard. While this study is focused on the region extending from southern Ontario to Quebec, the results also apply to other ENA sites which share similar characteristics.

Horizontal-to-vertical (H/V) component spectral ratios of Fourier amplitude spectra and/or response spectra (e.g., pseudo-spectral acceleration, PSA) are known to be a measure of site amplification, particularly effective at identifying the predominant site frequency (e.g., Nakamura, 1989; Lermo and Chávez-Garcia, 1993; Kawase et al., 2011). Horizontal-component shear-wave motions are amplified in near-surface sediment layers, whereas amplification on the vertical component is counterbalanced by the ray path refracting toward the vertical. Thus, the vertical component amplification may be considered negligible relative to that of the horizontal component, so that H/V ratios are a good approximation of site amplification. Modeling site amplification is important in the

development of ground-motion prediction equations (GMPEs), and for mapping the intensity of ground motion (e.g., ShakeMaps; Wald et al., 1999).

In this study, we use seismograph station and microtremor H/V measurements, from southern Ontario and Quebec, to develop a regional-scale model of site amplification suitable for use in applications such as ShakeMap. This model consists of functions, categorized by sediment class, which capture the average H/V trend of that class. The key descriptive variables of these functions are the peak frequency of response (f_{peak}), and to a lesser extent, the overall stiffness (or type) of the deposit. Using digitized maps of depth-to-bedrock (sediment thickness) and surficial geology, correlations are defined between depth-to-bedrock and f_{peak}, and surficial geology and peak amplitude of response (A_{peak}). From these correlations, the site amplification functions are developed, based on the assumption that H/V ratios act as a proxy for site amplification. We develop a set of amplification functions which is applicable to sites whose f_{peak} is known; e.g., at seismograph stations, or locations where microtremor studies have been conducted. A second set of functions is introduced to account for sites where f_{peak} can only be roughly estimated due to lack of site-specific information. These functions can then be applied to make simple and practical estimates of site response across the region. We emphasize that the intent here is to provide a broad-brush regional model, rather than a microzonation.

Ghofrani and Atkinson (2014) compared the effectiveness of using H/V spectral ratios as a descriptive variable to model site response with that of the time-averaged shear-wave velocity to 30 m (V_{S30}). This evaluation was done using two databases: a comprehensive ground-motion database from Japan, and the international NGA-West 2 database. They concluded that using H/V spectral ratios – instead of V_{S30} – as a site descriptor variable is advantageous since H/V ratios provide a more accurate characterization of amplification for deeper sediment deposits, and are more readily obtained. Ghofrani and Atkinson (2014) described the H/V characteristics for two types of regions. Regions with predominantly-shallow sediment sites (Class I), such as Japan and China, display strong H/V spectral ratios with A_{peak} at intermediate-to-high

frequencies (> 2 Hz), while regions with deeper gradational sediment sites (Class II), such as California and Italy, have A_{peak} values at lower frequencies (< 1 Hz).

In eastern Canada, the use of V_{S30} as a site response variable is problematic, as it is not available in most places and proxies like topographic slope do not work well in this region, which has subdued topographic relief. Moreover, V_{S30} does not convey information on the most important variable controlling site amplification in this region, which is depth-to-bedrock, or equivalently, peak frequency, as we will show in this article.

2.2 Database Information and the Computation and Classification of H/V Curves

The ground-motion data used in this study are the response spectral amplitudes from an online seismograph database for the region (www.seismotoolbox.ca). The database includes response spectra for 55 events of **M** 3.0 to 5.1 recorded on 38 seismograph stations: 36 in southern Ontario and 2 on the Island of Montreal, during the time period of 1996 to 2014. These stations are located throughout the region and rest on sites composed of various surficial geologies, with the majority being on bedrock or till. The instrument-corrected acceleration time series and 5%-damped PSAs were obtained by processing the Standard for the Exchange of Earthquake Data (SEED) waveform files through the program ICORRECT (Assatourians and Atkinson, 2008). To ensure adequate signal strength, the magnitude-distance limitations suggested by Atkinson (2004) were applied. As a result, all records used in this study had a hypocentral distance under 800 km, while most records were within 400 km. To compute a station's H/V ratio for a given record, the geometric mean of the horizontal-component PSA was divided by the vertical component PSA, at frequency points from 0.1 to 20 Hz, spaced in increments of 0.1 logarithmic units. The station's average (H/V) spectrum was obtained by log-averaging the H/V values for each frequency over all events (i.e., we obtain the mean value of log(H/V) as a function of frequency). We note that logarithms throughout this article are of base 10.

Sediment thickness and surficial geology data for Ontario are compiled by the Ontario Geological Survey (OGS) and made available online by the Ministry of Northern Development and Mines. These data are available in Keyhole Markup Language format for easy viewing in Google Earth. The website also provides an associated cross-section viewer (CrossSection.exe) which shows bedrock elevation, ground elevation and sediment thickness. These parameters are provided in units of meters, with a site's sediment thickness (depth-to-bedrock) being the difference between the ground and bedrock elevations. We queried this database to obtain surficial geology and depth-to-bedrock information as needed. Since the digitized map of surficial geology shows highly localized variability, including several different categories of sediment and bedrock, we simplify the mapped surficial sediment materials into four main site classes. In order of decreasing stiffness, these classes are: bedrock, till, sand/clay, and very soft organic sediment/fill. Furthermore, we assume that the entire sediment column is uniformly that given by the surficial geology map. We acknowledge that this is a simplification in areas where the surficial unit is not representative of the underlying stratigraphy, and that this simplification results in significant uncertainty in the amplification model.

Most of the 38 seismograph stations used in this study were examined in a previous similar study by Kolos (2010), where various sources were consulted for station depth-to-bedrock values. In this study, for stations with no depth-to-bedrock information available in Kolos (2010), the information from the OGS CrossSection algorithm is used to estimate depth. A simple inspection of all sediment sites' H/V spectra and their depth-to-bedrock values reveals a strong correlation between the peak frequency of the H/V ratio (f_{peak}) and the depth-to-bedrock (shown later). This is expected because the peak frequency of amplification is inversely proportional to the thickness of the amplifying layer, with the degree of amplification being dependent on the seismic impedance contrast (Aki and Richards, 2002). **Figure 2-1** shows a representation of the overall study area's sediment thickness and the locations of the seismograph stations. Note that sediments in southern Ontario are intermediate-to-deep in most areas, while the eastern parts of the province have thinner sediments, with some deeper pockets.
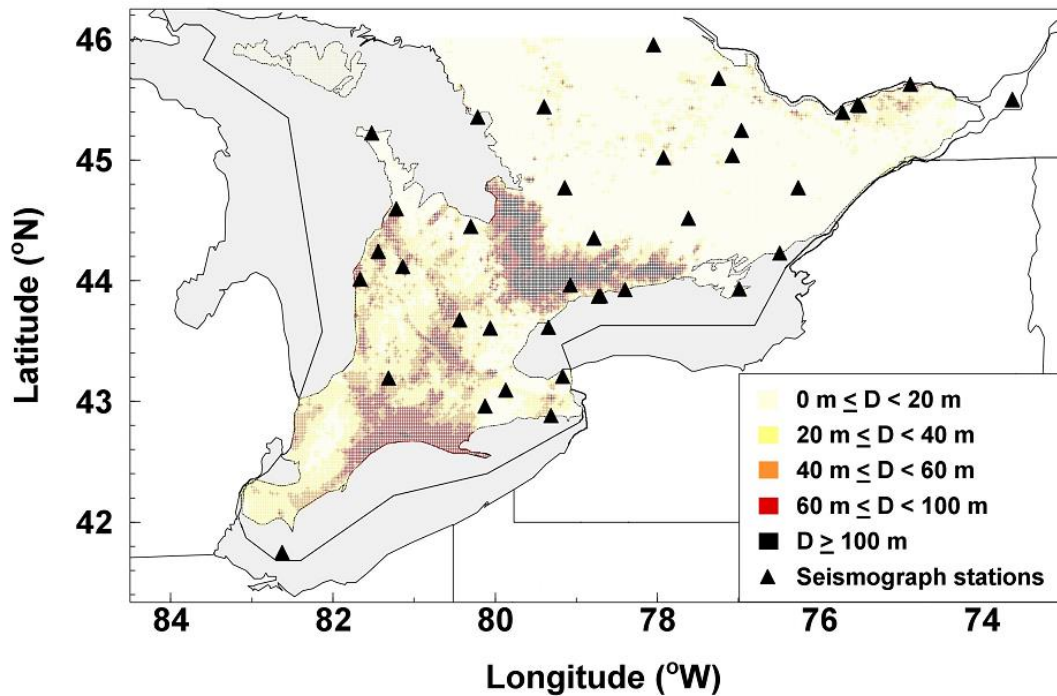
Figure 2-1: Sediment thickness (D) across southern Ontario and the locations of seismograph stations used in this study.

In Ontario, the digitized surficial geology map is used to estimate which of the four site classes applies to each station, while in Montreal this information is extracted from a dataset of boreholes, provided by the City of Montreal. In the majority of cases, the surficial geology is consistent with that expected based on the H/V spectral shape: sediments are associated with peaked spectra (with a greater A_{peak} seen in softer sediments), while bedrock is associated with flatter spectra. Where there are discrepancies between the surficial geology map and a station's H/V spectral appearance, the spectral shape is used to determine the site class. The latter is deemed to be a better indicator since the map sometimes shows boundaries between different geologies in very close proximity to a station, and the map resolution is rather poor. After determining the surficial geology associated with each station, the H/V spectra are grouped by geological category. We follow the approach of Ghofrani and Atkinson (2014) to generalize the H/V curve for each site type; we plot all sediment spectra and the amplitude of H/V as a function of f/f_{peak}. This normalizes the spectra in frequency space so that sites with

different values of f_{peak} can be overlaid, allowing an average H/V for the site class to be computed. The generic Gaussian-shaped model from Ghofrani and Atkinson (2014) is used to describe the average H/V curves for each of the three sediment classes in eastern Canada; we simply adjust the coefficients to better match the observed H/V curves. This approach is motivated by the similarity in H/V spectral shapes for Japan and eastern Canada. Both are regions that are characterized by sediment layers lying on top of much harder rock, resulting in a significant velocity contrast and large horizontal ground motion amplifications at a predominant site frequency. It should be noted that the eastern Canada ground motions used in this study are weak, so sediment non-linearity did not need to be considered in the amplification model. In cases where stronger motions are to be considered, such as higher-**M** scenario events, non-linearity is expected to reduce A_{peak} and shift f_{peak} to lower frequencies. For such events, a non-linear component can be added to the model in order to reduce the amplifications (e.g., Seyhan and Stewart, 2014).

2.3 H/V Characteristics and Correlation between Peak Frequency and Depth to Bedrock

Appendices A and **B** show the tabulated log(H/V) ratios and the associated standard deviations for all 38 seismograph stations, as well as the number of records used to calculate these values. **Appendix C** summarizes the site and H/V characteristics of these stations. These characteristics are used to develop the key relationships between variables, as shown later.

Another source of information on H/V is the results of microtremor surveys, in which seismic noise is collected for a brief time and the H/V ratios of the noise samples are calculated (Nakamura 1989; Bard 1999). Extensive microtremor studies have been conducted in Ottawa/Gatineau and Montreal (e.g., Motazedian and Hunter, pers. comm., 2015; Rosset and Chouinard, 2009; Chouinard and Rosset, 2012), and the H/V information from these studies is used to supplement the H/V spectra from seismographic stations. Generally, the H/V spectra obtained from microtremor surveys are consistent with those from earthquake studies (e.g., Lermo and Chávez-Garcia, 1993). However the H/V spectra from earthquake studies are usually better-behaved and have less variability in both A_{peak} and f_{peak}, provided that multiple earthquake records (e.g., > 5 recordings) are

available to calculate H/V ratios. The use of multiple records, along with the procedures recommended in Ghofrani and Atkinson (2014), result in a very stable pick for f_{peak}.

The relationship between f_{peak} and depth-to-bedrock is an inverse relationship, in which shallower deposits have higher peak frequencies. The stiffness of the deposit, which can be indicated by shear wave velocity, should also play a role in the relationship, as described by (Kramer, 1996):

$$f_{peak} = Vs_{av}/(4D), \tag{2.1}$$

where D is depth-to-bedrock (m) and Vs_{av} is the time-averaged shear wave velocity (m/s). Equation (2.1) suggests that we should be able to find a shear-wave velocity profile that is consistent with the observed relationship between f_{peak} and D. We consider a few trial relationships between shear wave velocity and depth that would achieve consistency and be in reasonable agreement with studies of how shear wave velocity increases with depth.

For the city of Montreal, Rosset et al. (2015) compiled Vs measurements for sand and clay and modeled the behavior of Vs versus depth (up to 35 m) for these two site types. A simple relationship that is intermediate to their Vs versus depth curves for sand and clay is given by:

$$Vs_{av} = -0.0058D^2 + 2.2401D + 205.5356, 0 < D \leq 120 \text{ m.} \tag{2.2}$$

Similarly, Motazedian et al. (2011) presented a Vs_{av} relation for the city of Ottawa:

$$Vs_{av} = 0.88D + 123.86, 0 < D \leq 120 \text{ m.} \tag{2.3}$$

The depth ranges presented in Rosset et al. (2015) and Motazedian et al. (2011) are extended to enable a comparison of the Vs-depth relations for these two cities (which are within the study area) against compiled data. A quick inspection shows that equation (2.2), which represents typical velocities for sediments in Montreal, yields much higher velocities than equation (2.3), for the Ottawa area. We therefore propose an arbitrary velocity-depth profile that is somewhere between the two:

$$Vs_{av} = 0.2762D + 190.2911, \; 0 < D \leq 120 \text{ m}, \tag{2.4a}$$

$$Vs_{av} = 223.4351 \text{ m/s}, \; D > 120 \text{ m}. \tag{2.4b}$$

The Vs_{av}-depth relationships given by equations (2.2), (2.3) and (2.4) are summarized in **Figure 2-2**, and will be used to help explain the observed relationships between f_{peak} and D. We note that since equations (2.2), (2.3) and (2.4) are derived from sites that are primarily of sand/clay, future studies obtaining velocity profiles from different site types in the region are suggested in order to better constrain the relationship between f_{peak} and D. Moreover, the velocity-depth profile described by equation (2.4) is proposed arbitrarily – i.e., there is no optimization or regression procedure behind its derivation.
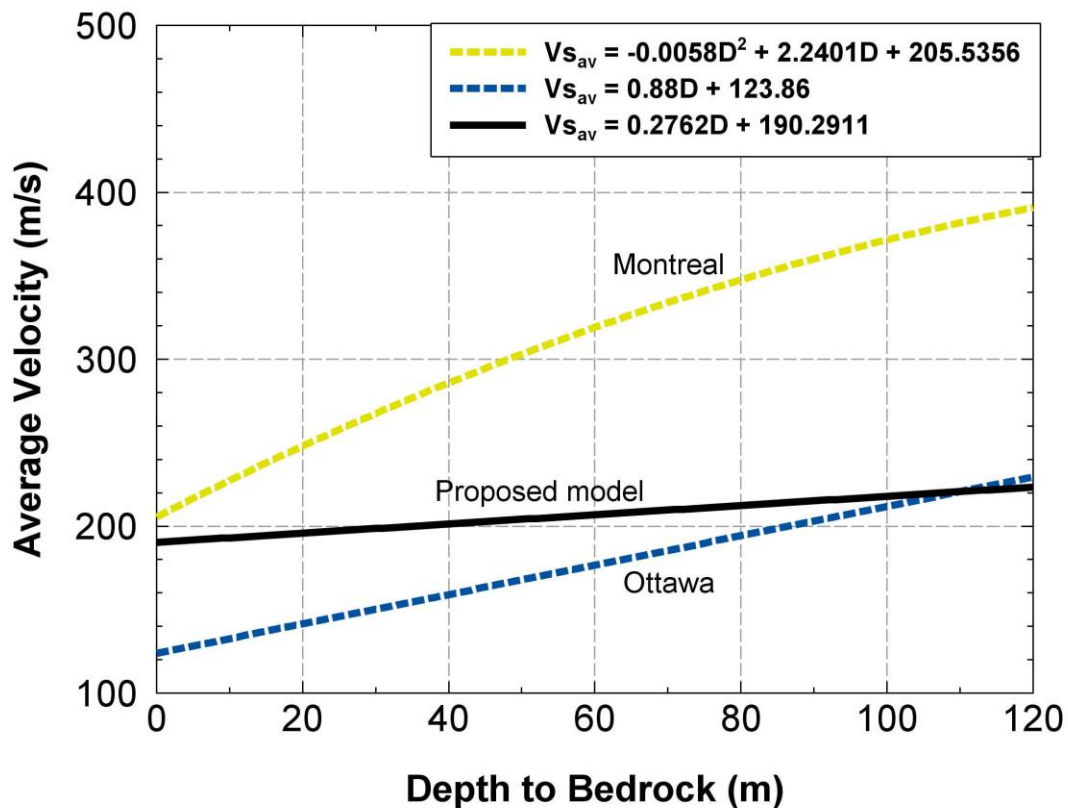
Figure 2-2: Average velocity-depth profiles for the study region. The dashed lines represent profiles for the cities of Montreal and Ottawa, while the solid black line is the profile proposed for the entire region. Note that these profiles are derived primarily from sand/clay sites.

To consider how we might expect the relationship between f_{peak} and D to behave, we refer to equation (2.1). For each value of D, we calculate a time-averaged layer velocity according to the example velocity-depth profiles and find the corresponding value of f_{peak}. **Figure 2-3** plots the expected relationship, in comparison to observations based on the H/V spectra. We include the f_{peak} and depth-to-bedrock data from seismograph stations (**Appendix C**), as well as the comparable information from microtremor surveys in Montreal and Ottawa/Gatineau. It should be noted that for Ottawa/Gatineau, Motazedian and Hunter (pers. comm., 2015) provide data for depth to firm ground, wherein the interface can range from compact till to bedrock. Regardless of the type of interface, depth to firm ground is treated as depth-to-bedrock and included in **Figure 2-3**. We acknowledge that this contributes to the uncertainty in f_{peak} and depth.
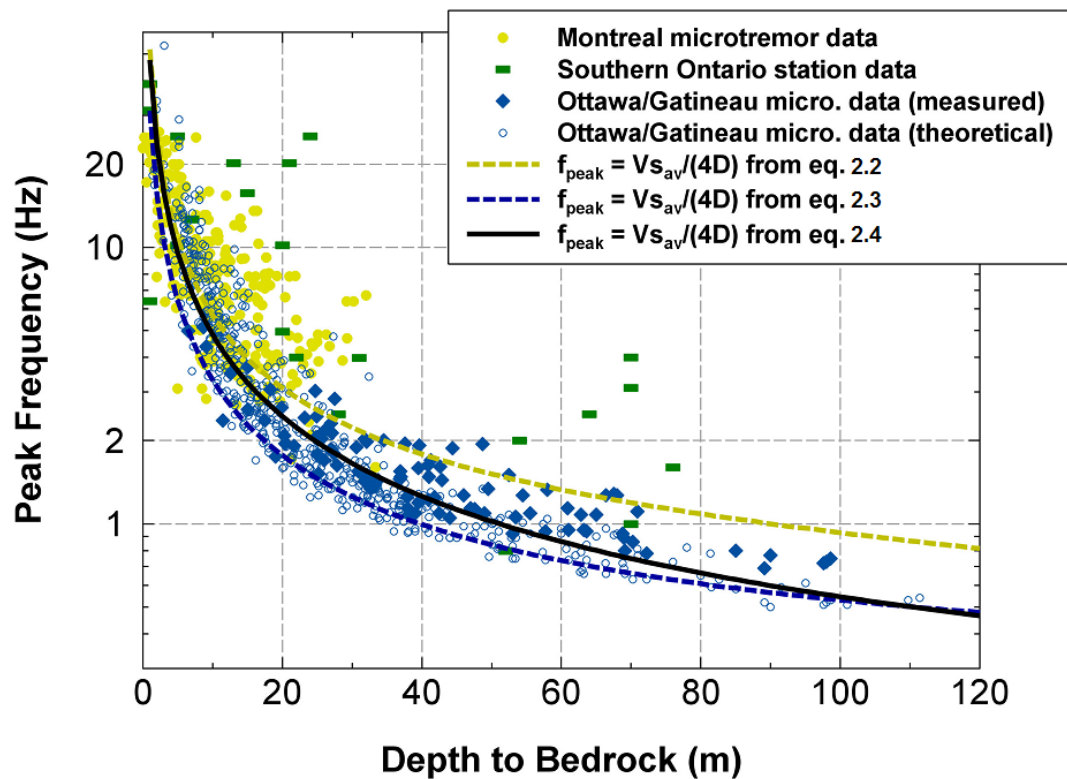
Figure 2-3: Site peak frequencies plotted as a function of depth to bedrock. Three $f_{peak} = Vs_{av}/(4D)$ relations, based on three average velocity profiles (discussed in text), are superimposed.

Using the velocity profile given by equation (2.4), when given D, the error in estimating $\log(f_{peak})$ against all observed data has a standard deviation of 0.2. Thus, if the depth-to-bedrock is known, the peak frequency of the site can be inferred to within approximately a factor of 1.6. We note that, in practice, additional uncertainty in estimating f_{peak} arises from a number of sources, including the uncertainty in estimating depth-to-bedrock itself. These uncertainties are important to consider in the application of the results, as discussed later.

The earthquake and microtremor data follow the same general trends, but the f_{peak} values from seismograph station measurements show larger scatter and are generally higher for equivalent depths. Differences exist between sub-regions and datasets that may partly explain these discrepancies. For instance, most of the microtremor data were collected in the Ottawa area, where soft, low-Vs post-glacial sediments make up approximately 65% of the cover (Motazedian et al., 2011). This is in contrast to other areas of southern Ontario where most seismograph stations are located. Site conditions here are primarily of higher-Vs till, with an underlying stratigraphy that can be complex (Hunter, pers. comm., 2015). Another possible explanation for the differences between datasets are the different depth-to-bedrock information sources. In particular, it may be difficult to extract information on f_{peak} for deep sites from weak-motion seismographic data due to inherent signal-to-noise limitations at low frequencies. This explains why most measured f_{peak} values are in the range of 2 to 10 Hz: it is a result of prevalent site conditions and suitable signal-to-noise ratio conditions.

2.4 Peak Amplitudes of Response, H/V Spectral Shapes and Amplification Functions

In general, peak amplitudes of response are shown to increase as sediment stiffness decreases. In **Figures 2-4** to **2-6**, we show the seismograph station H/V spectra for sites on sediment, grouped by their surficial geology. In descending order of stiffness, these sediment types are till, sand/clay and very soft organic sediment/fill. Their average H/V spectra have A_{peak} values of 3.0, 5.2 and 9.5, respectively. As sites within each class have similar shapes and amplitudes but are characterized by different peak frequencies, we describe their shapes using a dimensionless frequency measure normalized by the

peak, f/f$_{peak}$. This shifts all curves to peak at a value of f/f$_{peak}$ = 1. In **Figure 2-6**, it should be noted that only one station (TORO) is on soft organic sediment, hence the lone H/V spectrum seen in this figure.
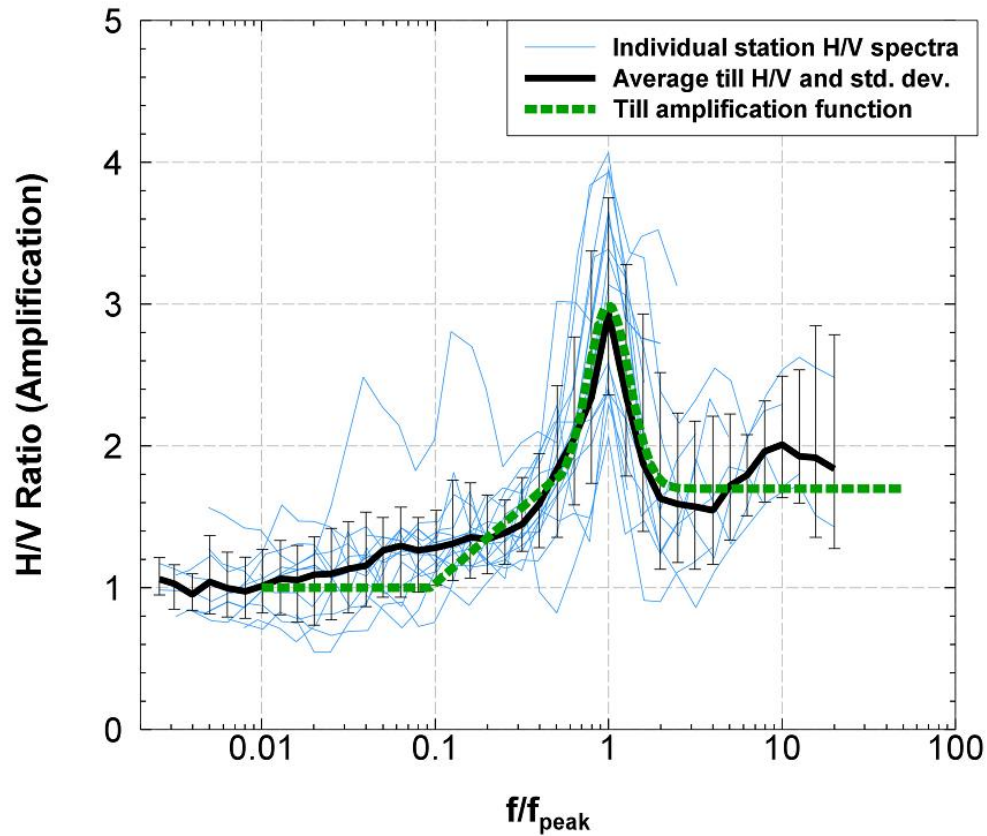
Figure 2-4: H/V spectra from 15 seismograph stations on till, plotted by f/f$_{peak}$ with the weighted average H/V curve and till amplification function. The spectra have an average A$_{peak}$ of 3.0.
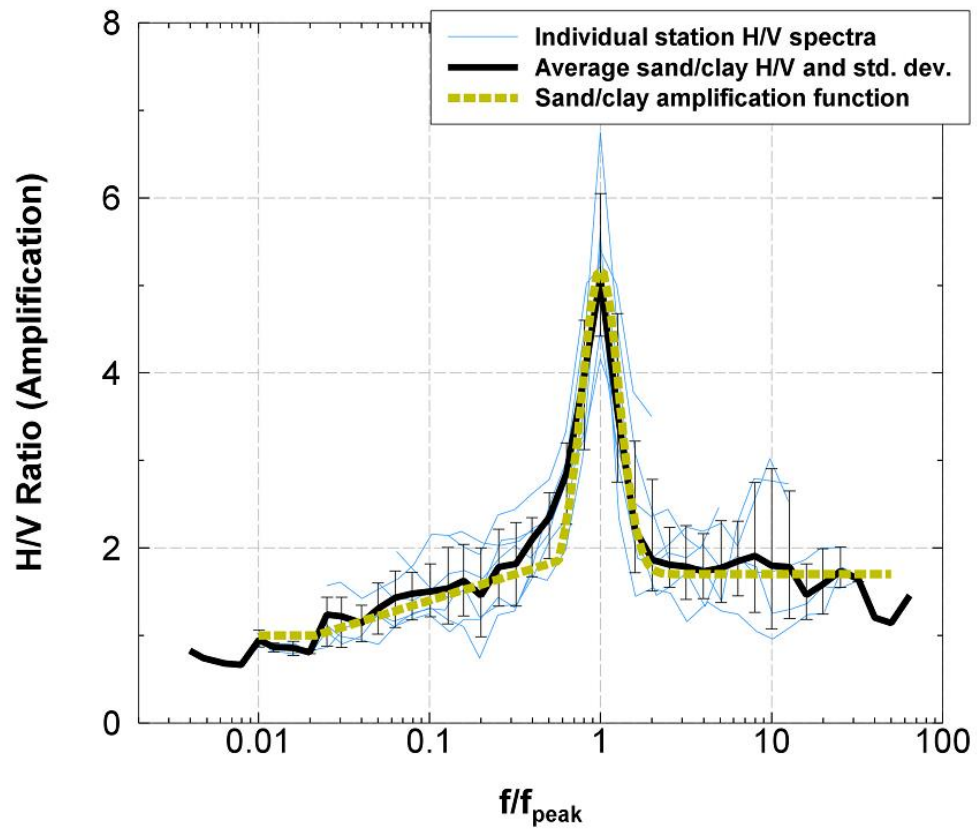
Figure 2-5: H/V spectra from 7 seismograph stations on sand/clay, plotted by f/f$_{peak}$ with weighted average H/V curve and sand/clay amplification function. The spectra have an average A$_{peak}$ of 5.2.
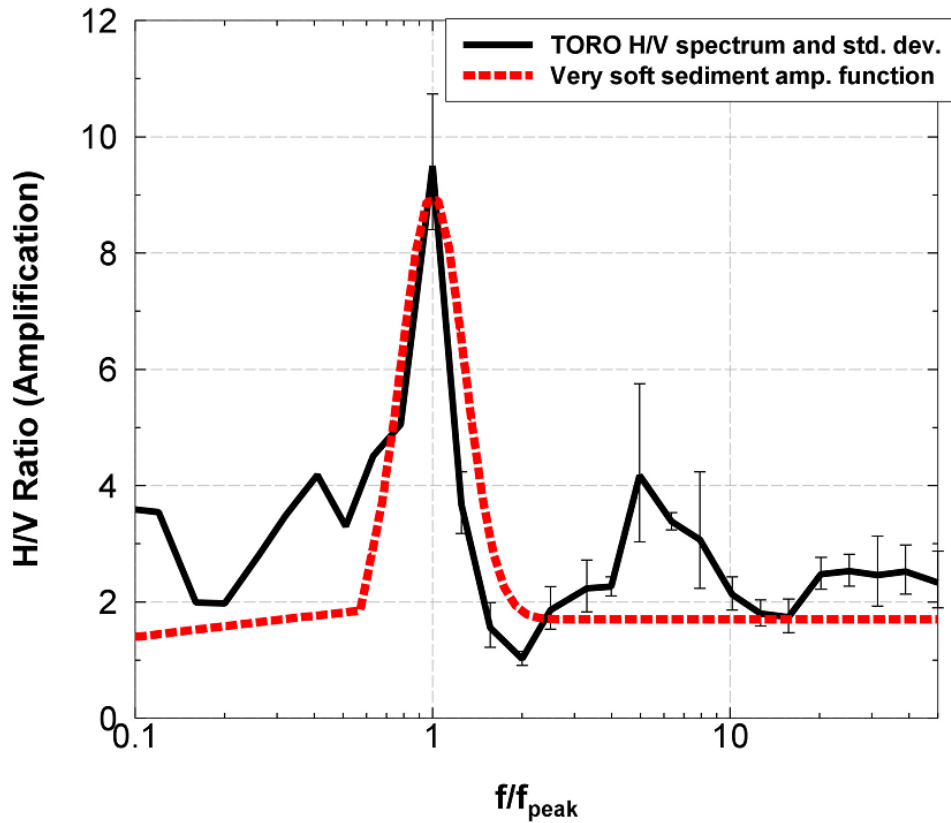
Figure 2-6: H/V spectrum for TORO, the only site on very soft sediment/fill, plotted by f/f$_{peak}$, and the soft organic sediment amplification function. The H/V spectrum has an A$_{peak}$ of 9.5.

The 15 stations on till have A$_{peak}$ values between 2.1 and 4.1, while the 7 stations on sand/clay have maximum amplitudes between 4.2 and 6.7. The amplification functions for the three sediment classes can be represented as two-piece functions of f/f$_{peak}$ which follow the average H/V trend for their respective sediment class. They have a condition that the minimum amplification (A$_{min}$) = 1 where necessary. The till amplification function can be described by

$$A_{Till}(f/f_{peak}) = 1.07X + 2.1, \; f/f_{peak} < 0.6 \tag{2.5a}$$

$$A_{Till}(f/f_{peak}) = 1.3\exp(-(X/0.17)^2) + 1.7, \; f/f_{peak} \geq 0.6, \tag{2.5b}$$

where $X = \log(f/f_{peak})$. Similarly, equation (2.6) describes amplification on sand/clay while equation (2.7) describes very soft organic sediment amplification:

$$A_{Sand/clay}(f/f_{peak}) = 0.6X + 2.0, \; f/f_{peak} < 0.6 \tag{2.6a}$$

$$A_{Sand/clay}(f/f_{peak}) = 3.5\exp(-(X/0.15)^2) + 1.7, \; f/f_{peak} \geq 0.6, \tag{2.6b}$$

$$A_{Organic}(f/f_{peak}) = 0.6X + 2.0, \; f/f_{peak} < 0.6 \tag{2.7a}$$

$$A_{Organic}(f/f_{peak}) = 7.31\exp(-(X/0.15)^2) + 1.7, \; f/f_{peak} \geq 0.6, \tag{2.7b}$$

where, similar to till, $X = \log(f/f_{peak})$. We note that the function for soft organic sediments is not well calibrated as we have only a single station on this site type.

It is also useful to consider the H/V spectra and amplification profile expected for bedrock sites, as these are often used to represent a reference condition in seismological and engineering applications. An amplification function for bedrock sites can also be used in the same manner as the functions for sites with sediment cover. In **Figure 2-7**, we show the H/V spectra and their average for all bedrock sites in the study region. Note the similarity of shapes and amplitudes for these sites, allowing a single robust average H/V curve to be defined.
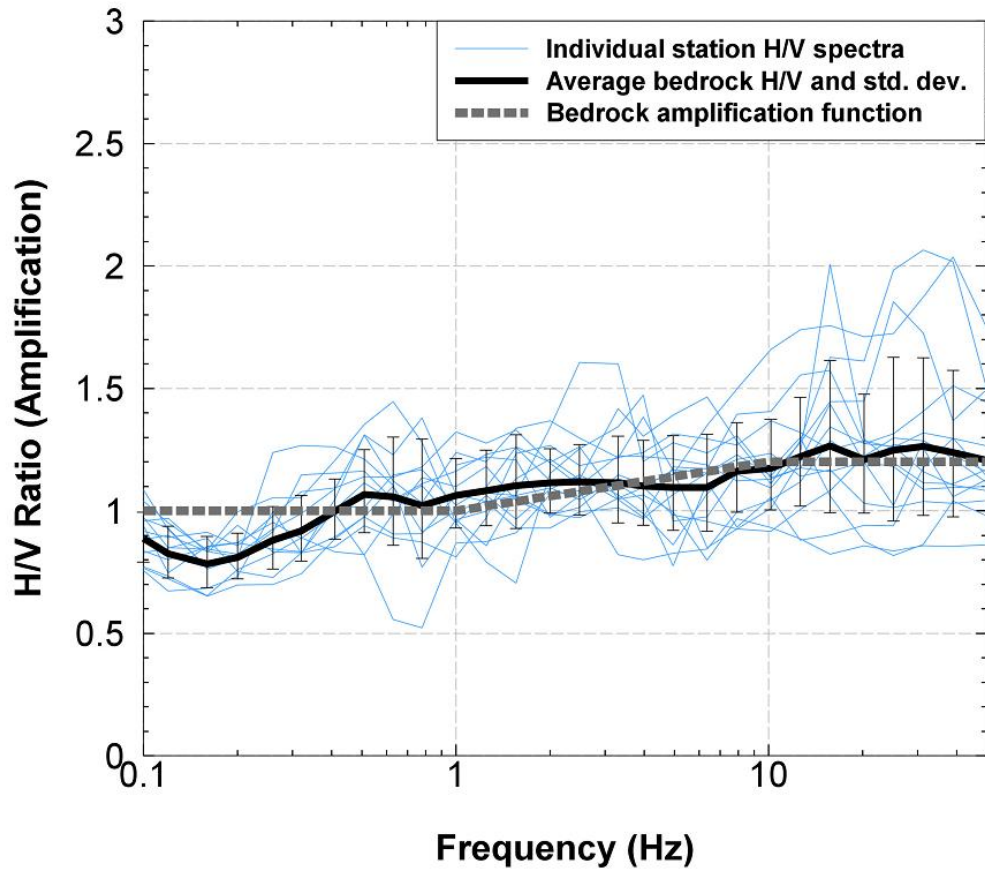
Figure 2-7: H/V spectra from 15 seismograph stations on bedrock with the weighted average H/V curve and bedrock amplification function. The spectra rise gently with increasing frequency.

Figure 2-7 shows that the bedrock spectra are relatively flat with a gentle rise as frequency increases. To capture the average H/V trend, a three-piece bedrock amplification function is used:

$$A_{Bedrock}(f) = 1, \ f \le 1 \ Hz \tag{2.8a}$$

$$A_{Bedrock}(f) = 0.2(\log(f)) + 1, \ 1 \ Hz < f < 10 \ Hz \tag{2.8b}$$

$$A_{Bedrock}(f) = 1.2, \ f \ge 10 \ Hz. \tag{2.8c}$$

The average bedrock H/V spectral ratio and $A_{Bedrock}(f)$ are in good agreement with previous studies, as described in Siddiqqi and Atkinson (2002).

The four amplification functions are plotted together in **Figure 2-8**. In this plot, the sediment amplification functions have their A_{peak} values normalized to an f/f_{peak} value of 1, but the bedrock function is not normalized (i.e., it is plotted versus frequency in Hz). The A_{peak} values of the till, sand/clay and organic amplification functions are 3.0, 5.2 and 9.0, respectively. These are slightly larger A_{peak} values than those seen in the H/V ratios for Japan in Ghofrani and Atkinson (2014), possibly due to stronger velocity contrasts at the base of the profile in Ontario; however, the overall shapes are similar in ENA and Japan.
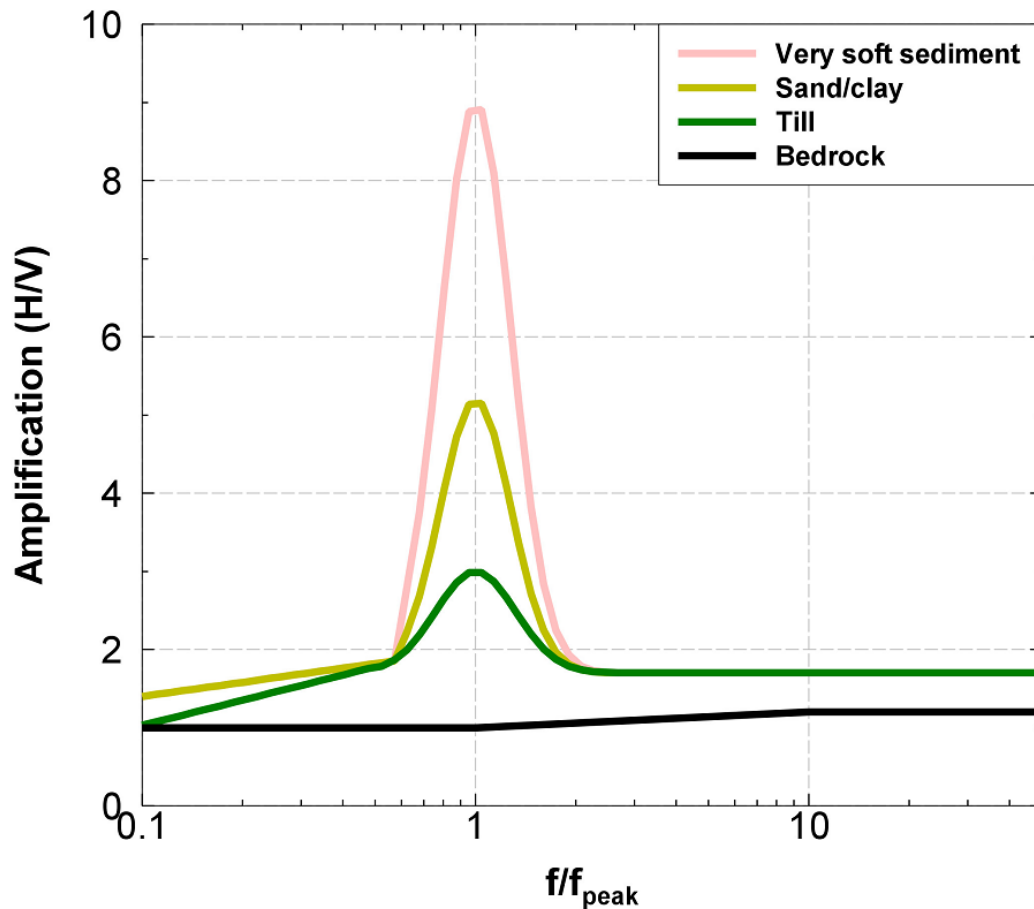
Figure 2-8: Comparison of site amplification functions for different surficial geology types. Till, sand/clay and very soft sediment/fill are plotted with respect to normalized frequency.

2.5   Amplification Functions for Sites with Unknown Peak Frequencies

The amplification functions obtained in the previous section were derived from ground-motion recordings collected at seismograph sites. We focused on the seismographic data due to the stability of the H/V spectra when gathered over multiple earthquake recordings. Moreover, it is particularly important to understand site amplification at seismographic sites, as this allows us to interpret seismographic data to obtain an understanding of the ground-motion field radiated by regional earthquakes. The

amplification functions are applicable for sites where the H/V ratios (or f_{peak} values) are known with confidence. For most locations, however, we have only an estimate of f_{peak} based on other information such as the sediment type and estimated depth-to-bedrock (e.g., such as from the OGS sediment thickness map in Ontario). As mentioned previously, the estimated depth-to-bedrock contains some uncertainty, and interpolating for sites between coordinates for which such information is available introduces more uncertainty. Only some of this uncertainty (excluding the component due to interpolation between locations) is represented in the standard deviation of equation (2.1), which gives f_{peak} to within a factor of ~1.6. Thus, we can say that our uncertainty in the estimate of f_{peak} for sites without a direct measurement based on H/V is at least a factor of 1.6, and is probably closer to a factor of two. A realistic model of site amplification across the region for use in ShakeMap or similar applications must account for this uncertainty.

If we are uncertain as to the peak frequency of response, it is preferable to assume a more generic amplification in which we have smoothed and broadened the peak over a range of frequencies, as well as making it gentler in amplitude. This will also help account for event-to-event variability in amplification at a site. To develop a smoothed broad-peak function, we consider the implications of one standard deviation in the value of f_{peak} (0.2 log units). For each sediment class's normalized average H/V curve, a Monte Carlo simulation is performed to generate 1000 identically-shaped curves, with random variability in f_{peak} within 0.2 log units (assuming a normal distribution in log frequency space). The average of these 1000 simulated curves is computed, which generates a curve that has a broadened peak. To capture the overall trend of this average curve, we alter the parameters of the Gaussian function from Ghofrani and Atkinson (2014). The results for this process for the three sediment classes are shown in **Figure 2-9** and the equations which describe the broad-peaked sediment amplification functions are given by equations (2.9) to (2.11). Since bedrock spectra have no peak frequency, the same function given by equation (2.8) also applies here.

$$A_{Till}(f/f_{peak}) = 1.25X + 2.39, \; f/f_{peak} < 0.6 \tag{2.9a}$$

$$A_{Till}(f/f_{peak}) = 0.5\exp(-(X/0.33)^2) + 1.8, \; f/f_{peak} \geq 0.6, \tag{2.9b}$$

$$A_{\text{Sand/clay}}(f/f_{\text{peak}}) = 1.5X + 3.15, \; f/f_{\text{peak}} < 0.6 \tag{2.10a}$$

$$A_{\text{Sand/clay}}(f/f_{\text{peak}}) = 1.5\exp(-(X/0.38)^2) + 1.8, \; f/f_{\text{peak}} \geq 0.6, \tag{2.10b}$$

$$A_{\text{Organic}}(f/f_{\text{peak}}) = 1.5X + 4.6, \; f/f_{\text{peak}} < 0.6 \tag{2.11a}$$

$$A_{\text{Organic}}(f/f_{\text{peak}}) = 2.8\exp(-(X/0.4)^2) + 2.3, \; f/f_{\text{peak}} \geq 0.6, \tag{2.11b}$$

where $X = \log(f/f_{\text{peak}})$, and we impose the condition that $A_{\text{min}} = 1$.
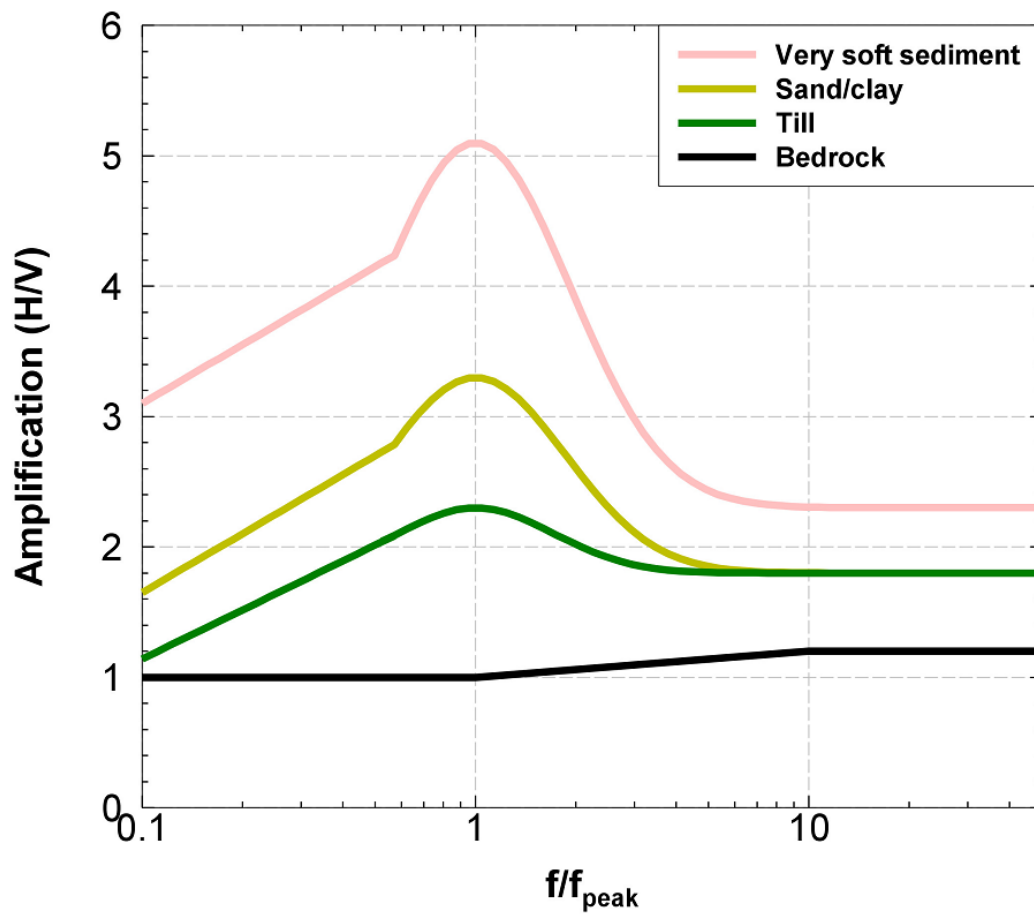
Figure 2-9: Suggested amplification functions for generic sites with poorly-known f_{peak}, normalized by f_{peak}.

2.6 Comparisons with a Typical Site Response Model Used in California

An interesting aspect of the amplification functions in **Figure 2-9** is that, even after broadening and dampening the peaks by considering an uncertainty of a factor of 1.6 in f_{peak}, the inferred average amplifications on sediments in eastern Canada are still much sharper and more pronounced than would be suggested by typical amplification functions that are applied in western North America. For example, a typical western site amplification model, derived from the NGA-West 2 database using V_{S30} as the site variable, is that given by Seyhan and Stewart (2012). By assuming weak-motion peak ground accelerations (PGAs) of $0.02g$ and a suitable, generic V_{S30} value for each type of deposit, we can compare the site amplification functions for southern Ontario to those of Seyhan and Stewart (2012), as shown in **Figure 2-10**. To make these comparisons, we assume nominal values for V_{S30} of 1000 m/s for till, 300 m/s for sand/clay and 150 m/s for soft/organic sediments.
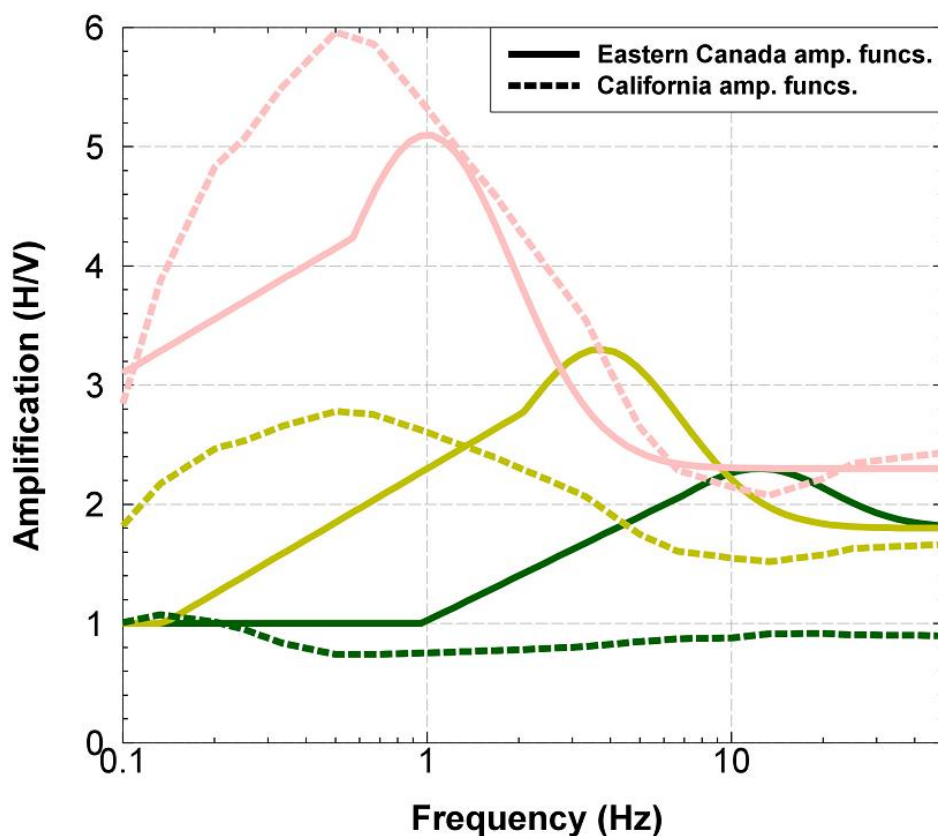
Figure 2-10: The three proposed generic sediment amplification functions for eastern Canada and the corresponding functions for California (Seyhan and Stewart, 2012) assuming nominal values of V_{S30} of 1000 m/s, 300 m/s and 150 m/s for till, sand/clay and soft soil, respectively. Light shades refer to very soft sediment/fill; intermediate to sand/clay; dark to till.

Note that till sites have, on average, high peak frequencies, while sand/clay sites have intermediate peak frequencies. Sites in western North America (primarily California data) have more subdued amplification profiles, with lower and broader peak frequencies, reflecting more gradational sediment profiles. The only sites in eastern Canada which could appear to have similar site amplification characteristics to the California functions are soft, deep sites with low peak frequencies. By contrast, most sediment profiles in eastern Canada are soft to stiff sediments of variable depth overlying much harder rock, resulting in a greater seismic impedance contrast. It should be noted that the Seyhan and

Stewart (2012) amplification functions were derived without consideration of the depth of the deposit; this has the effect of broadening the functions (similar to how the broad-peaked amplification functions for eastern Canada were derived). The difference seen in A_{peak} between the California functions and the H/V spectra for eastern Canada may be due partly to this broadening effect, and partly due to the higher impedance contrast in eastern Canada. One may also infer from the low peak frequency of the California sediment amplification functions, over all values of V_{S30}, that the California model is generally applicable to deep, gradational sites.

2.7   Summary and Conclusion

- A preliminary site amplification model is developed for eastern Canada based on the two predictive variables of f_{peak} and surficial geology type (bedrock, till, sand/clay, very soft organic sediment/fill). The intended use of this model is to predict levels of site amplification in a generalized sense, for application onto a real-time ShakeMap product for the region. More detailed studies, based on more subsurface geological information and velocity measurements in the field, are needed to refine this model.

- The value of f_{peak} in the site amplification model is a function of depth-to-bedrock. Similarly, A_{peak} is a function of surficial geology, or sediment stiffness. Sites in many parts of eastern Canada have pronounced amplification around a peak frequency, due to the sharp velocity contrast at the base of the profile.

- For use in ground-motion mapping applications, it is necessary to consider uncertainty in the value of f_{peak}. This uncertainty subdues and broadens the expected value of the amplification (by averaging over a range of f_{peak}). However, the functions are still sharper and more pronounced than in classic models for western regions.

- The use of sediment thickness and surficial geology as a way to characterize site response in Ontario is convenient since these data are readily available and correlate well with f_{peak} and A_{peak}, respectively. Moreover, these data exist for a large number

of sites in the region, unlike data for V_{S30}, which are scarce and only inferred for many seismograph stations.

- H/V spectra in eastern Canada have high values of A_{peak}; however, these apply to linear site amplification for weak-motions. Nonlinearity would be expected to dampen these amplifications and shift the peaks to lower frequencies.

References

Aki, K and Richards, P.G. (2002). Quantitative Seismology, 2nd edition. University Science Books. Sausalito, California. 700.

Assatourians, K. and Atkinson, G.M. (2008). Program: ICORRECT. Engineering Seismology Toolbox. Department of Earth Sciences, The University of Western Ontario. 40.

Atkinson, G.M. (2004). Empirical Attenuation of Ground-Motion Spectral Amplitudes in Southeastern Canada and the Northeastern United States. *Bulletin of the Seismological Society of America*, **94**, 3, 1079–1095.

Atkinson, G.M. and Assatourians, K. (2010). Attenuation and Source Characteristics of the 23 June 2010 M 5.0 Val-des-Bois, Quebec, Earthquake. *Seismological Research Letters*, **81**, 849–860.

Bard, P-Y. (1999). Microtremor measurements: a tool for site effect estimation? In: Irikura, K., Kudo, K., Okada, H., and Satasini, T., (eds) The Effects of Surface Geology on Seismic Motion. Balkema, Rotterdam, p. 1251–1279.

Chouinard, L. and Rosset, P. (2012). On the Use of Single Station Ambient Noise Techniques for Microzonation Purposes: the Case of Montreal; in Shear Wave Velocity Measurement Guidelines for Canadian Seismic Site Characterization in Soil and Rock, (ed.) J.A. Hunter and H.L. Crow; Geological Survey of Canada, Open File 7078, p. 85–93.

Ghofrani, H. and Atkinson, G.M. (2014). Site Condition Evaluation Using Horizontal-to-

Vertical Response Spectral Ratios of Earthquakes in the NGA-West 2 and Japanese Databases. *Bulletin of Soil Dynamics and Earthquake Engineering*, **67**, 30–43.

Kawase, H., Sánchez-Sesma, F.J. and Matsushima, S. (2011). The Optimal Use of Horizontal-To-Vertical Spectral Ratios of Earthquake Motions for Velocity Inversions Based on Diffuse Field Theory for Plane Waves. *Bulletin of the Seismological Society of America*, **101** (in press).

Kolos, D. (2010). Using Horizontal-to-Vertical Spectral Ratios to Estimate Shear Wave Velocities of Soil at South-Eastern Canadian Seismological Stations. The University of Western Ontario. Accelerated Master's Thesis. 64.

Kramer, S.L. (1996). Geotechnical Earthquake Engineering. Prentice-Hall, Inc. Upper Saddle River, New Jersey. 653.

Lermo, J. and Chávez-Garcìa, F.J. (1993). Site effects evaluation using spectral ratios with only one station. *Bulletin of the Seismological Society of America*, **84**, 1350–1364.

Motazedian, D., Hunter, J.A., Pugin, A., and Crow, H.L. (2011). Development of a V_{S30} (NEHRP) Map for the City of Ottawa, Ontario, Canada. *Canadian Geotechnical Engineering Journal*, **48**, 3, 458–472.

Nakamura, Y. (1989). A method for dynamic characteristics estimation of subsurface using microtremor on the ground surface. *Quarterly Report of RTRI*, **30**, 25–33.

Pal, J. and Atkinson G.M. (2012). Scenario Shakemaps for Ottawa, Canada. *Bulletin of the Seismological Society of America*, **102**, 2, 650–660.

Rosset, P. and Chouinard L. (2009). Characterization of site effects in Montreal, Canada. *Natural Hazards*, **48**, 295–308.

Rosset, P., Bour-Belveaux, M., Chouinard, L. (2015). Microzonation models for Montreal with respect to V_{S30}. *Bulletin of Earthquake Engineering*, **13**, 8, 2225–2239.

Seyhan, E. and Stewart, J.P. (2012). Site Response in NEHRP Provisions and NGA Models. *Earthquake Engineering*. **226**, 359–379.

Seyhan, E. and Stewart, J.P. (2014). Semi-empirical nonlinear site amplification from NGAWest2 data and simulations. *Earthquake Spectra*, **30**, 1241–1256.

Siddiqqi, J. and Atkinson, G.M. (2002). Ground-motion amplification at rock sites across Canada as determined from horizontal-vertical component ratio. *Bulletin of the Seismological Society of America*, **92**, 887–884.

Wald, D.J., Quitoriano V., Heaton, T.H. and Kanamori, H. (1999). Relationships between peak ground acceleration, peak ground velocity, and modified Mercalli intensity in California. *Earthquake Spectra,* **15**, 557–56.

Chapter 3

3 A Model for Estimating Amplification Effects on Seismic Hazards and Scenario Ground Motions in Southern Ontario

3.1 Introduction

The intensity of ground shaking that a locality experiences in any particular earthquake can vary considerably from site to site. A good example of this phenomenon is the moment magnitude (**M**) 6.9 Loma Prieta earthquake, which occurred in the San Francisco Bay area on 19 October 1989. This event produced a Modified Mercalli Intensity (MMI; Wood and Neumann, 1931) of VII to VIII in the epicentral region where great damage was observed mostly in older structures. However, even higher intensities of up to MMI IX were recorded at large distances, 100 km away, in parts of San Francisco and Oakland, California (Kramer, 1996), where several buildings, bridges and freeways collapsed. A main factor controlling this variability in ground shaking was local site conditions: sites on soft, unconsolidated San Francisco Bay mud observed larger amplitudes, especially on the horizontal component.

Southern Ontario, Canada's most densely-populated region, is characterized by a wide variety of site conditions, resulting in varied responses from site to site during an earthquake. Estimating this variability on a large geographical scale presents a challenge, especially when relevant site information is scarce. This challenge is addressed on a very broad scale in the national seismic hazard maps of the National Building Code of Canada (NBCC); the NBCC is updated every 5 years with the most recent version being released in 2015 (for an overview, see Humar, 2015). These maps provide 5%-damped horizontal-component pseudo-spectral acceleration (PSA) having an exceedance probability of 2% in 50 years. The PSA values are given for a reference site condition of National Earthquake Hazards Reduction Program (NEHRP) class C; this site condition is defined as having a time-averaged shear wave velocity in the upper 30 m (V_{S30}) of 360-760 m/s. Site amplification factors are provided in the 2015 NBCC to convert these motions to those for both firmer and softer sites. The approach and factors were based on empirical

site amplification studies in California (e.g., Borcherdt, 1970). This provides useful guidance for assessing hazard in a general sense, but contains oversimplifications for many types of deposits and may not be applicable for all regions. For example, Dowling et al. (2016) evaluated site amplification factors for Victoria and Vancouver on a site-specific basis, and concluded that the site factors in the 2015 NBCC tended to underestimate site response by 25% to 35% depending on the location, period and site class.

In eastern Canada there are many regions that are characterized by a soft layer overlying hard rock, and having a distinct peak site frequency; the response of such sites differs significantly from typical California deposits, which are characterized by gradational profiles in which stiffness increases gradually with depth. Considerable microzonation and site characterization work has been performed in southeastern Ontario and southern Quebec (e.g., Motazedian et al., 2011; Chouinard and Rosset, 2012; Nastev et al., 2016). Braganza et al. (2016) used these findings, along with site information for all of southern Ontario, to develop a regional-scale linear site amplification model. The model was derived using geological information on surficial geology and depth-to-bedrock, in concert with recorded horizontal-to-vertical (H/V) component ratios of PSA (5% damped) from earthquake motions, which provide an estimate of site amplification. The use of H/V spectral ratios as a proxy for site amplification is a well-known approach (e.g., Nakamura, 1989; Lermo and Chávez-García, 1993). The results of Braganza et al. (2016) were provided as a site amplification model that is a function of depth-to-bedrock and surficial geology. These parameters are used to estimate the site's peak frequency (f_{peak}) and degree of amplification. The use of f_{peak} as a site variable is an approach that is favoured in many regions (e.g., Zhao et al., 2006). The intended use of this amplification model is to aid in the development of ground-motion prediction equations (GMPEs) and to accurately estimate ground-motion intensities for applications such as ShakeMaps (e.g., Wald et al., 1999; Atkinson et al., 2015). **Figure 3-1** shows the linear amplification factors derived from the f_{peak}-based Braganza et al. (2016) model for low (1 Hz) and high (10 Hz) frequency ground motions.
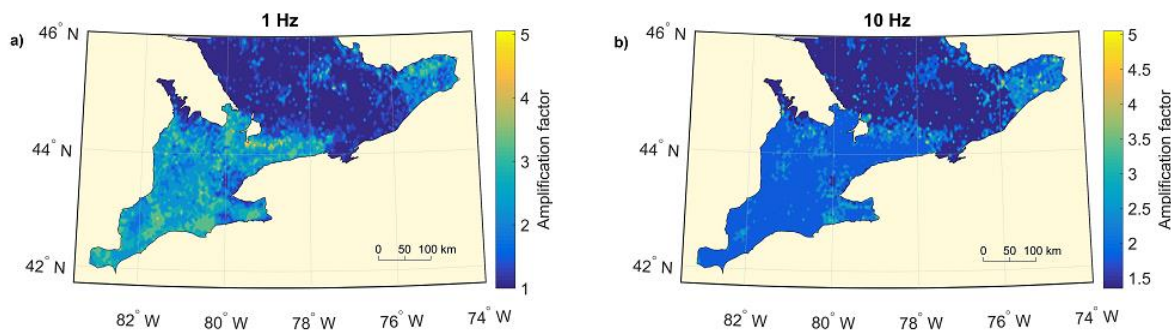
Figure 3-1: The Braganza et al. (2016) linear amplification model for southern Ontario, showing amplification factors for 1 Hz (a) and 10 Hz (b) ground motions. Soil nonlinearity may reduce these factors for strong levels of shaking.

In this study, the findings of Braganza et al. (2016) are expanded upon and the amplification model's applicability is tested on a regional scale. Ground-motion estimates and intensities are examined under different amplification models for the following cases:

- Motions experienced in Ottawa during the **M**5.0 Val-des-Bois, Quebec earthquake
- Motions expected in Ottawa for the 2015 NBCC 2% in 50 year reference motions
- Motions experienced in southern Ontario during the **M**5.0 Val-des-Bois, Quebec earthquake
- Motions expected in southern Ontario for a postulated **M**6.0 scenario event

The differences between amplifications based on f_{peak} and those based only on stiffness (V_{S30}) are demonstrated, and the advantages of using f_{peak} rather than V_{S30} in eastern Canada are discussed.

3.2 Derivation of the f_{peak}-based Amplification Model

Braganza et al. (2016) used the H/V component ratios of the 5%-damped PSA as an indicator variable for site response. In their approach, the site response is estimated from the peak frequency of the site and its surficial geology. The model was developed using H/V ratios at seismograph stations to estimate site amplification, which were correlated with local site conditions. The information on site conditions, including surficial geology and overburden thickness (i.e., depth-to-bedrock), is provided by the

Ontario Geological Survey (OGS) and can be accessed online (www.mndm.gov.on.ca/en/mines-and-minerals/applications/ogsearth). The H/V ratios were computed from PSA observations at seismograph sites and processed using the ICORRECT software of Assatourians and Atkinson (2008); this software corrects the seismographic records for instrument response and calculates the response spectrum. A relationship was determined between a site's depth-to-bedrock and peak frequency (i.e., the frequency at which the H/V ratio attains its maximum value). The peak amplitude of response (A_{peak}) was correlated with the type of surficial geology. Surficial geology was used as a proxy for stiffness rather than V_{S30} since reliable information for the latter is not available on a regional basis. Standard-shaped amplification curves developed in terms of these variables were derived for four generic surficial geologies (bedrock, till, sand/clay, and very soft sediment/fill) and for sites where f_{peak} is unknown. The functions for sediment are a function of a site's f_{peak}, with the value of A_{peak} increasing for softer sediments (i.e., A_{peak} increases from till to very soft sediment), as shown in **Figure 3-2**. We note that there is some uncertainty in the estimation of the H/V ratio, and additional uncertainty in the estimation of its peak frequency based on the site characteristics; these uncertainties were considered in the model development, as discussed by Braganza et al. (2016).
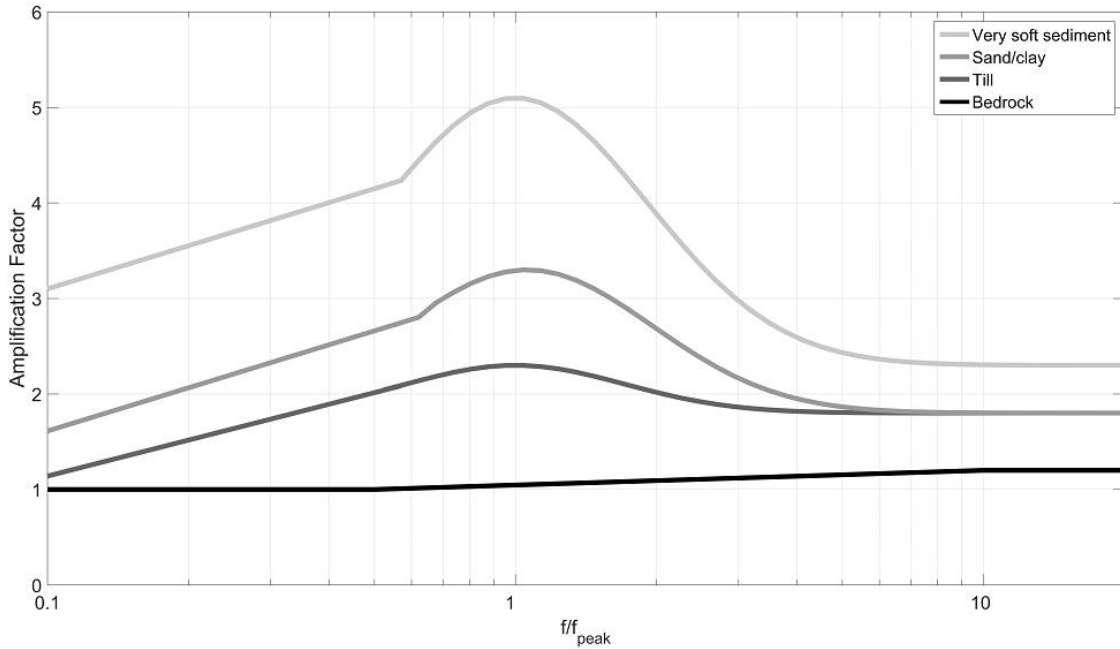
Figure 3-2: Linear amplification functions for sites with unknown f_{peak}, normalized by f_{peak}.

The linear amplification functions of **Figure 3-2** are normalized by using the dimensionless frequency measure f/f_{peak}, and can thereby be expressed as:

$$A_{Till}(f/f_{peak}) = 1.25X + 2.39, \; f/f_{peak} < 0.6, \tag{3.1a}$$

$$A_{Till}(f/f_{peak}) = 0.5\exp(-(X/0.33)^2) + 1.8, \; f/f_{peak} \geq 0.6, \tag{3.1b}$$

$$A_{Sand/clay}(f/f_{peak}) = 1.5X + 3.15, \; f/f_{peak} < 0.6, \tag{3.2a}$$

$$A_{Sand/clay}(f/f_{peak}) = 1.5\exp(-(X/0.38)^2) + 1.8, \; f/f_{peak} \geq 0.6, \tag{3.2b}$$

$$A_{Organic}(f/f_{peak}) = 1.5X + 4.6, \; f/f_{peak} < 0.6, \tag{3.3a}$$

$$A_{Organic}(f/f_{peak}) = 2.8\exp(-(X/0.4)^2) + 2.3, \; f/f_{peak} \geq 0.6, \tag{3.3b}$$

where $X = \log(f/f_{peak})$, and a condition is imposed that $A_{min} = 1$. Note that logarithms throughout this manuscript are of base 10. For bedrock sites (i.e., sites of NEHRP class A where $V_{S30} > 1500$ m/s), there is no peak frequency and the amplification rises gradually at higher frequencies:

$$A_{Bedrock}(f) = 1, f \leq 1 \text{ Hz,} \qquad (3.4a)$$

$$A_{Bedrock}(f) = 0.2(\log(f)) + 1, 1 \text{ Hz} < f < 10 \text{ Hz,} \qquad (3.4b)$$

$$A_{Bedrock}(f) = 1.2, f \geq 10 \text{ Hz.} \qquad (3.4c)$$

For the estimation of ground motions and intensity in this study, these generic amplification functions are used (in addition to site factors from the 2015 NBCC). The value of f_{peak} is estimated based on depth-to-bedrock information from the OGS or microzonation studies via the quarter-wavelength approximation (Kramer, 1996):

$$f_{peak} = Vs_{av}/4D, \qquad (3.5a)$$

where Vs_{av} is the time-averaged shear wave velocity (m/s) and D is the depth-to-bedrock (m). Vs_{av} is approximated using the empirical relation developed by Braganza et al. (2016):

$$Vs_{av} = 0.2762D + 190.2911, 0 < D \leq 120 \text{ m,} \qquad (3.5b)$$

$$Vs_{av} = 223.4351 \text{ m/s, } D > 120 \text{ m.} \qquad (3.5c)$$

The type of surficial geology, used to determine which site amplification function (**Figure 3-2**) is used, is obtained from the OGS information.

3.3   Methods Used to Estimate Ground Motion and Intensity

To map ground motions on a regional level, the region of interest is analyzed on a grid, calculating at each grid point the ground motions for a reference site condition, then multiplying these motions by the amplification terms reflecting the site conditions at that point. To map MMI, the motions are converted to felt intensity. In the following, the calculations for each of these elements are described.

3.3.1   Motions for a Reference Site Condition

The motions at each point, for the reference site condition, are calculated using the GMPEs described by Atkinson et al. (2015). They developed an empirically-calibrated model to provide event-specific GMPEs for southern Ontario, having

dependent variables of **M**, stress drop ($\Delta\sigma$), and hypocentral distance. The reference site condition is hard rock, with $V_{S30} = 2000$ m/s. For the Val-des-Bois earthquake, the recorded PSA data from the event were used to determine that the event is described by **M** = 5.1 and $\Delta\sigma = 690$ bars. The estimated source parameters are in reasonable agreement with other studies on this earthquake (e.g., Atkinson and Assatourians, 2010), and with the moment tensor value of **M** = 5.0. The value of stress drop for this event was higher than the average value for eastern Canadian events which resulted in relatively-strong shaking. To consider a larger scenario event, an event of **M** = 6.0 with a somewhat larger stress parameter of $\Delta\sigma = 830$ bars is used; due to the high stress value assumed for this scenario, its motions are roughly comparable to median-plus-sigma levels in terms of expected strength of shaking for **M** = 6.0 events (i.e., if we consider that such events could have stress drop values in the range from 300 to 900 bars). **Figure 3-3** plots the 1 and 10 Hz attenuation curves for these two considered events, showing the dependence of amplitude on distance (for hard rock). The GMPEs from Atkinson et al. (2015) provide the median motions for the specified stress drop values, but the adoption of relatively-high stress drop values implies the motions are biased high (i.e., motions are stronger than those for events of the same magnitude having average stress drops). Moreover, motions are often higher or lower at specific sites, relative to the median level for the event, by about a factor of two, due to the intra-event variability component of GMPEs.
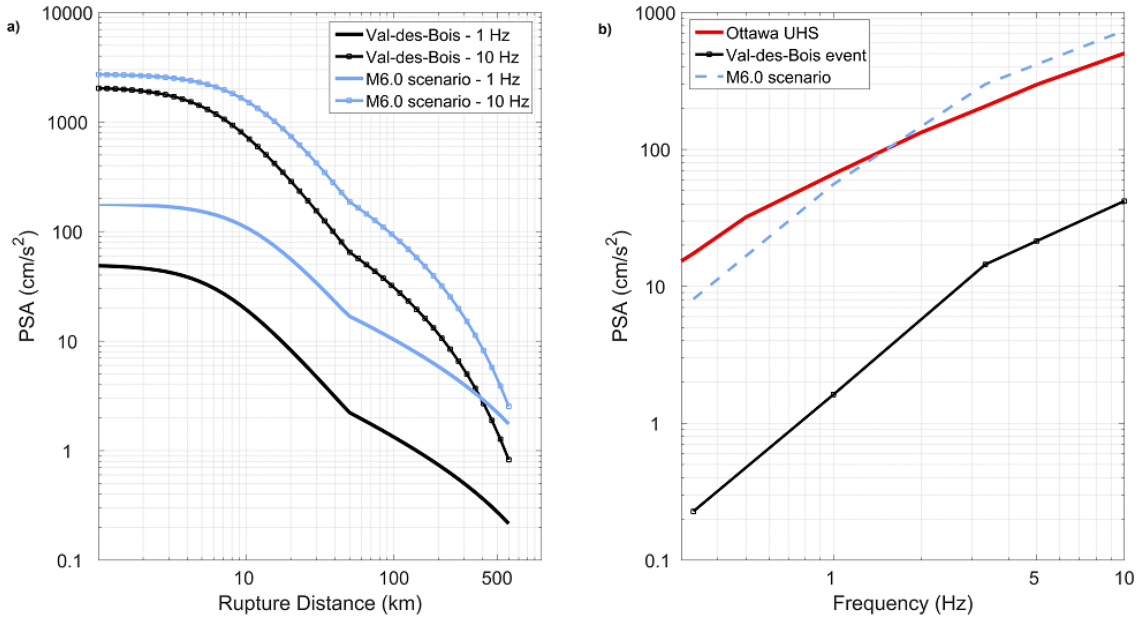
Figure 3-3: Attenuation curves for the Val-des-Bois and scenario M6.0 earthquakes for PSA at 1 and 10 Hz (a) and expected response spectra for the city of Ottawa for the Val-des-Bois and 2% in 50 year motions (b). The response spectrum for the M6.0 scenario event at a distance of 20 km is also shown. All curves are for a class A (hard rock) reference.

In addition to evaluating the motions from specific events, the motions specified by the 2015 NBCC (i.e., the mean-hazard PSA values given by the uniform hazard spectrum [UHS] for Ottawa for 2% in 50 years) are also considered. **Figure 3-3** also shows the Ottawa UHS in comparison to the response spectrum for the Val-des-Bois earthquake at Ottawa (~75 km from the epicenter), and for the **M**6.0 scenario at ~20 km, all for a class A reference site (V_{S30} = 2000 m/s). Note that the motions for Ottawa's UHS are provided for a class C reference condition in the 2015 NBCC and have been converted to class A as described in the next section. The motions for the mean-hazard Ottawa UHS, for 2% in 50 years, are much stronger than the **M**5.0 Val-des-Bois earthquake motions in Ottawa, and of similar amplitude to the **M**6.0 scenario event at a distance of approximately 20 km. This is as we would expect, because hazard contributions to the Ottawa UHS at the 2% in 50 year level tend to be dominated by

motions from moderate-to-large events ($\mathbf{M}$~5.5 to 6.6) at relatively close distances (< 50 km) (e.g., Pal and Atkinson, 2012).

3.3.2 Calculation of Site Amplifications Relative to the Reference Condition

Two amplification models – one based on f_{peak}, and the other based on V_{S30} (where the latter is the 2015 NBCC model) – are used to account for the effects of local soils on regional ground-motion estimates, in order to compare their implications. The 2015 NBCC site factors are tabulated for site classes A to E, for a few standard ShakeMap frequencies, i.e.,: 0.33, 1, 3.33 and 10 Hz, as well as peak ground velocity (PGV) and acceleration (PGA); the factors depend on the expected value of PGA for a reference class C (PGA_{ref}), in order to account for soil nonlinearity at strong shaking levels. For ShakeMap frequencies not listed in the 2015 NBCC, an interpolation in log-log space is made to estimate factors at neighbouring frequencies. Note that the 2015 NBCC amplifications are given relative to a value of 1.0 for a class C reference. These have been converted to the equivalent values relative to class A (i.e., relative to an amplification factor of 1.0 on hard rock sites) by dividing all factors for a given frequency by the corresponding factors for class A. **Table 3-1** summarizes the 2015 NBCC site factors used in this study for low levels of shaking ($PGA_{ref} < 0.1g$). These linear amplification factors are multiplied by the PSA values for hard rock in order to calculate the estimated motions under the V_{S30}-based approach to site classification. By contrast, the f_{peak}-based model of Braganza et al. (2016) calculates the applicable site amplification factors based on surficial geology and depth-to-bedrock, as described in the preceding section. Note that for the city of Ottawa, site information is provided as a V_{S30} class, for which an equivalent surficial geology is assigned in order to compute amplifications using the f_{peak}-based model. Similarly, for southern Ontario, surficial geologies are assigned an equivalent V_{S30} class for the purposes of using the 2015 NBCC model.

Table 3-1: Normalized 2015 NBCC site factors (class A reference), corresponding to ShakeMap parameters.

Site Class	2015 NBCC Site Factors					
	0.33 Hz	**1 Hz**	**3.33 Hz**	**10 Hz**	**PGV**	**PGA**
A	1.00	1.00	1.00	1.00	1.00	1.00
B	1.07	1.11	1.13	0.93	1.08	0.97
C	1.69	1.75	1.58	1.02	1.61	1.11
D	2.65	2.72	2.11	1.33	2.37	1.43
E	4.91	4.93	3.10	1.91	3.98	2.01

The linear amplification values described above are for low levels of shaking ($<$ 0.1g). For stronger shaking, the effect of soil nonlinearity on the amplification needs to be considered. For this purpose, the nonlinear component of the site amplification model of Seyhan and Stewart (2014) is used. They describe the total amplification effects as the sum of linear and nonlinear terms:

$$F_s = \ln(F_{lin}) + \ln(F_{nl}), \tag{3.6}$$

where F_s is the total site amplification in natural logarithmic units, F_{lin} is the linear component of the amplification, and F_{nl} is the nonlinear component. The F_{nl} component is given as

$$\ln(F_{nl}) = f_1 + f_2 \ln((PGA_r + f_3) / f_3), \tag{3.7}$$

where f_1, f_2 and f_3 are model coefficients, with f_2 being a function of site period and $V_{S30,}$ and PGA_r is PGA in units of g, as evaluated using the GMPE given by Boore et al. (2014). In this study, equation (3.7) is used to determine F_{nl}, which is then multiplied by the F_{lin} factors from the f_{peak} and 2015 NBCC models in order to adjust the amplification

factors for the effects of soil nonlinearity. F_s is then multiplied by the reference PSA at a given frequency to determine the ground acceleration. It should be noted that Seyhan and Stewart (2014) did not find significant regional differences in nonlinearity of soils; thus, this adjustment is likely reasonable for use with the linear site factors for southern Ontario. Moreover, like the F_{lin} term, the F_{nl} term is applied to all sites and is used for all events in this study for the purposes of estimating ground motions and shaking intensities.

3.3.3   Conversion of Ground Motion to Intensity

To compute estimates of felt intensity that would be experienced for the computed motions, the ground-motion-to-intensity conversion equation (GMICE) between PGV and MMI as given in Atkinson and Kaka (2007) is used:

$$MMI = 4.37 + 1.32(\log PGV) + 0.47 - 0.19\mathbf{M} + 0.26\log(R) \text{ for } \log PGV \le 0.48, \quad (3.8a)$$

$$MMI = 3.54 + 3.03(\log PGV) + 0.47 - 0.19\mathbf{M} + 0.26\log(R) \text{ for } \log PGV > 0.48, \quad (3.8b)$$

where R is the fault or hypocentral distance (km). Other GMICE for making intensity estimates were also considered, including those of Worden et al. (2012) and Dangkua and Cramer (2011). However, at all distances for the Val-des-Bois event, the Worden et al. (2012) relationship yielded consistently low estimates compared to Did You Feel It reports, while the Dangkua and Cramer (2011) relationship yielded consistently high estimates. Thus, the Atkinson and Kaka (2007) GMICE was selected as it appeared to be more applicable, at least for this event.

3.4 Ground Motions and Intensity for the City of Ottawa

For the city of Ottawa, estimates of median ground-motion amplitudes and MMI are made for the Val-des-Bois earthquake, as well as for the 2% in 50 year 2015 NBCC spectrum. The site parameters are obtained using information from Motazedian et al. (2011), which includes information on depth-to-bedrock and NEHRP class (V_{S30}) across the city. This site information is more accurate than that available in most parts of Ontario, because it was collected from a comprehensive microzonation study. To

calculate amplifications using the f_{peak} approach, a surficial geology type is assigned based on V_{S30}, and the depth-to-bedrock is used to calculate f_{peak} via equation (3.5). By contrast, the 2015 NBCC model uses the NEHRP class based on V_{S30} as input.

Panels a) and b) in **Figure 3-4** show the estimated horizontal-component amplitudes of PSA at 1 and 10 Hz (in log units) for the **M**5.0 Val-des-Bois earthquake for the city of Ottawa, using the f_{peak}-based model. The differences in predicted amplitudes between the 2015 NBCC and f_{peak} models are also shown in panels c) and d), in log units. This earthquake was sufficiently far from Ottawa (> 50 km) that the local site conditions are the main factor controlling differences in motions experienced across the city. In general, the strongest motions are in the Orléans area, which is approximately 17 km east of downtown and is characterized by soft sediments with depths between 30 to 100 m that amplify motions strongly (Motazedian et al., 2011). Throughout the city, 1 Hz motions are strongest primarily on class E sediments of 30-60 m depth, while 10 Hz motions are strong on sediments of shallow to intermediate depth (1-40 m), of varying site class. The ground-motion pattern is mostly a consequence of the thickness and stiffness of the sediments, as reflected in the f_{peak}-based model.
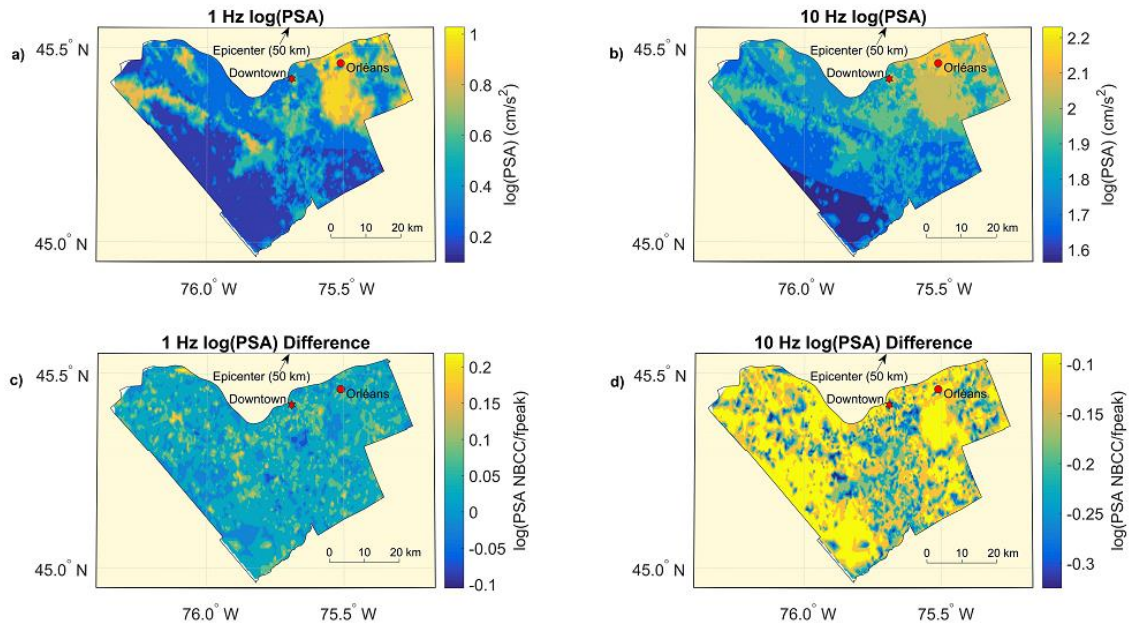
Figure 3-4: Estimated 1 Hz (a) and 10 Hz (b) log(PSA) for Ottawa for the M5.0 Val-des-Bois earthquake, using the f_{peak}-based amplification model. The difference between the NBCC and f_{peak}-based amplification models are shown for 1 Hz (c) and 10 Hz (d) motions, in log units. The locations of Orléans (discussed in text) and downtown Ottawa are indicated.

Comparing the two amplification models, in most cases they result in similar ground-motion amplitudes, to within 10% to 40%. The NBCC model usually predicts higher 1 Hz motions with the greatest model differences (up to a factor of 1.8) seen in areas of shallow (< 10 m) sediments, generally on NEHRP site class C. For 10 Hz motions, by contrast, the f_{peak} model yields higher estimated ground motions. At this higher frequency, the largest differences (up to a factor of 2.5) are observed on similar site types (i.e., shallow class C sites). These differences occur because the NBCC model usually predicts greater amplifications at low frequencies and less amplification at high frequencies, relative to the f_{peak}-based model. The f_{peak}-based model is more specific to the regional geologic conditions, involving sediment over hard, glaciated bedrock, which sets up large amplification near the site's peak frequency of response. There are negligible differences between models for hard rock sites, for which both have amplifications near unity.

The motions experienced during the Val-des-Bois earthquake are weaker than the 2% in 50 year motions used for design in Ottawa in the 2015 NBCC. **Figure 3-5** shows the variability of motions across Ottawa for the 2% in 50 year spectrum for PSA at 1 and 10 Hz (including the effects of nonlinearity), using the f_{peak}-based model. As with the Val-des-Bois event, the strongest predicted 1 Hz motions are on soft sediments of intermediate depth, while the strongest 10 Hz motions for this event are primarily associated with stiffer (class C) and shallower sites. Soft sediment effects do not show up as strongly, due to the greater effects of nonlinearity at high frequencies. Also note that, across events, F_{lin} is constant at a given site while only F_{nl} changes. Hence, the log(PSA) ratio between models remains the same regardless of the event.
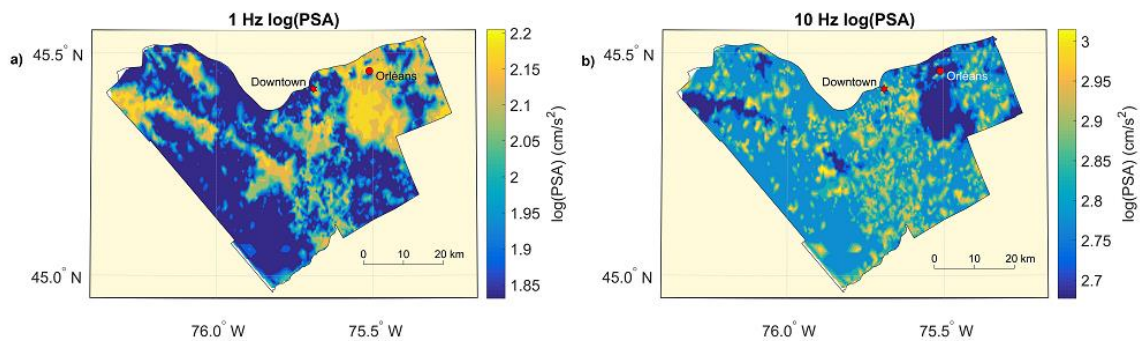
Figure 3-5: Estimated 1 Hz (a) and 10 Hz (b) horizontal log(PSA) for Ottawa from its 2% in 50 year probability ground motions, using the f_{peak}-based amplification model.

3.5 Felt Intensity Comparisons for Downtown Ottawa

Direct comparisons between observed and estimated MMI for the **M**5.0 Val-des-Bois earthquake are made for Ottawa using intensity observations available from the Geological Survey of Canada (Stephen Halchuk, pers. comm., 2016). **Figure 3-6** shows the details of the surficial geology and depth-to-bedrock in central Ottawa for which most intensity reports are available; Pal and Atkinson (2012) examined reports for the same area. Note that sites with greater depth-to-bedrock are associated with softer sediments. These deeper, soft sites are those that amplify intermediate-to-long periods.
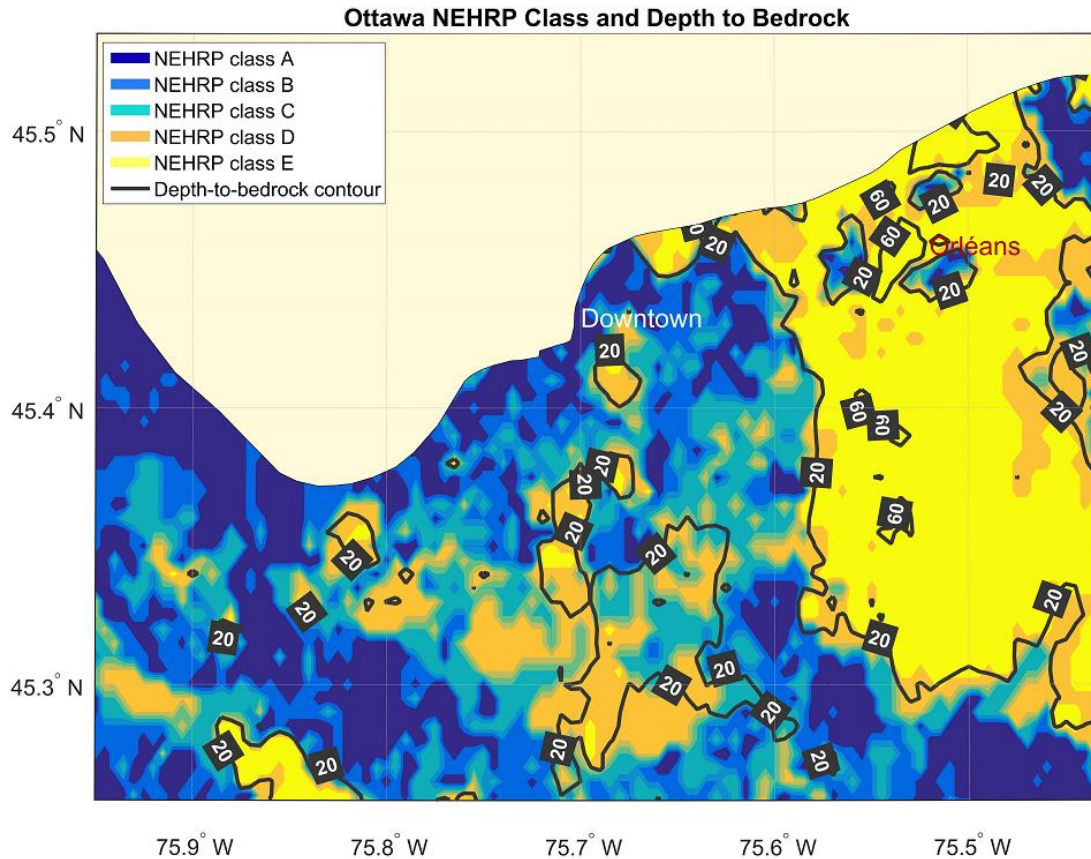
Figure 3-6: Estimated NEHRP site class and depth-to-bedrock from microzonation information (Motazedian et al., 2011) for downtown Ottawa and Orléans. Pal and Atkinson (2012) examined reported felt intensity for the M5.0 Val-des-Bois earthquake for this area.

Similar to the method outlined in Pal and Atkinson (2012), the area shown on **Figure 3-6** is subdivided into a 24 x 18 grid of cells and the MMI for each cell is estimated using the event-specific GMPE for the Val-des-Bois earthquake to compute the expected PGV within each grid cell for the reference site condition. The PGV is amplified using the f_{peak}-based amplification model (assuming that the PGV is associated with a frequency near 1.3 Hz), and then converted to MMI using the empirical relation between PGV and MMI (equation 3.8). This enables a comparison between predicted and observed intensities within a relatively small area. Within this grid, there are 123 cells having a minimum number (*n*) of 3 intensity reports. **Figure 3-7** shows the predicted

MMI for the Val-des-Bois earthquake, along with the differences between observed and predicted MMI. Note that observed MMI is averaged within each cell for which $n \geq 3$.
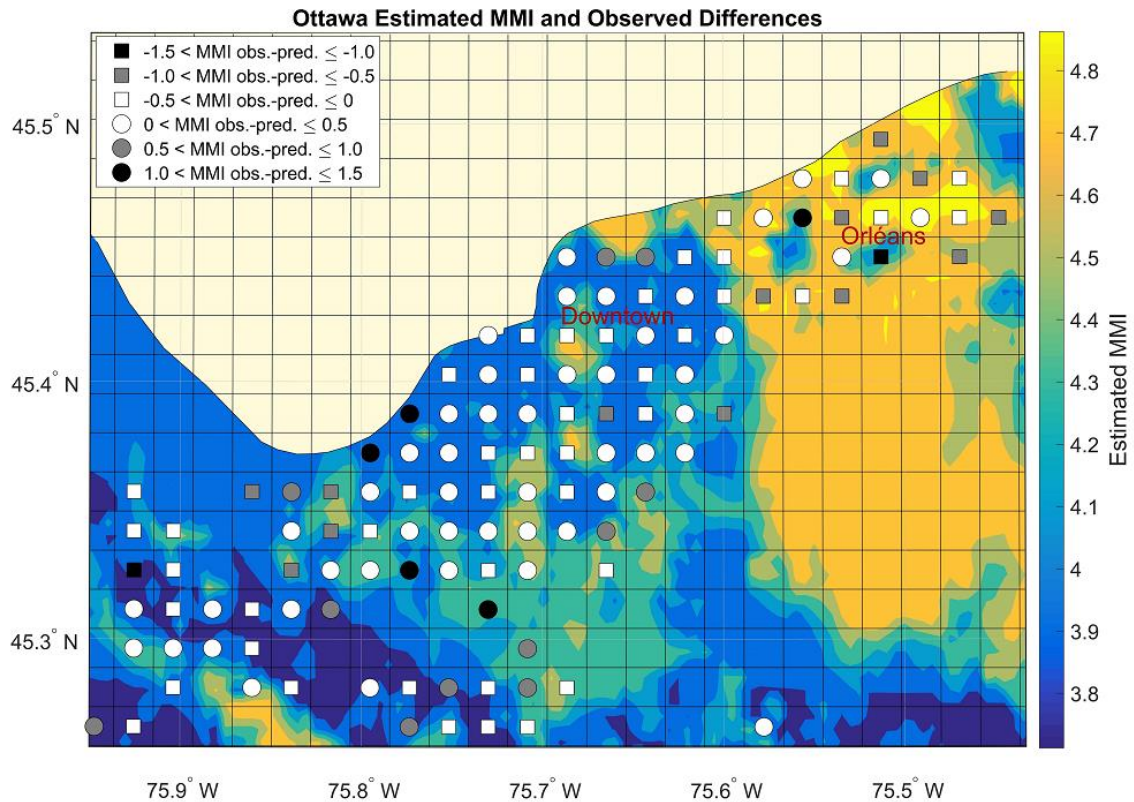
Figure 3-7: Estimated MMI for the M5.0 Val-des-Bois earthquake, along with differences between observed and predicted intensities.

The average absolute value of the differences between the observed MMI and MMI predicted by the f_{peak}-based model is 0.4 ± 0.3 intensity units. It is interesting to note that the NBCC and f_{peak} models predict MMI to within 0.05 ± 0.05 units of each other on average, in spite of larger differences in the frequency content of the predicted motions at many sites (thus, a separate figure is not provided for the NBCC model MMI values); the reasons for this similarity are discussed in more detail later. There are only 7 cells for which the discrepancy between observed and predicted intensity exceeds 1 unit; in most cases the observations and predictions agree to within 0.5 units. Higher intensities are estimated in the Orléans area where softer and deeper sites are more prevalent. This is consistent with the intensity reports for this event, although the

predicted MMIs tend to be higher than the observations by about 0.5 units in this area. Around downtown and to the south, where site conditions are highly variable, the differences between observed and predicted MMI values do not appear to be systematic. Overall, the agreement between observations and predictions is considered to be satisfactory, especially in light of the significant uncertainties in both the observations and predictions. Specifically, the observations are limited and suffer from deficiencies in the method by which the Geological Survey of Canada codes intensities, which is not consistent with standard practice for internet intensity reports (Atkinson et al., 2014). Moreover, the predicted MMI values have significant uncertainties from both the prediction of the motions in the cells and their conversion to intensity. All these factors affect the computed intensity differences in each grid cell.

3.6   Ground Motion and Intensity Maps for Southern Ontario

Ground motion and intensity estimates are extended to all of southern Ontario. In this case, the site information needed to compute amplification factors is obtained from maps of depth-to-bedrock and surficial geology provided by the OGS, interpolated on a grid with a spacing of 500 m. On this grid, the 1 and 10 Hz PSA are computed for the **M**5.0 Val-des-Bois earthquake from the event-specific GMPE, and amplified using both amplification models. Note that to compute amplifications using the NBCC approach, a V_{S30} class is assigned based on surficial geology. We believe that this simple proxy method is appropriate for regional-scale assessments of ground shaking. It is possible to assign a V_{S30} class using other methods, such as the topographic slope proxy, as described by Allen and Wald (2007). Using their method, topographic slope measurements from elevation data are correlated with V_{S30} measurements to develop coefficients for predicting V_{S30} in various regional settings (e.g., active tectonic and stable continental regions). First-order approximations of V_{S30} are provided for southern Ontario, which show that class D sites dominate the Ottawa area and St. Lawrence Valley, and regions southwest of Toronto; particularly the flatter areas around Sarnia, London, and Windsor. By contrast, most other areas in the region are characterized by stiffer class B and C soils. While this method provides a good first-order estimate of amplification (which is part of a larger, continental-scale map), the V_{S30}-surficial geology

proxy using geological data from southern Ontario is deemed much more suitable for site characterization purposes in this region.

Figure 3-8 shows the effects of both attenuation and site condition on the expected ground motions using the f_{peak} model. The amplitudes decay with distance from the source, but there are pockets of higher and lower motion, especially at 1 Hz, due to local site conditions. The predicted motions are in general quite weak, as it was a moderate event occurring outside the region.
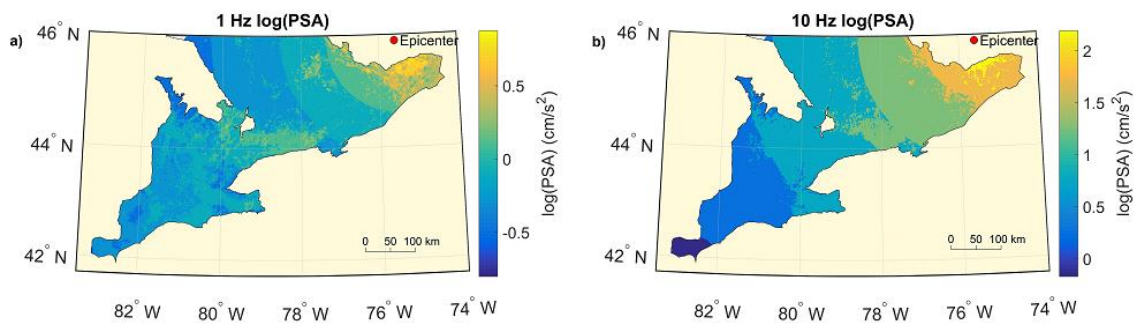
Figure 3-8: Estimated 1 Hz (a) and 10 Hz (b) horizontal log(PSA) for southern Ontario for the M5.0 Val-des-Bois earthquake, using the f_{peak}-based amplification model.

It is interesting to repeat the above exercise considering a stronger scenario earthquake with higher levels of ground shaking. The selected scenario is an event of **M**6.0 with a relatively-high stress drop ($\Delta\sigma = 830$ bars) arbitrarily located in the Southern Great Lakes Seismic Zone near Niagara Falls within a band of moderate seismicity, as shown in **Figure 3-9**. Estimates of horizontal log(PSA) are shown, in addition to the differences between the motions as computed from the two amplification models. Motions are computed only for sites in Ontario, for which compiled digital databases on depth-to-bedrock and surficial geology are available. Moreover, note that NEHRP classes from the 2015 NBCC model are assigned a surficial geology for the purposes of making ground motion estimates on a regional scale.

Across all of southern Ontario, the differences in predicted log(PSA) between the NBCC and f_{peak} approaches – due entirely to the amplification models – are not large on

average (0.01 ± 0.10 for 1 Hz; -0.16 ± 0.10 for 10 Hz PSA). However, the NBCC model predicts higher 1 Hz motions by a factor of 1.4 (0.15 log units) in 10% of grid cells, with 3% of cells having differences that exceed a factor of 2 (0.3 log units); the maximum difference is 0.43 log units (factor of 2.7). At 10 Hz, differences in motions are also as large as a factor of 2.7, but in this case the higher motions are predicted by the f_{peak}-based model. **Figure 3-9** shows an example of a subregion for where these differences can be more pronounced, and where nonlinear effects would show up more strongly. For both 1 and 10 Hz motions, the greatest differences between models occur in areas that contain mostly soft sediments of shallow (< 10 m) depths.
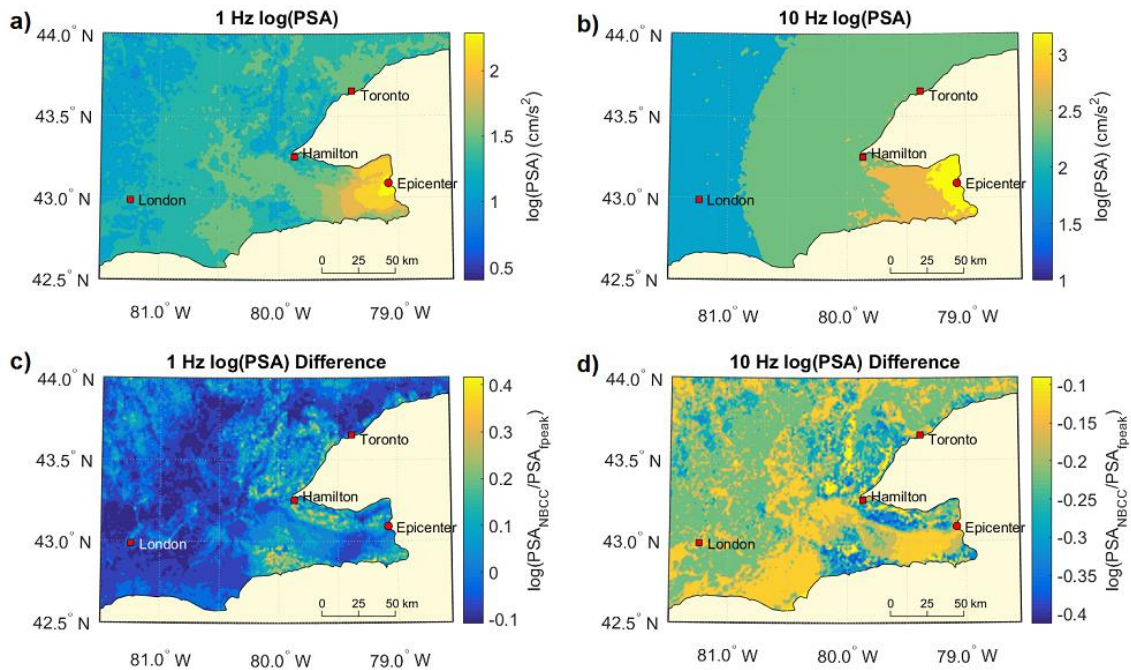
Figure 3-9: Estimated 1 Hz (a) and 10 Hz (b) horizontal log(PSA) for a subregion of southern Ontario for a scenario M6.0 earthquake, using the f_{peak}-based amplification model. The estimated log(PSA) differences computed from the NBCC minus the f_{peak}-based amplification models are shown for 1 Hz (c) and 10 Hz (d) motions.

On **Figure 3-10**, the estimated MMI for the Val-des-Bois earthquake across Ontario is shown; these values agree well with average intensity values from the USGS

(http://earthquake.usgs.gov/earthquakes) for the cities of Windsor (2.3), London (2.9), Barrie (3.4), Toronto (3.3), Kingston (3.1) and Ottawa (4.2). The NBCC and f_{peak} models give a similar range in predicted MMI for this event; the average value of the absolute MMI differences between the models is 0.1 ± 0.1 intensity units, with the NBCC model predicting MMI between 0.2 units less to 0.5 units greater than the f_{peak} model. The reason for these small discrepancies arises from the fact that MMI is estimated from PGV, for which the difference in amplification factors between models is very small for most sites. In general, **Figure 3-10** shows that predicted intensities are highest – around 4 – in the Ottawa area and St. Lawrence Valleys, where soft clays of intermediate to deep depths are predominant. Intensities of 3 to 4 are consistent as epicentral distance increases toward the southwest, likely due to the intermediate to deep soils that are more prevalent in this region of the province, and which add to amplification effects. Contrast this to the region north of Barrie; here, predicted intensities drop below 3 despite closer epicentral distances since the area is dominated by outcropping bedrock.
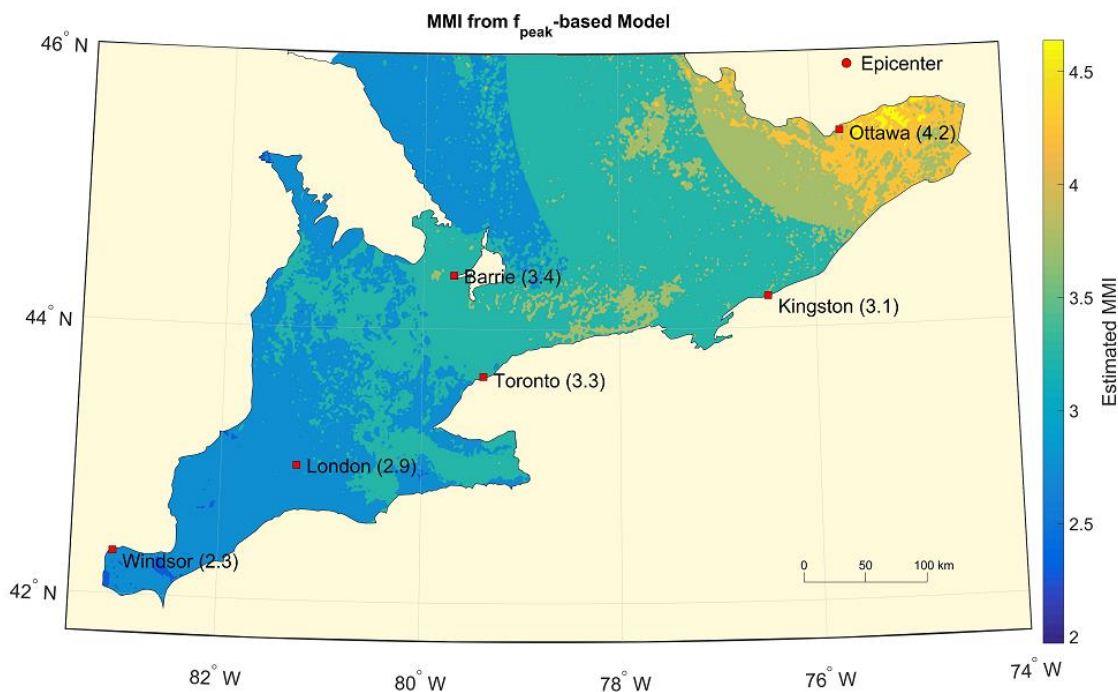
Figure 3-10: Estimated intensity map of southern Ontario for the M5.0 Val-des-Bois earthquake using the f$_{peak}$-based model. Observed intensities for six cities are superimposed for comparison.

The small percentage of sites that result in significant differences in predicted intensities between models are soft and very shallow (< 3 m), of which there are not many. However, these sites are more prevalent in the Niagara Peninsula area along western Lake Ontario. **Figure 3-11** shows the predicted intensities and model differences in this region for the **M**6.0 scenario earthquake. For this type of event, the motions would be felt (MMI 3) to distances of about 500 km, and thus would be felt across all of southern Ontario. This scenario provides a better sense of the intensity behaviour in the event of a large regional earthquake in a populous region. **Figure 3-11** shows that both amplification models generally predict similar intensities, with maximum values of about 7.5 near the epicenter; however, differences in estimated MMI are as large as 1.1 units. These anomalies are seen up to 80 km from the epicenter in areas that contain very shallow sand/clay and soft organic sediments. In most cases where there are predicted intensity differences between models, the NBCC model predicts the higher values since MMI is estimated from PGV, a parameter with lower-frequency characteristics.
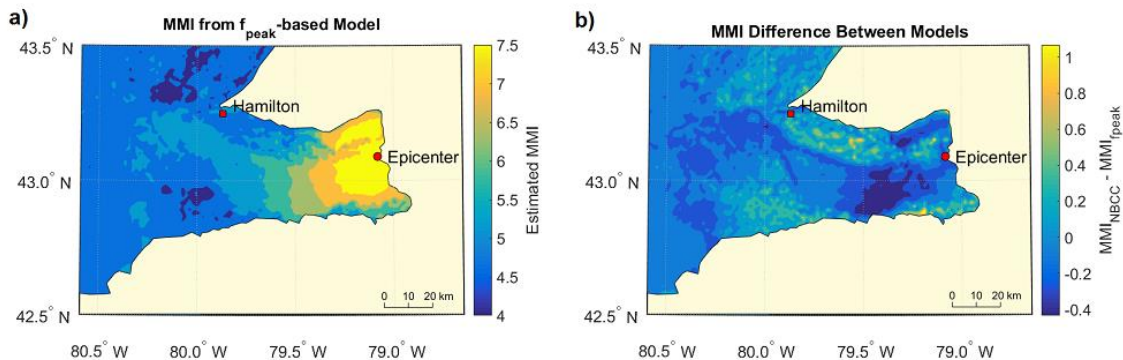
Figure 3-11: Estimated intensity map of the Niagara Peninsula region of southern Ontario for a scenario M6.0 earthquake using the f_{peak}-based model (a). The intensity differences computed from the NBCC and f_{peak}-based models are also shown (b).

3.7 Summary and Conclusions

In this study, two amplification models are used – one from the 2015 NBCC and the other a model from Braganza et al. (2016), derived from depth-to-bedrock (f_{peak}) and surficial geology – to estimate ground-shaking intensities and low (1 Hz) and high (10

Hz) frequency ground motions for regional earthquakes. While the two models generally predict similar intensities, they differ in their projections of the relative strength of ground motion at low and high frequencies. The differences can be as much as a factor of 2.7 at both 1 and 10 Hz. In general, the NBCC model – derived from amplification data for California sites – predicts higher motions at low frequencies, whereas the f_{peak}-based model predicts higher motions at high frequencies. The latter model is believed to be more applicable in Ontario since it was derived from empirical earthquake data in southern Ontario, and reflects the dominant site conditions of the region (sediment of shallow to intermediate depths overlying hard, glaciated bedrock).

Using V_{S30} in southern Ontario as a parameter to predict site amplification is problematic since this information is not reliably available for most sites. Moreover, site peak frequency (f_{peak}) is a more applicable site variable than V_{S30} for sites in Ontario. It is more readily available, and provides information for deeper sites (Hassani and Atkinson, 2016). The f_{peak}-based amplification model from Braganza et al. (2016), which uses depth-to-bedrock and surficial geology as inputs, provides a robust method for estimating regional amplification in southern Ontario. For future building code developments, the use of f_{peak} as a site response variable is recommended, in addition to (or in place of) V_{S30}. For assessing site-specific cases, f_{peak} can be easily approximated in situ via ambient noise methods (e.g., Chouinard and Rosset, 2012).

References

Allen, T.I. and Wald, D.J. (2007). Topographic slope as a proxy for global seismic site conditions (V_{S30}) and amplification around the globe: U.S. Geological Survey Open-File Report, 2007-1357, 69 p.

Assatourians, K. and Atkinson, G.M. (2008). Program: ICORRECT. Engineering Seismology Toolbox. Department of Earth Sciences, The University of Western Ontario. 40.

Atkinson, G.M. and Kaka, S. I. (2007). Relationships between Felt Intensity and

Instrumental Ground Motion in the Central United States and California. *Bulletin of the Seismological Society of America*, **97**, no. 2, 497–510.

Atkinson, G.M. and Assatourians, K. (2010). Attenuation and Source Characteristics of the 23 June 2010 **M** 5.0 Val-des-Bois, Quebec, Earthquake. *Seismological Research Letters*, **81**, no. 5, 849–860.

Atkinson, G.M., Assatourians, K. and Lamontagne, M. (2014). Characteristics of the 17 May 2013 M 4.5 Ladysmith, Quebec, Earthquake. *Seismological Research Letters*, **85**, no. 3, 755-762.

Atkinson, G.M., Hassani, B., Singh, A., Yenier, E. and Assatourians, K. (2015). Estimation of Moment Magnitude and Stress Parameter from ShakeMap Ground-Motion Parameters. *Bulletin of the Seismological Society of America*, **105**, no. 5, 2572–2588.

Boore, D. M., Stewart, J. P., Seyhan, E., and Atkinson, G. A. (2014). NGA-West2 equations for predicting PGA, PGV, and 5% damped PSA for shallow crustal earthquakes. *Earthquake Spectra*, **30**, no. 3, 1057–1085.

Borcherdt, R. D. (1970). Effects of local geology on ground motion near San Francisco Bay. *Bulletin of the Seismological Society of America*, **60**, no. 1, 29–61.

Braganza, S., Atkinson, G.M., Ghofrani, H., Hassani, B., Chouinard, L., Rosset, P., Motazedian, D. and Hunter, J. (2016). Modeling Site Amplification in Eastern Canada on a Regional Scale. *Seismological Research Letters*, **87**, no. 4, 1008-1021.

Chouinard, L. and Rosset, P. (2012). On the Use of Single Station Ambient Noise Techniques for Microzonation Purposes: the Case of Montreal; in Shear Wave Velocity Measurement Guidelines for Canadian Seismic Site Characterization in Soil and Rock, (ed.) J.A. Hunter and H.L. Crow; Geological Survey of Canada, Open File 7078, p. 85–93.

Dangkua, D. T. and Cramer, C. H. (2011). Felt Intensity versus Instrumental Ground Motion: A Difference between California and Eastern North America? *Bulletin of the Seismological Society of America*, **101**, no. 4, 1847–1858.

Dowling, J., Liam Finn, W.D., Ventura, C.E., Bebamzadeh, A. and Fairhurst, M. (2016).

An alternative approach to site factors for NBCC 2015. *Canadian Journal of Civil Engineering*, **43**, 1017–1024.

Hassani, B. and Atkinson, G. M. (2016). Applicability of the NGA-West2 Site Effects Model for Central and Eastern North America. *Bulletin of the Seismological Society of America*, **106**, no. 2, 653–664.

Humar, J. (2015). Background to some of the seismic design provisions of the 2015 National Building Code of Canada. *Canadian Journal of Civil Engineering*, **42**, 940–952.

Kramer, S.L. (1996). Geotechnical Earthquake Engineering. Prentice-Hall, Inc., Upper Saddle River, New Jersey.

Lermo, J. and Chávez-García F.J. (1993). Site effects evaluation using spectral ratios with only one station. *Bulletin of the Seismological Society of America*, **84**, 1350–1364.

Motazedian, D., Hunter, J.A., Pugin, A., Khaheshi Banab, K., Crow, H.L. (2011). Development of a V_{S30} (NEHRP) Map for the City of Ottawa, Ontario, Canada. *Canadian Geotechnical Engineering Journal*, **48**, no. 3, 458–472.

Nakamura, Y. (1989). A method for dynamic characteristics estimation of subsurface using microtremor on the ground surface. Quarterly Report of RTRI, **30**, 25–33.

Nastev, M., Parent, M., Ross, R., Howlett, D. and Benoit, N. (2016). Geospatial modelling of shear-wave velocity and fundamental site period of Quaternary marine and glacial sediments in the Ottawa and St. Lawrence Valleys, Canada. *Soil Dynamics and Earthquake Engineering*, **85**, 103-116.

NBCC. (2015). National Building Code of Canada, 14th Edition, Canadian Commission on Building and Fire Codes, National Research Council of Canada, Ottawa, Ontario, Canada.

Pal, J. and Atkinson G. M. (2012). Scenario Shakemaps for Ottawa, Canada. *Bulletin of the Seismological Society of America*, **102**, no. 2, 650–660.

Seyhan, E. and Stewart, J. P. (2014). Semi-empirical nonlinear site amplification from NGA-West2 data and simulations. *Earthquake Spectra*, **30**, no. 3, 1241–1256.

Wald, D.J., Quitoriano, V., Heaton, T.H., Kanamori, H. (1999). Scrivner, C.W. and

Worden, C.B. 1999. 'Trinet ShakeMaps': Rapid Generation of Peak Ground
Motion and Intensity Maps for Earthquakes in Southern California. *Earthquake
Spectra*, **15**, no. 3, 537-555.

Wood, H.O. and Neumann, F. (1931). Modified Mercalli Intensity Scale of 1931. *Bulletin
of the Seismological Society of America*, **21**, no. 4, 277–283.

Worden, C. B., Gerstenberger, M. C., Rhoades D. A. and Wald, D. J. (2012).
Probabilistic Relationships between Ground-Motion Parameters and Modified
Mercalli Intensity in California. *Bulletin of the Seismological Society of America*,
102, no. 1, 204–221.

Zhao, J. X., Irikura, K., Zhang, J., Fukushima, Y., Somerville, P.G., Asano, A., Ohno, Y.,
Oouchi, T., Takahashi, T. and Ogawa, H. (2006). An empirical site-classification
method for strong-motion stations in Japan using H/V response spectral ratio.
Bulletin of the Seismological Society of America, **96**, no. 3, 914–925.

Chapter 4

4 Assessment of the Spatial Variability of Site Response in Southern Ontario

4.1 Introduction

Southern Ontario is a region of low-to-moderate seismicity that experiences a few felt earthquakes per year. The ground motion distribution from such events is controlled by magnitude, distance, and, to a very significant extent, local and regional site effects. Horizontal-component earthquake ground motions are amplified because incoming shear waves slow down as they travel through softer sediment layers; the net amplification on the vertical component is generally observed to be negligible in comparison to that on the horizontal component. Amplification from vertical propagation of transverse shear waves will occur at the peak frequency (f_{peak}; or site period, T) related to the average shear wave velocity (V_{Sav}) and thickness (D) of the soft sediment layer by (Kramer, 1996):

$$f_{peak} = V_{Sav}/4D. \tag{4.1}$$

Therefore, the ratio of the horizontal-to-vertical component motion (H/V) is a good first-order measure of frequency-dependent site amplification (e.g., Lermo and Chávez-García, 1993; Atkinson and Cassidy, 2000). Earthquake records in southern Ontario show that the H/V ratio varies strongly with frequency, with the peak frequency (f_{peak}) of response being dependent on a site's depth-to-bedrock, and the peak amplitude (A_{peak}) being dependent on surficial geology (Braganza et al., 2016). Seismographs in southeastern Ontario are mostly sited on bedrock, and tend to exhibit fairly flat earthquake H/V spectra (($H/V)_{EQ}$) compared to records from stations to the west and southwest, which are mostly on sediment of varying stiffness and thickness. At soil sites, $(H/V)_{EQ}$ commonly exhibits a distinct spectral peak at the site's predominant frequency, which has an inverse relationship with the depth-to-bedrock (or resonator depth), as predicted by equation (4.1).

Correlating H/V spectral properties with site conditions or using H/V spectra as a proxy for earthquake site amplification has become common practice, both on large and

small scales (e.g., Di Alessandro et al., 2012; Ghofrani and Atkinson, 2014; Chouinard and Rosset, 2012). Braganza et al. (2016) correlated f_{peak} and A_{peak} of $(H/V)_{EQ}$ spectra in southern Ontario with regional information on depth-to-bedrock and surficial geology (bedrock, till, sand/clay and very soft sediment) in order to develop a generalized model of site amplification for the region. The Braganza et al. (2016) model characterizes the overall shape of the H/V spectra for a site in southern Ontario by f_{peak} and A_{peak} when given a site's depth-to-bedrock and surficial geology as input variables. For non-bedrock sites, for which f_{peak} is unknown and must be estimated based on depth-to-bedrock, the uncertainty in its value is considered by widening the peak by $\pm$ 1 standard deviation; see Braganza et al. (2016) for more details. The resulting site amplification functions for southern Ontario are shown in **Figure 4-1**.
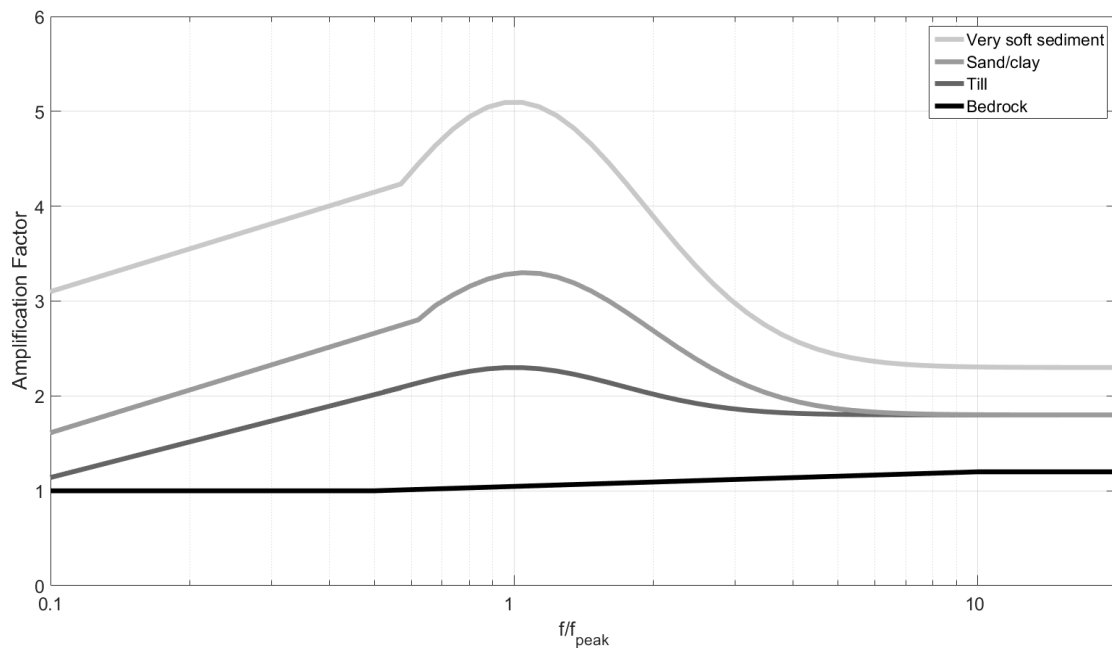
Figure 4-1: Site amplification functions from Braganza et al. (2016) for sites in southern Ontario (f_{peak} to be determined from regionally mapped depth-to-bedrock estimates). The functions for sediment (till, sand/clay and very soft sediment) are normalized to a dimensionless f/f_{peak} value of 1, whereas the function for bedrock is a function of frequency (Hz).

In this study, we examine the degree of spatial variation of the main site variable (f_{peak}) for regional amplification hazard (microzonation) mapping purposes. To determine this variation, we conduct single-instrument ambient noise surveys at varying distances up to 1 km from 10 seismograph stations in southern Ontario. Establishing the spatial variability of f_{peak} is important for regional ShakeMap (Wald et al., 1999; Atkinson et al., 2015) applications, and it capitalizes on available drift thickness (depth-to-bedrock) information (compiled by the Ontario Geological Survey [OGS] and made available online by the Ministry of Northern Development and Mines at www.mndm.gov.on.ca), which is provided on an interpolated grid with a spacing of ~0.5 km. Thus, an estimate of the variation one can expect in f_{peak} up to 1 km away from a site where the variable is known or approximated enables us to assess the confidence in applying an interpolated site amplification grid to the region for the purposes of estimating and mapping ground motions and shaking intensities. We emphasize that the focus of this study is on the spatial variation of f_{peak} in southern Ontario from a statistical viewpoint, and not on the underlying causes for these variations (e.g., subsurface geological effects or heterogeneities).

4.2   Microtremor Technique Background

The idea of using spectral ratios from ambient noise or microtremor ($(H/V)_{MT}$) recordings to measure f_{peak} and amplification was popularized by Nakamura (1989); see Molnar et al. (2016) for a recent review. Ambient noise is generally assumed to be primarily composed of surface waves; in reality, each site will have varying contributions of body, surface, and diffracted (scattered) wavefields. The noise is generated across a wide frequency spectrum, with natural phenomena (wind, tides, fluctuations in atmospheric pressure, etc.) comprising lower (< 1 Hz) frequency content and anthropogenic activity (vehicular traffic, machinery) comprising higher ($\geq$ 1 Hz) frequency content. While there can be differences between $(H/V)_{EQ}$ and $(H/V)_{MT}$, the microtremor technique yields reliable estimates of the peak frequency of a soil layer, particularly in regions where there exists a strong impedance contrast between the bedrock and overlying sediment layer (Lermo and Chávez-García, 1994; Bard, 1999). The field efficiency and demonstrated reliability of the $(H/V)_{MT}$ technique has led to

worldwide applications. The (H/V)$_{MT}$ methodology is expected to be an effective hazard mapping tool in southern Ontario, as much of the region is characterized by unconsolidated Holocene sediments overlying firm glacial sediments (shear wave velocity [V$_S$] ≈ 580 m/s; e.g., Motazedian et al., 2011) or hard bedrock (V$_S$ ≈ 2800 m/s; Boore and Joyner, 1997), setting up ideal conditions for producing a dominant site response peak.

4.3   Survey Analysis and Methodology

The 10 seismograph stations surveyed in this study are located throughout southern Ontario on sediments of varying type and thickness. In selecting sites to survey, our aim was to pick sites with fairly distinct spectral peaks in (H/V)$_{EQ}$, as well as sites of varying sediment conditions. Ease of access was also a consideration. **Figure 4-2** shows a map of surveyed seismograph stations and their approximate site conditions. Information for site conditions (depth-to-bedrock and/or surficial geology) at stations is either inferred, measured in previous studies, or is provided by the OGS (Braganza et al., 2016).
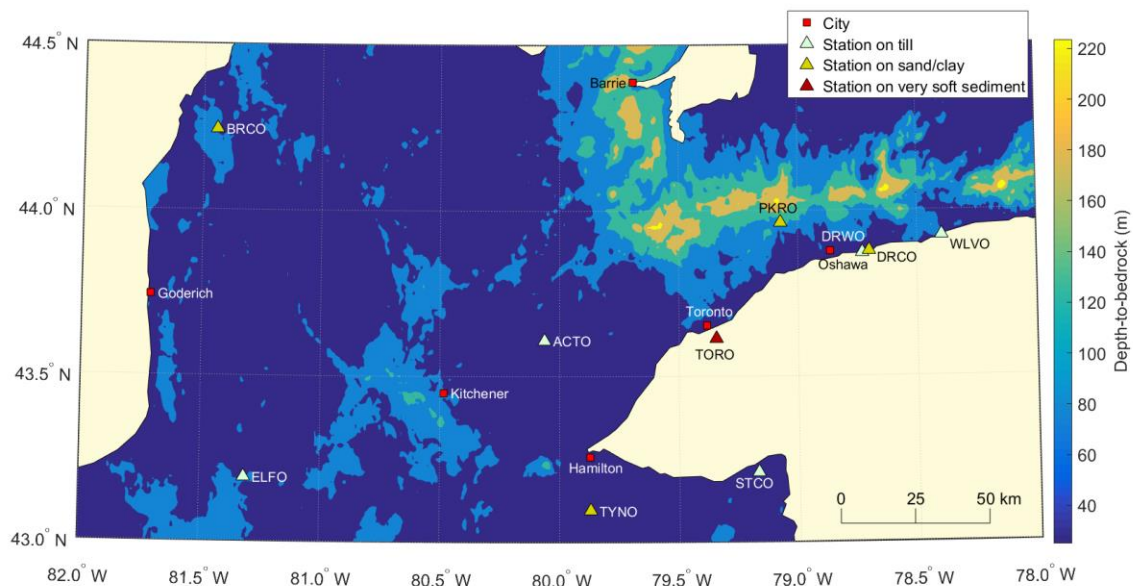
Figure 4-2: The locations and estimated site conditions of the 10 surveyed seismograph stations. Stations are on sediments of varying type and thickness. Note

that station TORO is located on a small, man-made peninsula south of the city of Toronto.

The instrument used to record ambient noise at the 10 stations is the MoHo s.r.l. Tromino® (**Figure 4-3**; http://moho.world/en/tromino/), which is an ultra-portable instrument with 3 accelerometric channels and a low frequency limit of 0.1 Hz. Record processing details are provided in **Appendix D**. Note that the processing of the $(H/V)_{MT}$ time series is based on Fourier spectra (in units of mm/s), whereas $(H/V)_{EQ}$ are from 5%-damped pseudo-spectral acceleration (PSA, in units of cm/s^2). However, the differences between spectral ratios based on Fourier and response spectra are minimal, and have negligible impact on the determination of f_{peak}.

Figure 4-3: The MoHo s.r.l. Tromino® used to perform ambient noise surveys in this study.

To measure variations in f_{peak} as a function of distance, the Tromino® was placed at the following distances from each surveyed seismograph station: 0, 40, 80, 160, 500 and 1000 m. The shorter survey spacing at closer distances should facilitate detection of

any very local subsurface features. We conducted the surveys in as straight a line as possible to capture any effects of a dipping subsurface interface. However, in some cases, this was not logistically possible; obstacles such as lakes, construction sites, fenced areas, private property, etc., acted as barriers and/or forced some survey distances to be omitted. For additional information on how surveys were carried out and on general Tromino® deployment methods, we refer to the guidelines in Molnar et al. (2016). Details on methodology for this study are also provided in **Appendix D**.

To ensure a proper analysis of the $(H/V)_{MT}$ of each survey, it is necessary to inspect the individual spectral components (i.e., the two horizontal and single vertical components). Records are considered to be good if there is a clear divergence between the two horizontal components and the vertical component near the predominant site frequency, resulting in a clear peak in $(H/V)_{MT}$. This results in an "eye-shape" appearance in the individual spectral components where the vertical component is reduced over a narrow frequency bandwidth (Castellaro and Mulargia, 2009). The horizontal-component amplitude in this frequency bandwidth increases due to increasing contributions of Love waves relative to Rayleigh waves (Castellaro, 2016). If a record shows no clear divergence between the vertical and horizontal spectra, resulting in no clear peak in the overall $(H/V)_{MT}$, it is considered to be poor. Factors that can alter the H/V appearance and cause poor results are: poor instrument coupling with the ground; environmental variables such as rain, wind and other noise contributions; and the type of material on which the instrument is placed (e.g., natural versus stiff artificial soil; Castellaro and Mulargia, 2009). An example of a poor and good recording is shown in **Figure 4-4**. Regardless of the cause(s) for a poor record, such spectra are excluded from further analysis.
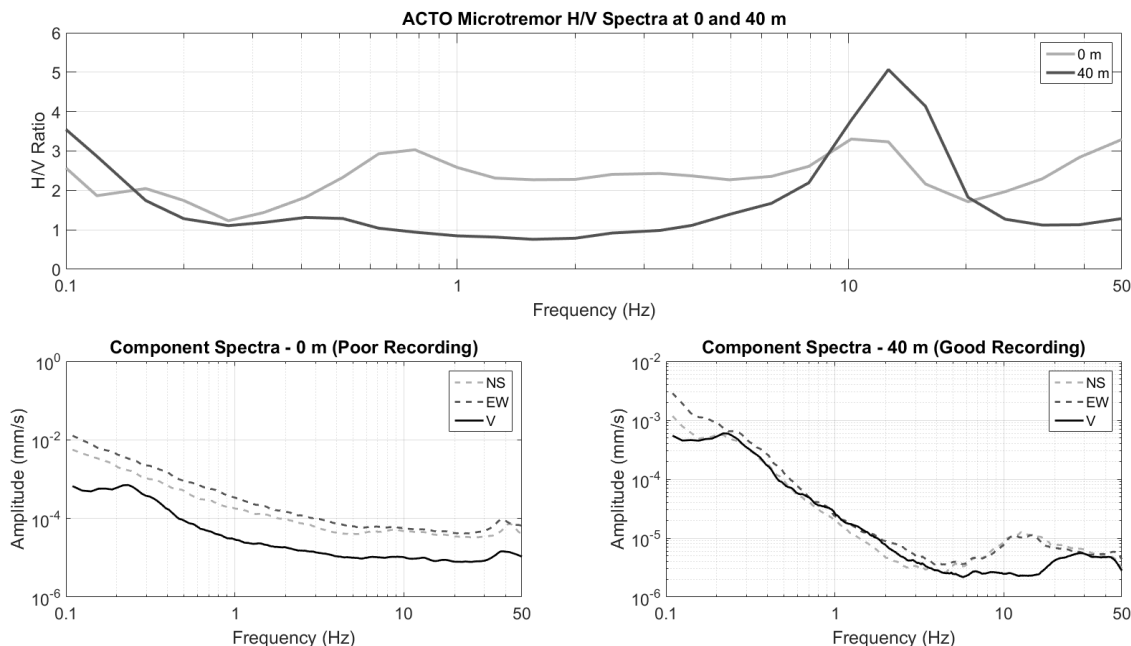
Figure 4-4: Examples of poor and good ambient noise recordings near station ACTO. Individual component spectra for the 0 m survey do not exhibit a distinct "eye-shape" divergence between the vertical and horizontal components, resulting in a (H/V)$_{MT}$ that is without a clear peak. By contrast, the 40 m survey shows a divergence between components at ~8-15 Hz, resulting in a clear spectral peak at ~13 Hz.

4.4 (H/V)$_{MT}$ Spectral Shape Types and Variation in f$_{peak}$ with Distance

In **Figures 4-5** and **4-6**, we present examples of sediment sites (stations TORO and PKRO) that show consistent single peaks in both their (H/V)$_{EQ}$ and (H/V)$_{MT}$ spectra. TORO is believed to be a very soft site, with sediments of ~70 m thickness, while PKRO is underlain by sand/clay of ~76 m thickness (Braganza et al. 2016). For these plots, the H/V ratios that are output from the ambient noise records have been averaged over the same log-spaced frequency bins used for the (H/V)$_{EQ}$ spectra.
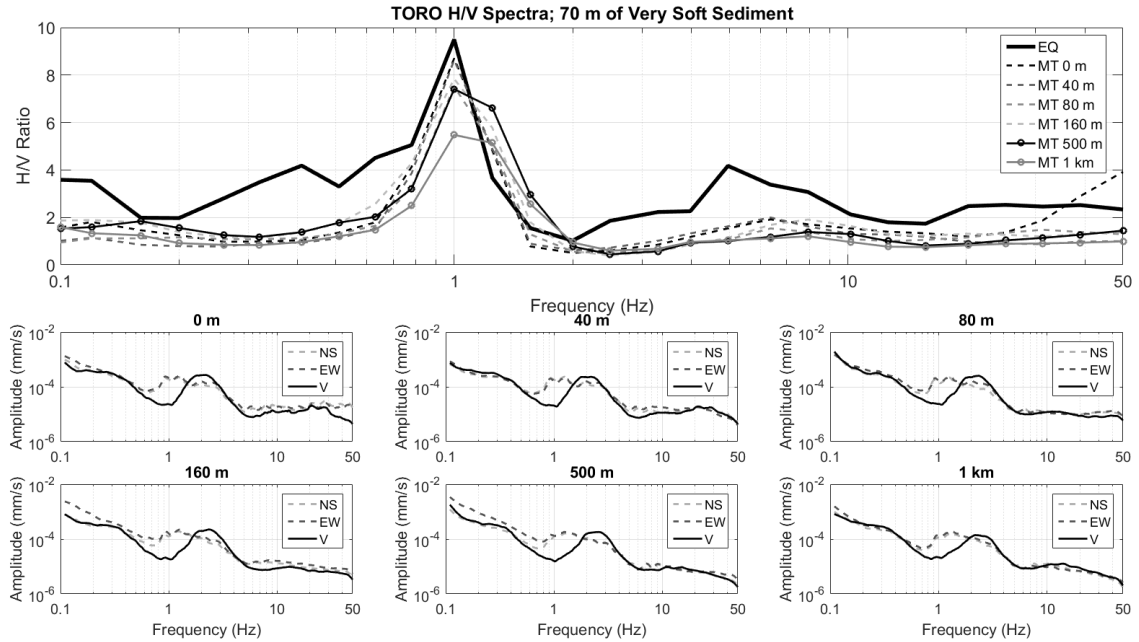
Figure 4-5: Station TORO's (H/V)$_{EQ}$ (heavy line) and the six (H/V)$_{MT}$ surveys, at distances up to 1 km. All surveys show a consistent f$_{peak}$ of 1.0 Hz.
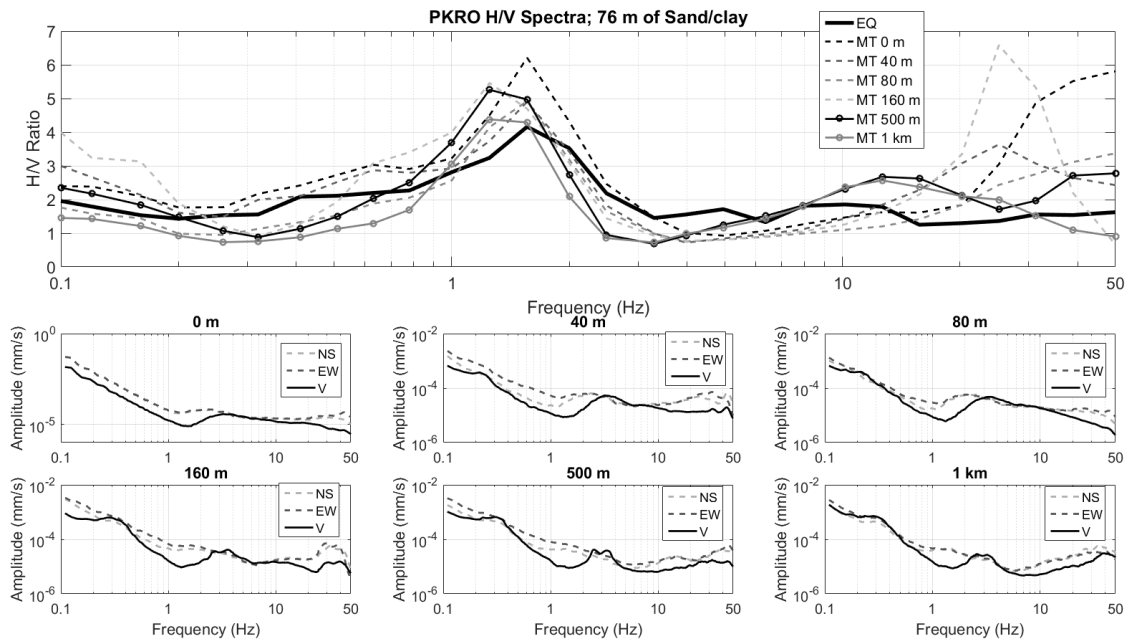
Figure 4-6: Station PKRO's (H/V)$_{EQ}$ (heavy line) and the six (H/V)$_{MT}$ surveys, at distances up to 1 km. An f$_{peak}$ of 1.6 Hz is seen at distances < 80 m, which decreases to 1.3 Hz (0.1 log units) from 160 m to 1 km.

Figure 4-5 shows that the f_{peak} results from $(H/V)_{MT}$ at station TORO are consistent with results based on $(H/V)_{EQ}$: from the station up to 1 km away, the value of f_{peak} is 1.0 Hz. An obvious divergence in the individual component spectra between the horizontal and vertical amplitudes is also seen around this frequency. The high A_{peak} value near the station implies a strong impedance contrast at depth. At the furthest distances (500 and 1000 m), the spectral peaks start to broaden and reduce in amplitude, likely related to changes in subsurface conditions; however, the value of f_{peak} remains the same. In **Figure 4-6**, we observed that the 1.6 Hz f_{peak} from $(H/V)_{MT}$ for PKRO is in agreement with that from $(H/V)_{EQ}$ for distances up to 80 m. At further distances, the $(H/V)_{MT}$ spectra widen and f_{peak} decreases to 1.3 Hz. The resonator depth appears to be relatively stable at PKRO, which results in only a small change in f_{peak} over a 1 km distance. Overall, TORO and PKRO are sites with a similar depth-to-bedrock (estimated at 70 and 76 m, respectively) and thus exhibit similar peak frequencies, near 1.0 Hz. The peak amplitudes at TORO, a site with inferred soft sediment, are generally higher than they are at PKRO, which is a stiffer site. For both sites, the values of f_{peak} are consistent between the earthquake and microtremor surveys, but the A_{peak} values differ by up to a factor of 3 to 4.

Figures 4-7 and **4-8** show the H/V spectra of stations ELFO and DRWO, both of which are on relatively stiff material (till). These spectra exhibit wider peaks in their $(H/V)_{EQ}$, and there is a suggestion of a secondary peak.
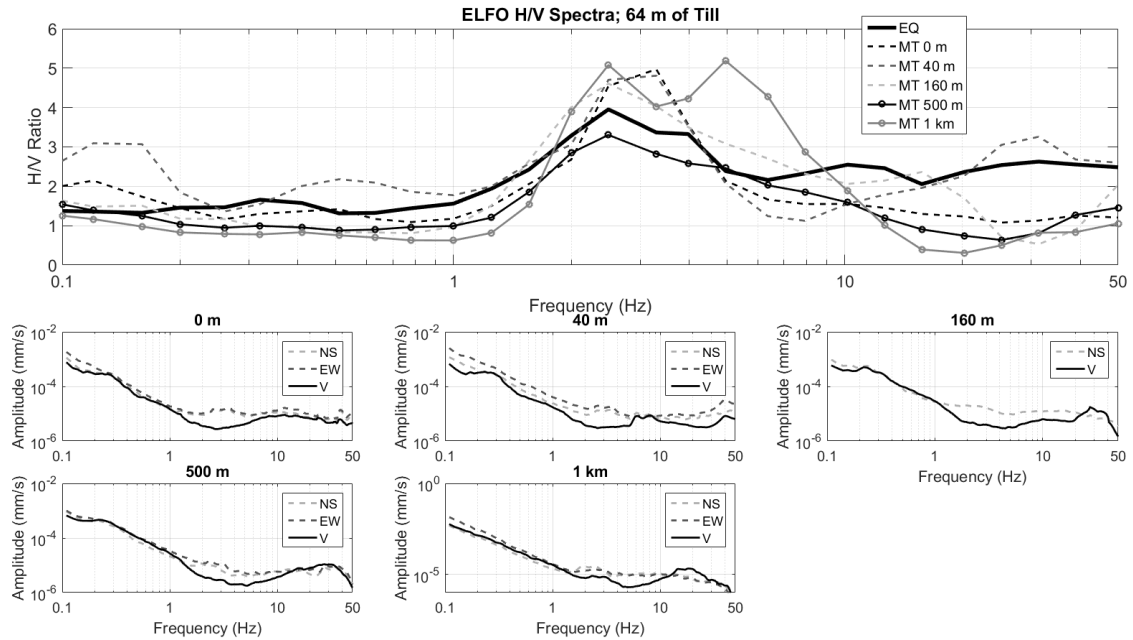
Figure 4-7: Station ELFO's (H/V)$_{EQ}$ exhibits a fairly broad peak with f$_{peak}$ at 2.5 Hz, followed by a secondary smaller peak at 4.0 Hz. This is reflected in the (H/V)$_{MT}$, which show either double peaks or broad spectra at all survey distances.
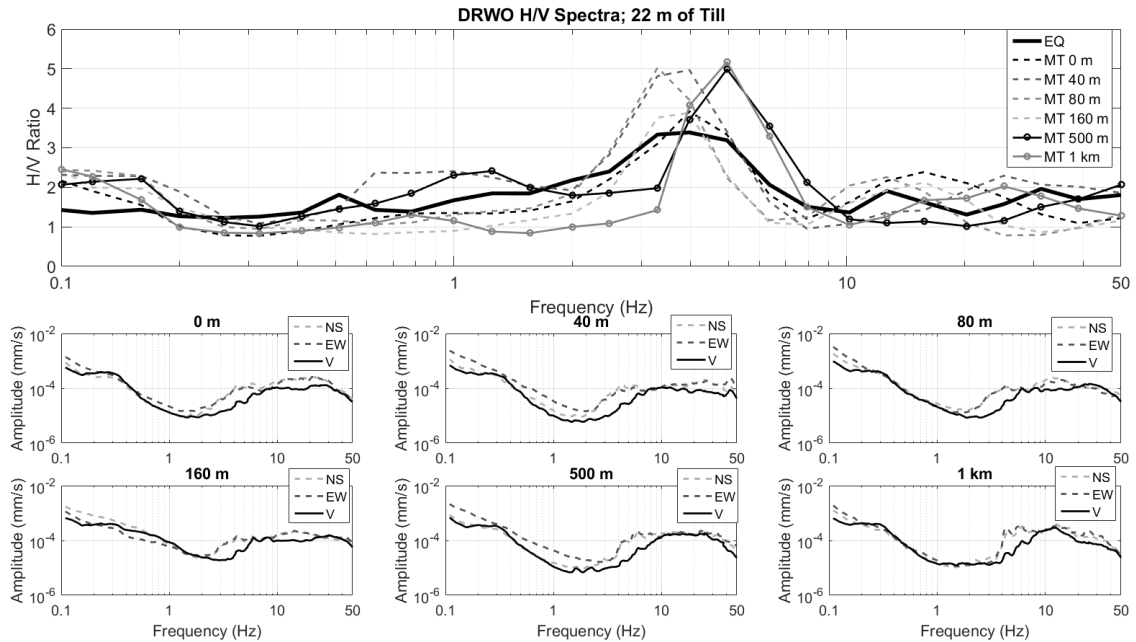
Figure 4-8: DRWO's (H/V)$_{EQ}$ has an f$_{peak}$ at 4.0 Hz, but the spectrum is similar in H/V ratio between 3.3 Hz to 5.0 Hz. The (H/V)$_{MT}$ show f$_{peak}$ variations in this entire range, with a higher f$_{peak}$ of 5.0 Hz for the 500 and 1000 m surveys.

The (H/V)$_{EQ}$ at ELFO is 2.5 Hz, and (H/V)$_{MT}$ surveys show log(f$_{peak}$) to be within 0.1 units of this value, except for the 1 km survey, which shows a secondary – and slightly greater – peak at 5.0 Hz. DRWO's (H/V)$_{EQ}$ f$_{peak}$ is at 4.0 Hz, but the H/V ratio is similar from 3.3 Hz to 5.0 Hz. The (H/V)$_{MT}$ log(f$_{peak}$) values at all distances are consistently within ± 0.1 log units of the f$_{peak}$ from (H/V)$_{EQ}$. It is also noted that higher values of f$_{peak}$ are associated with shallower sites; DRWO has an estimated depth-to-bedrock of 22 m, while is it 64 m at ELFO. Lastly, in **Figures 4-9** and **4-10** we present examples of ambient noise records that show evidence of poor coupling and/or have some wind/noise contamination, but from which f$_{peak}$ can still be discerned.
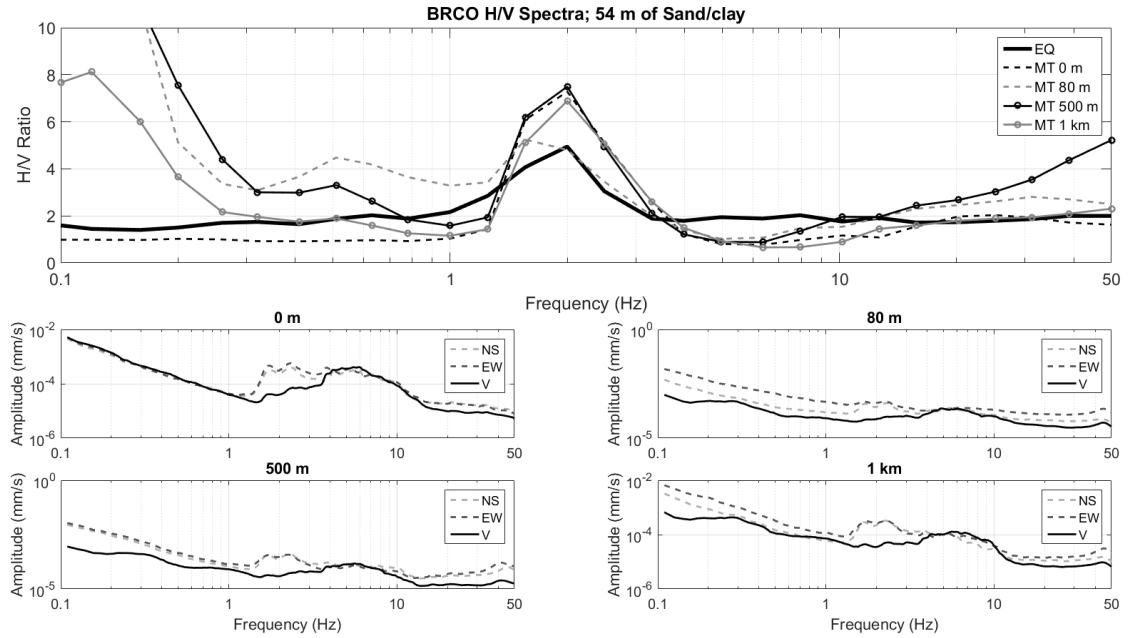
Figure 4-9: (H/V)$_{MT}$ at station BRCO show noise contamination below ~1 Hz, but the spectra still show a general agreement in f$_{peak}$ (2.0 Hz) with that from the (H/V)$_{EQ}$.
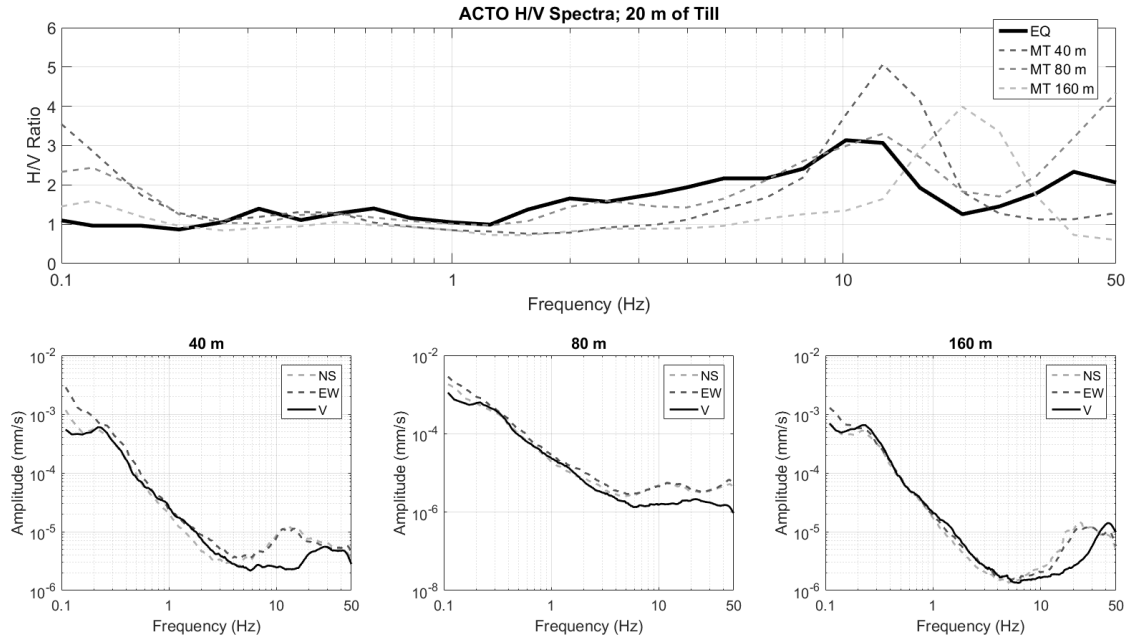
Figure 4-10: H/V ratios at station ACTO. The 40 and 80 m surveys exhibit a log(f_peak) that is within 0.1 units of the f_peak from (H/V)_EQ (10.2 Hz), while the 160 m survey shows greater variation (0.3 log units higher).

For station BRCO (**Figure 4-9**), (H/V)$_{MT}$ show rising amplitudes below ~1 Hz, which are likely the result of windy conditions on the day that the measurements were taken. The exception is the 0 m record, which was taken from a survey performed previously when weather conditions were favorable. At this site, f$_{peak}$ for all useable surveys is either in complete agreement (2.0 Hz) with the (H/V)$_{EQ}$, or is within 0.1 log units. In **Figure 4-10**, surveys for ACTO at 40 and 80 m show log(f$_{peak}$) from (H/V)$_{MT}$ and (H/V)$_{EQ}$ that agree to within 0.1 log units, while the 160 m survey has an f$_{peak}$ that is higher by 0.3 log units (20.2 Hz, compared to 10.2 Hz).

As mentioned previously, the purpose of measuring f$_{peak}$ as a function of distance is to determine the confidence with which we can interpolate f$_{peak}$ between grid points that have a known or estimated value based on depth-to-bedrock, which has been mapped on a ~0.5 km spaced grid. In **Table 4-1**, we summarize the findings of f$_{peak}$ versus distance and tabulate the average of the differences between log(f$_{peak}$) from (H/V)$_{EQ}$ and log(f$_{peak}$) from (H/V)$_{MT}$, across all surveyed distances. Note that, for a given survey

distance, the average difference is computed as the average of all absolute value log(f_{peak}EQ/f_{peak}MT). An "N/A" is shown for surveys that are associated with poor records. (For H/V spectral ratio plots of stations DRCO, STCO, TYNO and WLVO, please see **Appendix D**).

Table 4-1: The f_{peak} values from all (H/V)$_{EQ}$ and (H/V)$_{MT}$ at the 10 stations. The average difference between log(f_{peak}EQ/f_{peak}MT) is computed as the average of all absolute value log(f_{peak}EQ/f_{peak}MT).

Station	f_{peak} from (H/V)$_{EQ}$ (Hz)	f_{peak} from (H/V)$_{MT}$ at Survey Distance (Hz)					
		0 m	**40 m**	**80 m**	**160 m**	**500 m**	**1 km**
ACTO	10.2	N/A	12.7	12.7	20.2	N/A	N/A
BRCO	2.0	2.0	N/A	1.6	N/A	2.0	2.0
DRCO	10.2	10.2	N/A	N/A	N/A	N/A	12.7
DRWO	4.0	4.0	4.0	3.3	4.0	5.0	5.0
ELFO	2.5	3.3	3.3	N/A	2.5	2.5	5.0
PKRO	1.6	1.6	1.6	1.6	1.3	1.3	1.3
STCO	5.0	4.0	5.0	4.0	4.0	4.0	4.0
TORO	1.0	1.0	1.0	1.0	1.0	1.0	1.0
TYNO	4.0	N/A	N/A	N/A	N/A	N/A	5.0
WLVO	15.7	N/A	N/A	N/A	N/A	6.4	6.4

Average Difference (log units)	0.03	0.04	0.06	0.08	0.10	0.13

Table 4-1 shows that, at zero separation distance, f_{peak} from $(H/V)_{MT}$ generally agrees with that of $(H/V)_{EQ}$, with the average difference being 0.03 log units. This difference increases to 0.13 log units for separation distances of 1 km. The results of all 1 km surveys, in addition to the averaged earthquake H/V at each station, are summarized in **Figure 4-11**.
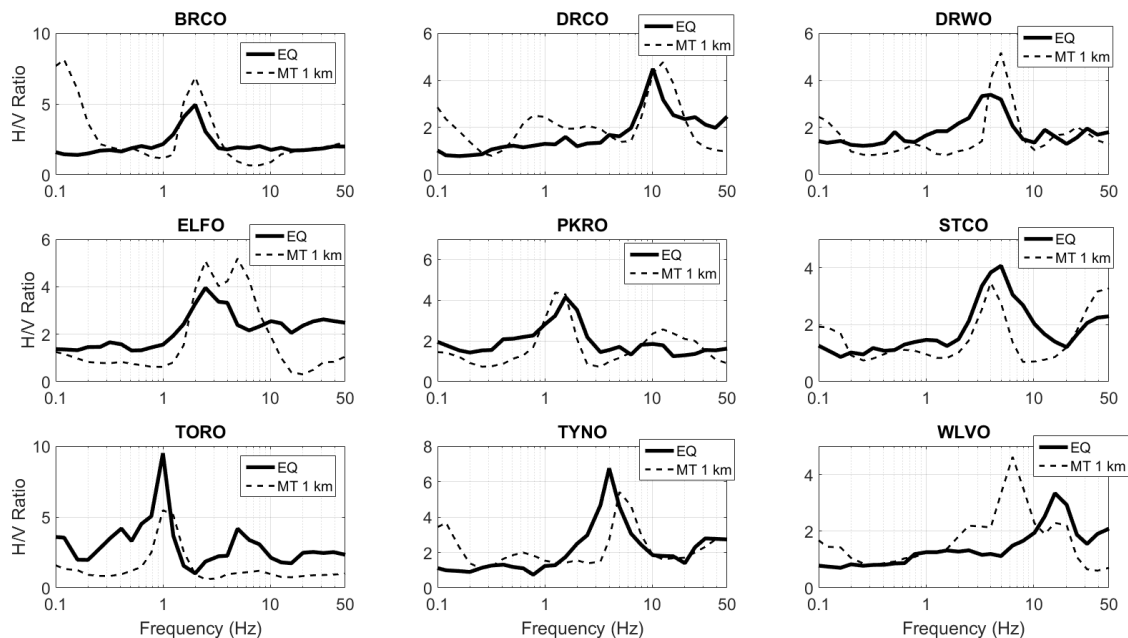
Figure 4-11: The averaged earthquake H/V ratios at 9 seismograph stations, in addition to the ambient noise H/V ratios at 1 km distance from each station. f_{peak} is shown to be in agreement to within 0.13 log units, on average.

There are a few obvious caveats with the results in **Table 4-1**; specifically, the sample size is small as there are only 10 surveyed stations, with some records that are poor or show no f_{peak}. Moreover, the nature of southern Ontario's geology as well as logistical constraints have the surveys covering a relatively small area (the greater Toronto area and

southwestern Ontario), and only one straight-line survey is performed per station. Furthermore, because $\log(f_{peak})$ is a multiplicative measure of deviation in f_{peak}, it implies a multiplicative change in soil depth. We might therefore expect this deviation to be greater for shallower sites, since a subsurface dipping interface would impact a factor in depth more steeply at such a site than it would for a deeper site. In other words, the factor of change in f_{peak} should ultimately be controlled by the local geology. Regardless of the reasons (e.g., local geology) for the change in f_{peak}, our aim is to use the results of the ambient noise records to gain a basic understanding of how the fundamental parameter controlling site amplification in this region, f_{peak}, can be expected to vary as a function of distance.

4.5   Summary and Conclusions

In this study, we perform ambient noise surveys at 10 seismograph stations in southern Ontario to detect how the site parameter f_{peak} varies as a function of distance. The f_{peak} from earthquake H/V spectra is compared with that from ambient noise at survey distances of 0, 40, 80, 160, 500 and 1000 m from each station. Results show that, on average, $\log(f_{peak})$ is constant to within approximately 0.13 base 10 log units, over distances up to 1 km. While this study surveys only 10 stations and is further limited by some poor ambient noise recordings that are not useable, it yields a preliminary idea of how one can expect f_{peak} to vary as a function of distance in southern Ontario. This has practical applications when it comes to approximating or interpolating this fundamental site parameter for regional hazard mapping purposes. The method of mapping f_{peak} with distance can also be applied in regions where the amplification spectra are likely to exhibit spectral peaks near the site's peak frequency (i.e., in regions that are characterized by a strong seismic impedance contrast between their soil and bedrock layers, such as Japan, Taiwan and China [Ghofrani and Atkinson, 2014]).

In southern Ontario, there will be additional uncertainty in f_{peak} when it is approximated via an estimated site variable (i.e., depth-to-bedrock). Underlying geological structures, heterogeneities and dipping bedrock in some sub-regions could cause f_{peak} to vary more drastically than is typically observed in this study. For these reasons, the amplification functions in Braganza et al. (2016), displayed in **Figure 4-1**,

were adjusted (widened by $\pm$ 1 std. dev. in estimating f_{peak} from depth-to-bedrock in southern Ontario, or 0.2 log units) to account for some of this uncertainty.

References

Atkinson, G.M., and Cassidy, J.F. (2000). Integrated use of seismograph and strong-motion data to determine soil amplification: Response of the Fraser River delta to the Duvall and Georgia Strait earthquakes. *Bulletin of the Seismological Society of America*, **90**, 1028–1040.

Atkinson, G.M., Hassani, B., Singh, A., Yenier, E., and Assatourians, K. (2015). Estimation of Moment Magnitude and Stress Parameter from ShakeMap Ground-Motion Parameters. *Bulletin of the Seismological Society of America*, **105**, no. 5, 2572-2588.

Bard, P.-Y. (1999). Microtremor measurements: A tool for site effect estimation? State-of-the-art paper, Second International Symposium on the Effects of Surface Geology on seismic motion, K. Irikura, K. Kudo, H. Okada, and T. Satasini (Editors), Yokohama, 1–3 December 1998, **3**, 1251–1279.

Boore, D.M., and Joyner, W.B. (1997). Site Amplifications for Generic Rock Sites. *Bulletin of the Seismological Society of America*, **87**, no. 2, 327–341.

Braganza, S., Atkinson, G.M., Ghofrani, H., Hassani, B., Chouinard, L., Rosset, P., Motazedian, D., and Hunter, J. (2016). Modeling Site Amplification in Eastern Canada on a Regional Scale. *Seismological Research Letters,* **81**, no. 4, 1008-1021.

Castellaro, S. (2016). The complementarity of H/V and dispersion curves. *Geophysics*, 81, no. 6, T323-T338.

Castellaro, S. and Mulargia, F. (2009). The effect of velocity inversions on H/V. *Pure Applied Geophys*ics, **166**, 567–92.

Chouinard, L., and Rosset, P. (2012). On the use of single station ambient noise techniques for microzonation purposes: The case of Montreal, in Shear Wave Velocity Measurement Guidelines for Canadian Seismic Site Characterization in Soil and Rock, J. A. Hunter and H. L. Crow (Editors), Geological Survey of Canada, Open File 7078, 85–93.

Di Alessandro, C., Bonilla, L.F., Boore, D.M., Rovelli, A., and Scotti, O. (2012). Predominant-Period Site Classification for Response Spectra Prediction Equations in Italy. *Bulletin of the Seismological Society of America*, **102,** no. 2, 680-695.

Ghofrani, H., and Atkinson, G.M. (2014). Site condition evaluation using horizontal-to-vertical response spectral ratios of earthquakes in the NGA-West 2 and Japanese databases. *Bulletin of Soil Dynamics and Earthquake Engineering*, **67**, 30-43.

Kramer, S. L. (1996). Geotechnical Earthquake Engineering, Prentice-Hall, Inc., Upper Saddle River, New Jersey, 653.

Lermo, J. and Chávez-García, F.J. (1993). Site effects evaluation using spectral ratios with only one station. *Bulletin of the Seismological Society of America*, **83**, 1574-1594.

Lermo, J. and Chávez-García, F.J. (1994). Are microtremors useful in site response evaluation? *Bulletin of the Seismological Society of America*, **84**, 1350-1364.

Molnar, S., Cassidy, J.F., Castellaro, S., Cornou, C., Crow, H., Hunter, J.A., Matsushima, S., Sànchez-Sesma, F.J., and Yong, A. (2016). Application of MHVSR For Site Characterization: State-of-the-Art, 16th World Conference on Earthquake Engineering, Paper no. 4946.

Motazedian, D., Hunter, J.A, Pugin, A., and Crow, H.L. (2011). Development of a V_{S30} (NEHRP) map for the City of Ottawa, Ontario, Canada. *Canadian Geotechnical Engineering Journal,* **48**, no. 3, 458–472.

Nakamura, Y. (1989). A method for dynamic characteristics estimation of subsurface using microtremor on the ground surface. Q. Rep. Railway Tech. Res. Inst. 30, 25-33.

Wald, D.J., Quitoriano, V., Heaton, T.H., Kanamori, H. (1999). Scrivner, C.W. and Worden, C.B. (1999). 'Trinet ShakeMaps': Rapid Generation of Peak Ground Motion and Intensity Maps for Earthquakes in Southern California. *Earthquake Spectra*, **15**, no. 3, 537-555.

Chapter 5

5   Discussion, Conclusions and Future Work

5.1   Discussion

The key parameter in the site amplification model is the site's peak frequency of response, or f_{peak}, which has an inverse relationship with the site's depth-to-bedrock. We test how well the model estimates f_{peak} using information from a microzonation study in the Greater Toronto Area (GTA). Mihaylov (2011) developed a 3-component data acquisition system and used the H/V spectral ratio method (Nogoshi and Igarashi, 1971; Nakamura, 1989, 2000) to measure ambient noise and record H/V spectral ratios at 187 sites across the GTA. From these measurements, f_{peak} was determined at each of these sites and an interpolated map of this site response parameter was produced for the region. **Figure 5-1** shows this map, in addition to the locations of nearby seismograph stations (ACTO, TORO and PKRO) and their values of f_{peak} (from averaged earthquake H/V data).
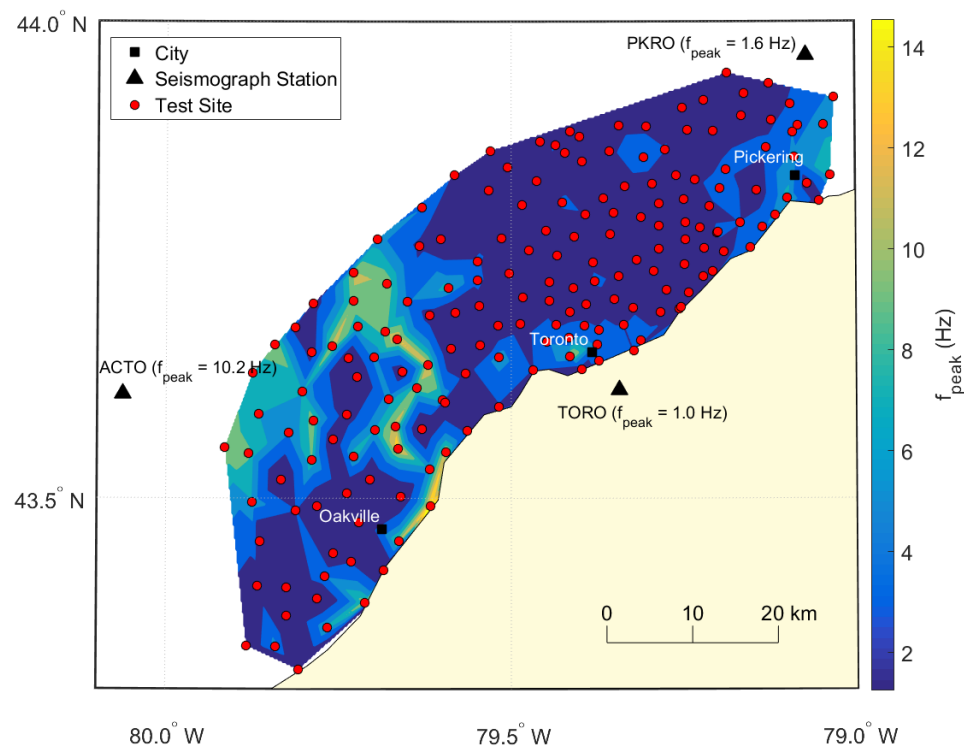
Figure 5-1: Map of the study area (Greater Toronto Area) from Mihaylov (2011), in addition to interpolated values of f$_{peak}$, determined from ambient noise surveys at 187 test sites. Nearby seismograph stations (ACTO, TORO and PKRO) and their station f$_{peak}$ values are superimposed.

The f$_{peak}$ values at each of these sites can be estimated using equations (2.1) and (2.4) from chapter 2 in conjunction with drift thickness data from the Ontario Geological Survey (OGS) map, and compared with the measured f$_{peak}$ from Mihaylov (2011). At some test sites, Mihaylov (2011) noted that a more prominent H/V spectral peak was apparent at higher frequencies, which was recorded as the dominant frequency, compared to lower frequency peaks, which were noted as the fundmental frequency. For the comparison done in this study, if both a fundamental and dominant frequency was detected in the H/V spectrum, the latter is taken to be the site's f$_{peak}$. The results of the measured vs. estimated f$_{peak}$ comparison are shown in **Figure 5-2**.
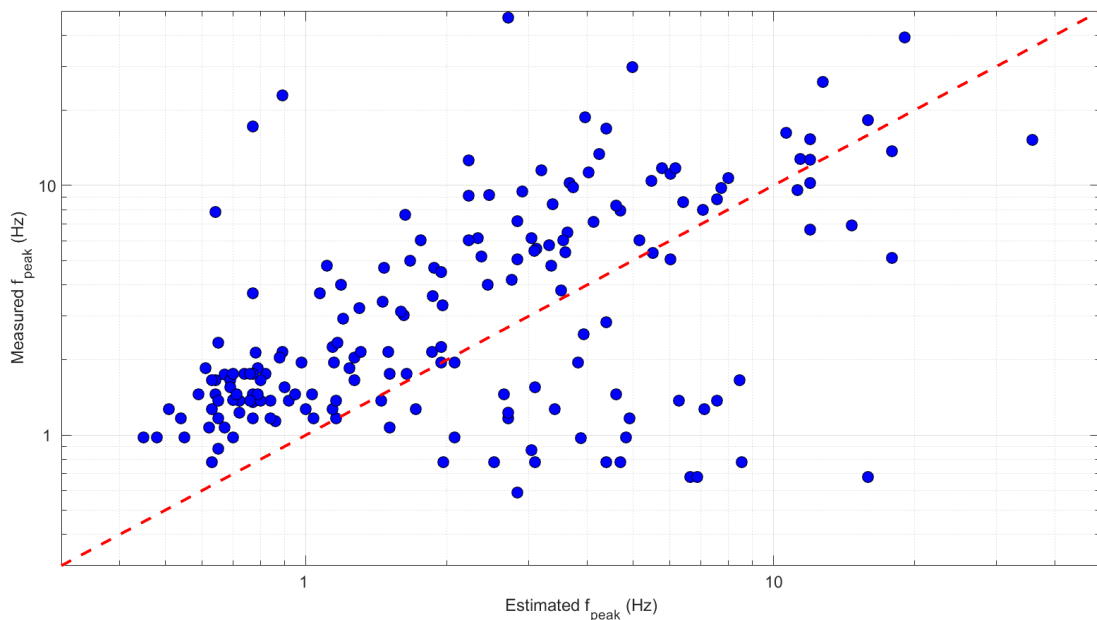
Figure 5-2: Measured f$_{peak}$, as determined from a microzonation study in the Greater Toronto Area (Mihaylov, 2011) versus estimated f$_{peak}$, as determined using equations (2.1) and (2.4) in conjunction with drift thickness information from the Ontario Geological Survey.

Figure 5-2 shows that there is a systematic bias in measured vs. estimated f_{peak}, where values for the former are consistently higher. There are several possibilities for this bias, including: the instrumentation used to measure f_{peak}, inaccurate drift thickness values from the OGS map, or a velocity-depth profile from equation (2.4) that is better suited to softer, low-velocity sediments, particularly at greater depths (Braganza et al., 2016; Motazedian et al., 2011; Rosset et al., 2015). **Figure 5-2** also shows that there are test sites for which measured f_{peak} is considerably lower (by > 1 log units) compared to the estimated f_{peak}. In these cases, it is possible that: (i) the test sites do not have the very shallow depth-to-bedrock that is indicated by the OGS map; (ii) the measured f_{peak} is very low due to a localized subsurface effect, or (iii) that measured f_{peak} is in error (too low).

In general, the results of this test show that the measured and estimated f_{peak} are within 0.35 log units (or a factor of 2.2), on average. The apparent bias warrants further investigation in future work.

5.2 Summary and Conclusions

Site amplification, the amplification of seismic waves and ground motions due to subsurface effects, is an important phenomenon that strongly influences felt effects and damage potential of earthquakes. The aim of this thesis was to develop and test a region-specific site amplification model for the purposes of estimating and mapping seismic hazard in southern Ontario.

In chapter 2, we develop a regional site amplification model that is based on two geological variables that are readily available: depth-to-bedrock, from which peak frequency of response (f_{peak}) is estimated, and surficial geology, which provides an estimate of the peak amplitude of response (A_{peak}). Chapter 3 tests this model against another amplification model from the 2015 National Building Code of Canada (NBCC), which is based on the traditionally-used site parameter, shear-wave velocity in the top 30 metres of soil (V_{S30}). The two models predict low and high frequency ground motions differently, and based on southern Ontario's geology, we suggest that the model based on f_{peak} is more applicable. In chapter 4, we test the spatial variability of this important site

response parameter (f_{peak}) for mapping purposes, and find that it is spatially stable to within approximately 0.13 base 10 log units, over distances up to 1 km.

5.3 Future Work

This is the first comprehensive site amplification model that is specific to southern Ontario and which uses the f_{peak} parameter as a site response variable. Thus, further field studies and calibration will be needed in order to further test and refine the model. As mentioned in chapter 2, simplifications are made with respect to the region's geology; there will be smaller areas with more complex subsurface features that create amplification effects which are not adequately captured by the f_{peak}-based model in this thesis. In chapter 4, a basic idea of the spatial variability of f_{peak} in the region is gained, but as mentioned, more surveys are needed. The apparent bias in f_{peak} inferred from depth-to-bedrock relative to that measured by microtremor surveys in the GTA warrants further investigation. Overall, the initial results obtained in this thesis support f_{peak} as an appropriate site response parameter – especially compared to V_{S30} – in southern Ontario. This model can be used in regional ShakeMap applications. Moreover, the model can be used as a guide to site-specific amplification factors for building-code applications, by measuring the value of f_{peak} for the site.

References

Braganza, S., Atkinson, G.M., Ghofrani, H., Hassani, B., Chouinard, L., Rosset, P., Motazedian, D., and Hunter, J. (2016). Modeling Site Amplification in Eastern Canada on a Regional Scale. *Seismological Research Letters,* **81**, no. 4, 1008-1021.

Mihaylov, D. (2011). Seismic Microzonation of Great Toronto Area and Influence of Building Resonances on Measured Soil Responses. The University of Western Ontario. PhD Thesis. 249.

Motazedian, D., Hunter, J.A., Pugin, A., and Crow, H.L. (2011). Development of a V_{S30} (NEHRP) Map for the City of Ottawa, Ontario, Canada. *Canadian Geotechnical Engineering Journal*, **48**, 3, 458–472.

Nakamura, Y. (1989). A method for dynamic characteristics estimation of subsurface using microtremor on the ground surface. *Quarterly Report of RTRI*, **30**, 25–33.

Nakamura, Y. (2000). Clear identification of fundamental idea of Nakamura's technique and its applications. *Proceedings of the 12th World Conference on Earthquake Engineering,* Auckland/New Zealand, 2000.

Nogoshi, M. and Igarashi, T. (1971). On the Amplitude Characteristics of Microtremor (Part 2) (in Japanese with English abstract). *Journal of the Seismological Society of Japan*, 24, 26–40.

Rosset, P., Bour-Belveaux, M. and Chouinard, L. (2015). Microzonation models for Montreal with respect to V$_{S30}$. *Bulletin of Earthquake Engineering*, **13**, 8, 2225–2239.

Appendices

Appendix A: The log horizontal-to-vertical (H/V) ratios of the 38 seismograph stations in eastern Canada.

Station	No. of Records Used		Frequency (Hz)														
	f < 1 Hz	f ≥ 1 Hz	0.1	0.2	0.3	0.5	0.8	1	1.6	2	2.5	3.3	5.0	7.9	10.2	15.7	20.2
ACTO	4	19	0.04	-0.06	0.15	0.11	0.06	0.02	0.14	0.22	0.20	0.25	0.34	0.38	0.50	0.29	0.10
ALFO	12	31	-0.01	-0.04	0.01	0.06	0.06	0.04	0.04	0.10	0.15	0.12	0.14	0.07	0.09	0.15	0.22
ALGO	7	25	0.20	0.18	0.26	0.33	0.29	0.38	0.42	0.45	0.52	0.70	0.62	0.28	0.31	0.34	0.36
BANO	5	30	-0.14	-0.21	-0.01	0.11	0.00	0.04	0.12	0.12	0.07	0.06	0.08	0.28	0.31	0.22	-0.04
BASO	2	10	-0.02	-0.03	-0.08	-0.03	-0.06	-0.09	0.09	0.10	0.07	0.09	0.07	-0.03	0.00	0.16	0.08
BMRO	2	9	-0.08	-0.12	-0.08	0.05	0.04	-0.02	-0.15	0.06	0.10	0.13	-0.02	0.06	0.04	0.30	0.11
BRCO	4	18	0.20	0.18	0.24	0.27	0.28	0.34	0.61	0.69	0.48	0.28	0.29	0.31	0.25	0.24	0.24
BUKO	5	20	-0.11	-0.12	-0.05	-0.09	0.06	0.04	0.02	-0.01	0.01	0.06	0.06	0.18	0.22	0.25	0.23
BWLO	2	9	-0.09	-0.16	-0.05	-0.14	-0.01	-0.06	0.06	0.14	0.19	0.17	0.17	0.14	0.17	0.16	0.19
CLPO	0	2	N/A	N/A	N/A	N/A	N/A	0.08	0.08	-0.01	0.03	0.05	-0.11	-0.03	0.02	-0.05	-0.03
CLWO	3	12	0.20	0.15	0.07	0.20	0.40	0.36	0.26	0.31	0.45	0.43	0.27	0.32	0.31	0.58	0.59
DELO	3	28	-0.12	-0.14	-0.08	0.12	0.14	0.03	0.03	0.04	0.02	0.05	-0.01	-0.03	-0.04	0.03	0.09
DRCO	2	7	0.01	-0.08	0.03	0.09	0.09	0.12	0.21	0.08	0.12	0.13	0.21	0.48	0.65	0.40	0.37
DRWO	3	13	0.15	0.10	0.10	0.26	0.14	0.22	0.27	0.34	0.38	0.52	0.50	0.18	0.13	0.21	0.12
ELFO	2	5	0.14	0.16	0.22	0.12	0.16	0.19	0.39	0.52	0.60	0.53	0.38	0.37	0.41	0.31	0.37

ELGO	2	6	-0.02	-0.07	0.09	0.07	0.23	-0.01	0.06	0.19	0.36	0.26	0.11	-0.07	0.05	0.16	0.21
HGVO	2	5	-0.10	-0.12	-0.06	-0.13	-0.26	-0.12	0.04	0.15	0.12	0.06	0.05	0.09	0.14	0.27	0.33
KGNO	7	33	-0.01	-0.09	-0.01	0.12	0.01	0.09	0.13	0.14	0.11	0.09	0.12	0.10	0.14	0.10	0.11
KLBO	3	17	0.02	0.00	0.02	0.13	0.11	-0.02	-0.02	0.04	0.06	0.03	-0.06	0.07	0.07	0.03	-0.06
LINO	3	6	-0.08	-0.18	-0.05	-0.10	-0.05	-0.01	0.04	0.08	0.09	0.02	0.07	0.12	0.22	0.37	0.56
MNT	7	16	-0.04	-0.07	0.03	0.06	0.07	0.12	0.12	0.08	0.04	0.09	0.08	0.05	0.05	0.07	0.08
MNTQ	6	20	0.04	-0.09	-0.04	0.01	0.07	0.01	0.10	0.08	0.10	0.02	0.00	-0.01	-0.03	-0.08	-0.07
MPPO	2	11	-0.03	-0.06	-0.05	-0.09	-0.28	-0.06	-0.04	0.03	0.03	-0.09	-0.08	0.00	0.01	0.11	0.08
ORHO	7	16	0.33	0.31	0.35	0.45	0.75	0.37	0.19	0.17	0.06	0.14	0.09	-0.02	0.04	0.10	0.25
ORIO	9	21	0.07	0.02	0.02	0.10	0.12	0.05	0.09	0.07	0.10	0.10	0.06	0.08	0.13	0.26	0.27
OTT	15	33	0.11	0.00	0.07	0.10	0.08	0.13	0.09	0.09	0.06	0.12	0.23	0.28	0.36	0.12	0.41
PECO	3	20	-0.05	-0.09	0.06	0.07	0.05	0.07	0.10	0.05	0.06	0.02	0.07	0.14	0.15	0.20	0.11
PEMO	11	28	-0.08	-0.07	0.04	0.06	0.04	0.08	0.11	0.15	0.12	0.13	0.13	0.13	0.18	0.31	0.47
PKRO	6	25	0.29	0.16	0.19	0.33	0.36	0.45	0.62	0.55	0.34	0.16	0.23	0.26	0.27	0.10	0.11
PLIO	3	6	-0.01	-0.09	0.10	0.08	-0.11	-0.02	0.03	0.13	0.21	0.20	0.1	0.12	0.06	0.13	0.11
PLVO	8	25	-0.08	-0.06	-0.08	-0.01	-0.04	0.03	-0.03	-0.03	0.00	0.01	0.03	0.09	0.06	0.16	0.16
PTCO	0	4	N/A	N/A	N/A	N/A	N/A	-0.02	0.05	0.08	0.05	0.15	0.14	0.10	0.05	0.21	0.21
SADO	9	33	-0.12	-0.16	-0.13	-0.01	-0.04	0.00	0.03	-0.01	-0.01	0.02	0.07	0.08	0.09	0.07	0.01
STCO	4	16	0.10	0.01	0.07	0.05	0.14	0.17	0.10	0.17	0.33	0.53	0.61	0.43	0.31	0.15	0.08
TOBO	3	13	0.04	0.05	0.10	0.17	0.16	0.06	-0.01	-0.06	0.07	0.15	0.23	0.18	0.21	0.48	0.48
TORO	1	4	0.56	0.30	0.54	0.52	0.70	0.98	0.19	0.01	0.27	0.35	0.62	0.49	0.33	0.24	0.39
TYNO	4	16	0.05	-0.05	0.10	0.07	-0.13	0.09	0.24	0.40	0.47	0.67	0.66	0.39	0.27	0.25	0.14
WLVO	7	26	-0.11	-0.08	-0.09	-0.07	0.08	0.10	0.12	0.11	0.12	0.07	0.05	0.22	0.29	0.52	0.47

**Appendix B: The standard deviations of the log horizontal-to-vertical (H/V) ratios
of the 38 seismograph stations in eastern Canada.**

Station	No. of Records Used		Frequency (Hz)														
	f < 1 Hz	f ≥ 1 Hz	0.1	0.2	0.3	0.5	0.8	1	1.6	2	2.5	3.3	5.0	7.9	10.2	15.7	20.2
ACTO	4	19	0.088	0.082	0.085	0.162	0.148	0.147	0.152	0.134	0.098	0.067	0.074	0.079	0.082	0.069	0.097
ALFO	12	31	0.167	0.179	0.151	0.124	0.127	0.133	0.125	0.108	0.106	0.125	0.184	0.151	0.115	0.102	0.122
ALGO	7	25	0.165	0.203	0.157	0.066	0.107	0.127	0.139	0.130	0.135	0.133	0.126	0.095	0.085	0.101	0.112
BANO	5	30	0.125	0.153	0.193	0.189	0.116	0.128	0.177	0.140	0.149	0.129	0.124	0.088	0.081	0.075	0.114
BASO	2	10	0.027	0.107	0.014	0.112	0.037	0.110	0.099	0.094	0.099	0.076	0.112	0.068	0.044	0.091	0.067
BMRO	2	9	0.017	0.096	0.010	0.058	0.141	0.140	0.142	0.124	0.103	0.077	0.070	0.067	0.049	0.098	0.053
BRCO	4	18	0.174	0.175	0.168	0.234	0.104	0.093	0.096	0.081	0.071	0.062	0.085	0.061	0.086	0.081	0.060
BUKO	5	20	0.134	0.129	0.176	0.142	0.129	0.147	0.149	0.110	0.115	0.106	0.070	0.062	0.087	0.087	0.124
BWLO	2	9	0.019	0.066	0.027	0.018	0.208	0.098	0.120	0.131	0.075	0.133	0.242	0.458	0.279	0.077	0.193
CLPO	0	2	N/A	N/A	N/A	N/A	N/A	0.107	0.057	0.128	0.043	0.076	0.028	0.026	0.145	0.098	0.026
CLWO	3	12	0.088	0.110	0.023	0.124	0.110	0.149	0.103	0.128	0.064	0.058	0.060	0.088	0.081	0.130	0.136
DELO	3	28	0.106	0.057	0.191	0.104	0.092	0.124	0.127	0.124	0.121	0.113	0.124	0.098	0.112	0.080	0.098
DRCO	2	7	0.101	0.039	0.207	0.297	0.270	0.057	0.074	0.097	0.076	0.085	0.103	0.080	0.096	0.152	0.147
DRWO	3	13	0.229	0.223	0.172	0.243	0.212	0.111	0.095	0.145	0.117	0.066	0.089	0.106	0.083	0.044	0.084
ELFO	2	5	0.267	0.259	0.302	0.204	0.352	0.115	0.138	0.070	0.087	0.063	0.076	0.080	0.093	0.054	0.107
ELGO	2	6	0.324	0.134	0.255	0.113	0.014	0.111	0.063	0.064	0.080	0.049	0.042	0.149	0.118	0.043	0.032

HGVO	2	5	0.139	0.083	0.072	0.106	0.110	0.164	0.129	0.085	0.094	0.102	0.072	0.071	0.055	0.087	0.158
KGNO	7	33	0.106	0.169	0.130	0.252	0.222	0.132	0.118	0.119	0.091	0.093	0.127	0.092	0.101	0.078	0.094
KLBO	3	17	0.170	0.233	0.163	0.196	0.190	0.160	0.144	0.141	0.131	0.071	0.128	0.087	0.066	0.146	0.183
LINO	3	6	0.092	0.127	0.238	0.260	0.138	0.182	0.213	0.227	0.232	0.163	0.081	0.047	0.117	0.150	0.277
MNT	7	16	0.214	0.232	0.255	0.210	0.192	0.147	0.188	0.184	0.147	0.137	0.140	0.141	0.107	0.088	N/A
MNTQ	6	20	0.121	0.064	0.131	0.214	0.211	0.143	0.158	0.133	0.142	0.106	0.106	0.130	0.098	0.151	0.142
MPPO	2	11	0.001	0.128	0.122	0.144	0.157	0.136	0.176	0.081	0.100	0.172	0.125	0.091	0.103	0.078	0.073
ORHO	7	16	0.165	0.159	0.164	0.161	0.200	0.094	0.137	0.101	0.155	0.132	0.117	0.150	0.171	0.230	0.203
ORIO	9	21	0.167	0.159	0.090	0.149	0.189	0.152	0.166	0.127	0.178	0.129	0.108	0.091	0.099	0.101	0.121
OTT	15	33	0.183	0.128	0.152	0.131	0.131	0.120	0.134	0.147	0.160	0.106	0.136	0.121	0.134	0.110	0.173
PECO	3	20	0.152	0.112	0.170	0.110	0.149	0.129	0.160	0.153	0.113	0.121	0.146	0.092	0.065	0.071	0.056
PEMO	11	28	0.109	0.108	0.159	0.199	0.200	0.151	0.140	0.148	0.137	0.123	0.137	0.134	0.110	0.120	0.156
PKRO	6	25	0.191	0.225	0.193	0.088	0.089	0.110	0.093	0.104	0.119	0.073	0.069	0.062	0.095	0.105	0.098
PLIO	3	6	0.206	0.198	0.104	0.137	0.037	0.082	0.125	0.159	0.097	0.124	0.079	0.099	0.105	0.122	0.136
PLVO	8	25	0.138	0.116	0.150	0.140	0.148	0.112	0.104	0.141	0.125	0.111	0.102	0.114	0.091	0.098	0.113
PTCO	0	4	N/A	N/A	N/A	N/A	N/A	0.106	0.098	0.051	0.133	0.058	0.113	0.067	0.040	0.038	0.074
SADO	9	33	0.143	0.181	0.152	0.151	0.165	0.162	0.176	0.159	0.142	0.132	0.145	0.121	0.137	0.115	0.141
STCO	4	16	0.193	0.129	0.097	0.077	0.078	0.136	0.122	0.134	0.079	0.089	0.082	0.054	0.104	0.161	0.172
TOBO	3	13	0.087	0.018	0.120	0.090	0.160	0.184	0.122	0.102	0.099	0.078	0.067	0.069	0.087	0.137	0.097
TORO	1	4	N/A	N/A	N/A	N/A	N/A	0.053	0.107	0.052	0.085	0.087	0.139	0.139	0.058	0.071	0.048
TYNO	4	16	0.089	0.113	0.133	0.180	0.103	0.138	0.114	0.060	0.082	0.083	0.113	0.115	0.076	0.157	0.213
WLVO	7	26	0.147	0.125	0.140	0.154	0.209	0.186	0.089	0.119	0.110	0.086	0.090	0.078	0.095	0.103	0.111

Appendix C: The 38 stations' site and horizontal-to-vertical (H/V) spectral characteristics

Station	Spectra Type	f_{peak} (Hz)	Log Peak Amplitude	Surficial Geology	Depth-to-bedrock (m)	Depth-to-bedrock Reference
ACTO	Peaked	> 10	0.50	Till	20	Kolos (2010)
ALFO	Peaked	> 10	0.38	Till	1	Spectrum appearance
ALGO	Peaked	4.0	0.73	Sand/clay	70	Kolos (2010)
BANO	Peaked	> 10	0.38	Till	7	Cross-section map (OGS)
BASO	Flat	N/A	N/A	Bedrock	0	Spectrum appearance
BMRO	Rising	N/A	N/A	Bedrock	0	Spectrum appearance
BRCO	Peaked	2	0.69	Sand/clay	54	Kolos (2010)
BUKO	Rising	N/A	N/A	Bedrock	0	Kolos (2010)
BWLO	Peaked	6.4	0.31	Till	1	Spectrum appearance
CLPO	Flat	N/A	N/A	Bedrock	0	Kolos (2010)
CLWO	Peaked	> 10	0.59	Till	21	Cross-section map (OGS)

DELO	Flat	N/A	N/A	Bedrock	0	Spectrum appearance
DRCO	Peaked	> 10	0.65	Sand/clay	5	Cross-section map (OGS)
DRWO	Peaked	4.0	0.53	Till	22	Cross-section map (OGS)
ELFO	Peaked	2.5	0.60	Till	64	Kolos (2010)
ELGO	Peaked	2.5	0.36	Till	28	Kolos (2010)
HGVO	Peaked	> 10	0.38	Till	1	Spectrum appearance
KGNO	Flat	N/A	N/A	Bedrock	0	Spectrum appearance
KLBO	Flat	N/A	N/A	Bedrock	0	Kolos (2010)
LINO	Peaked	> 10	0.73	Sand/clay	5	Kolos (2010)
MNT	Flat	N/A	N/A	Bedrock	0	Spectrum appearance
MNTQ	Flat	N/A	N/A	Bedrock	0	Spectrum appearance
MPPO	Flat	N/A	N/A	Bedrock	0	Kolos (2010)
ORHO	Peaked	0.8	0.75	Sand/clay	52	Cross-section map (OGS)

ORIO	Peaked	> 10	0.41	Till	7	Cross-section map (OGS)
OTT	Peaked	> 10	0.41	Till	13	Kolos (2010)
PECO	Rising	N/A	N/A	Bedrock	0	Spectrum appearance
PEMO	Peaked	> 10	0.56	Till	24	Kolos (2010)
PKRO	Peaked	1.6	0.62	Sand/clay	76	Cross-section map (OGS)
PLIO	Flat	N/A	N/A	Bedrock	0	Spectrum appearance
PLVO	Rising	N/A	N/A	Bedrock	0	Kolos (2010)
PTCO	Rising	N/A	N/A	Bedrock	0	Kolos (2010)
SADO	Flat	N/A	N/A	Bedrock	0	Spectrum appearance
STCO	Peaked	5.0	0.61	Till	20	Kolos (2010)
TOBO	Peaked	> 10	0.55	Till	1	Spectrum appearance
TORO	Peaked	1.0	0.98	Very soft sediment/fill	70	Kolos (2010)
TYNO	Peaked	4.0	0.83	Sand/clay	31	Kolos (2010)
WLVO	Peaked	> 10	0.52	Till	15	Kolos (2010)

Appendix D: Tromino deployment and processing methods, and horizontal-to-vertical (H/V) spectra plots for stations DRCO, STCO, TYNO and WLVO.

This appendix outlines the steps involved in deploying the Tromino® and processing the recorded data. Additional H/V plots for stations DRCO, STCO, TYNO and WLVO are also provided.

**Tromino® Settings, Deployment, Processing and Interpretation of f_{peak} from Data**

For all surveys, the high gain velocity channels of the Tromino® are collected at a sampling rate of 128 Hz; hence the Nyquist frequency is 64 Hz. Note however that H/V plots are only shown up to 50 Hz, and high amplitudes at very high frequencies are assumed to be caused by noise. Recorded data are uploaded and processed with the Grilla version 6.1 software package. Records are segmented in two-minute time windows and noisy windows are filtered. During processing, a 5% cosine tapering is applied, followed by a Fourier transform, to output ambient noise H/V spectral ratios as Fourier spectra (mm/s). Conversely, the $(H/V)_{EQ}$ are generated by computing the geometric mean of both horizontal log(PSA) spectra and dividing this by the vertical log(PSA) spectrum. Additional details of the computation of $(H/V)_{EQ}$ are described in Braganza et al. (2016).

Recording time lengths for each ambient noise survey are between 20 and 40 minutes, with the time interval increasing for deeper (e.g., ELFO, PKRO) and/or noisier sites, as recommended by Molnar et al. (2016). Surveys are performed at 0, 40, 80, 160, 500 and 1000 m from a seismograph station (with the 0 m survey being performed ~2-3 m from the seismometer vault). The exceptions are WLVO at 160 m and DRCO between 40 and 500 m, where private property and other site regulations only allowed for select measurements. There are a few instances where a record is quite poor in quality, so it is swapped with an earlier survey that was done at the same survey distance, using the same instrumentation, at an earlier time for a different study. Specifically, this is done for PKRO and BRCO at 0 m, and ELFO at 40 m. Whenever possible, the Tromino® was deployed on the same surface ground conditions that the seismograph station rested on. When this could not be achieved (i.e., private property, very soft farmland, or deep ravines on either side of a public road), the Tromino® was instead deployed on the

unpaved shoulder of the road. These instances occurred for surveys: DRWO at 80, 160 and 500 m, and PKRO at 1000 m.

$(H/V)_{MT}$ which contained large peak amplitudes at extreme ends of the frequency spectrum are considered to be related to high noise conditions. Such records were generally consistent with environmental surroundings; e.g., BRCO (see **Figure 4-8**) exhibits high amplitude H/V ratios at lower frequencies and surveys were performed on a fairly windy day; station STCO is near a fairly busy highway and thus higher $(H/V)_{MT}$ is seen at higher frequencies. Therefore, when determining f_{peak} from $(H/V)_{MT}$, anomalous A_{peak} values at very low or high frequencies (e.g., BRCO; PKRO 160 m survey) are not considered to be indicative of subsurface features.

**H/V Plots for Stations DRCO, STCO, TYNO and WLVO**
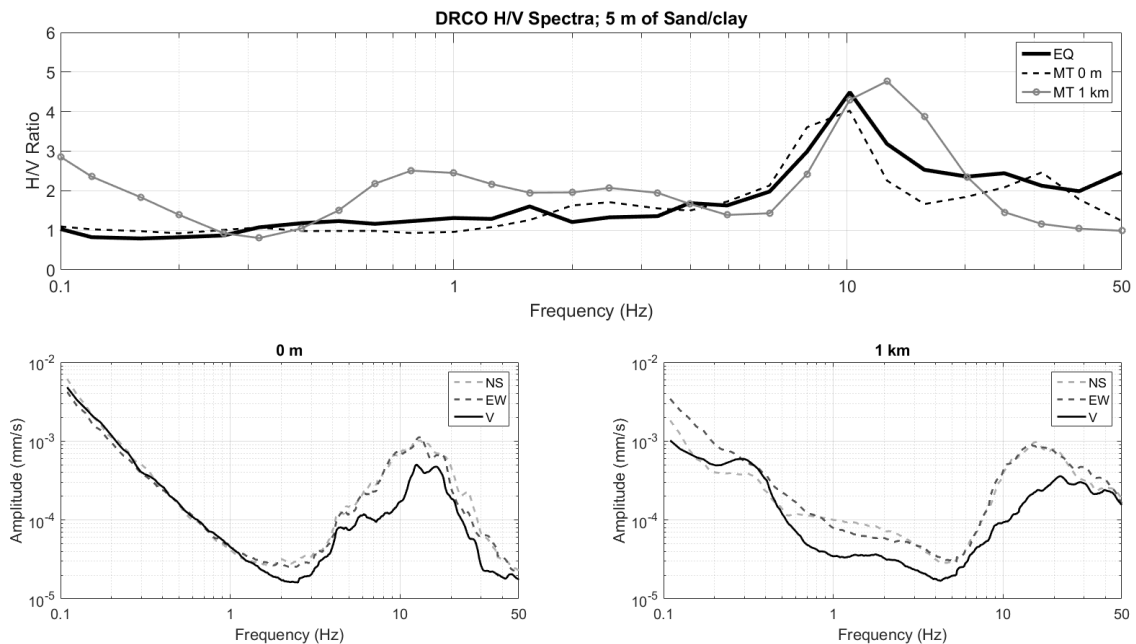
H/V spectra at station DRCO. f_{peak} from $(H/V)_{MT}$ at 0 m is in agreement with the f_{peak} from $(H/V)_{EQ}$ (10.2 Hz); at 1 km, f_{peak} is 0.1 log units higher. No surveys performed at 40, 80, 160 and 500 m due to logistical complications.
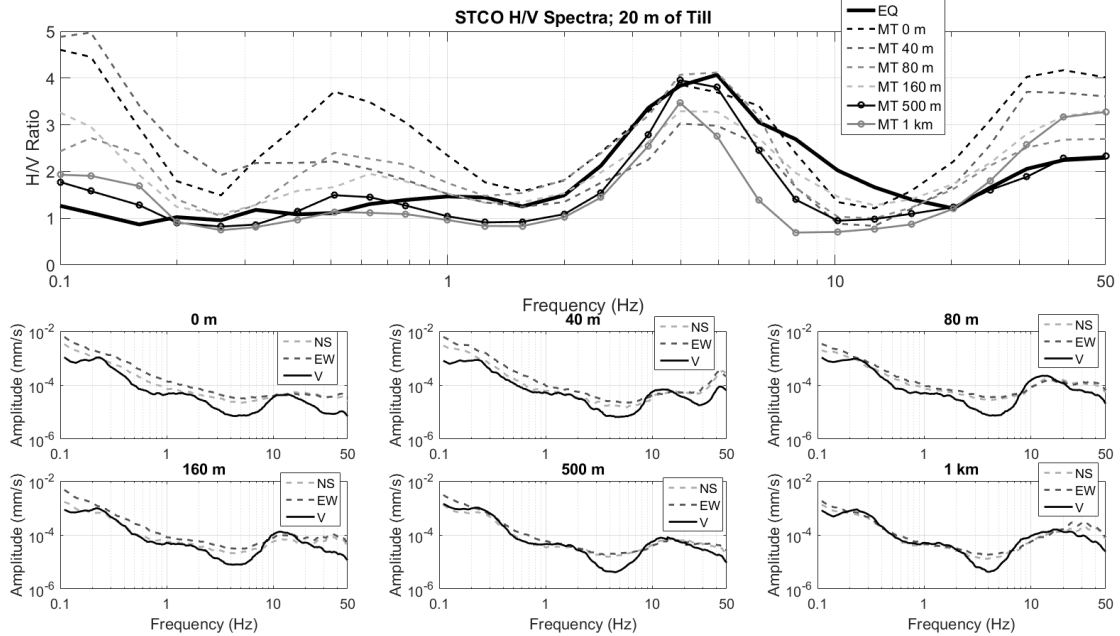
H/V spectra at station STCO. For all surveys, f_{peak} from $(H/V)_{MT}$ is in agreement with f_{peak} from $(H/V)_{EQ}$ (5.0 Hz) to within 0.1 log units.
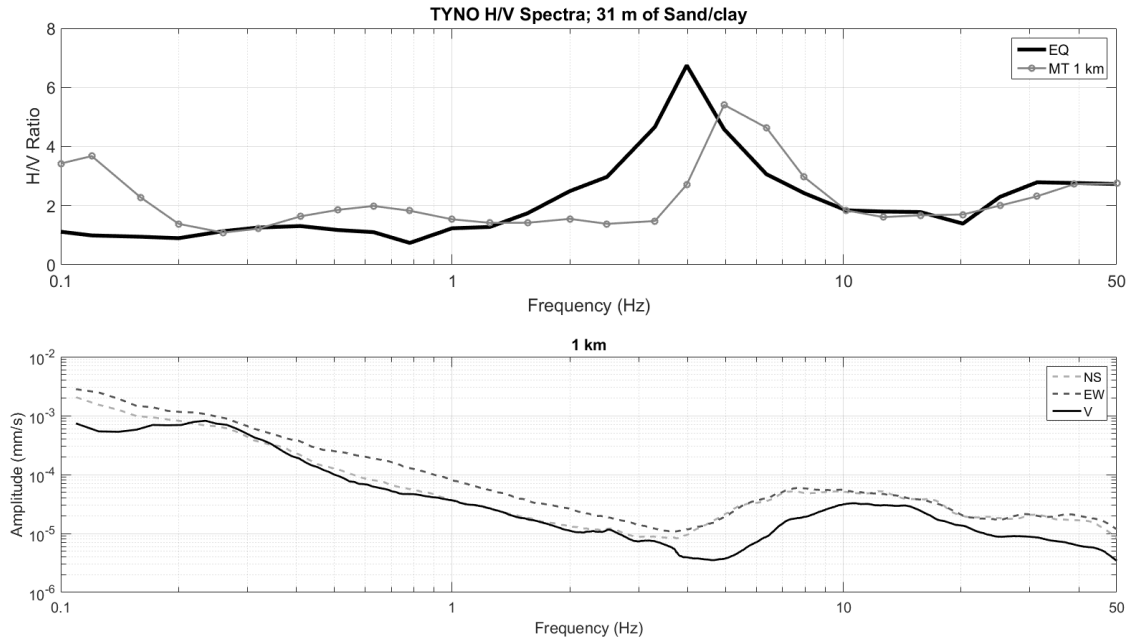
H/V spectra at station TYNO. For the lone good record (survey at 1 km), f_{peak} from $(H/V)_{MT}$ is greater than f_{peak} from $(H/V)_{EQ}$ (4.0 Hz) by 0.1 log units.
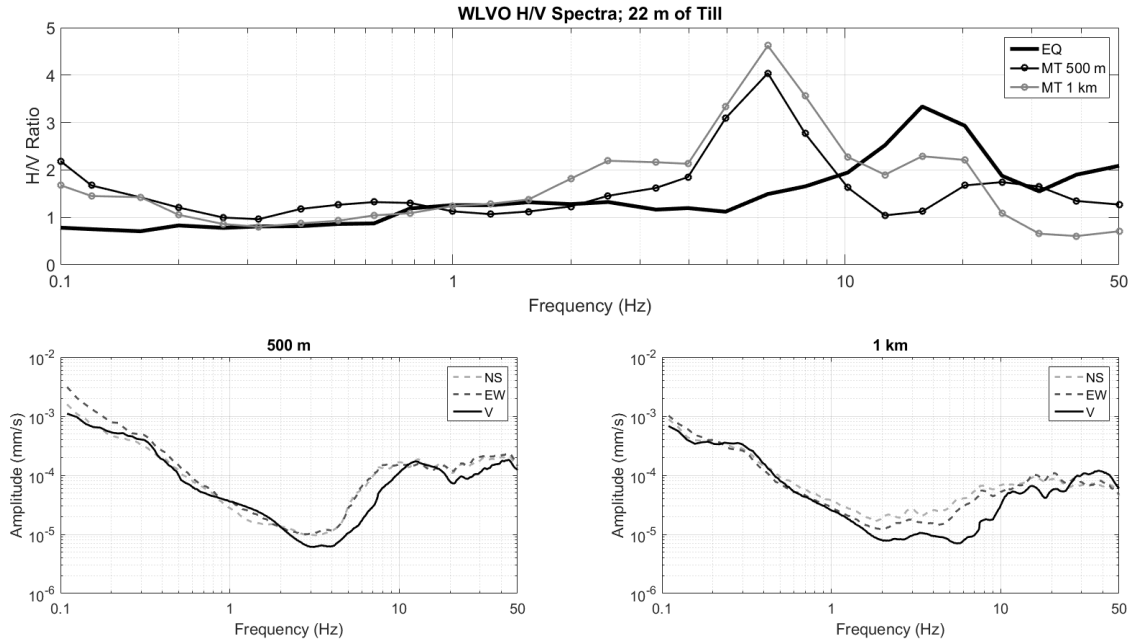
H/V spectra at station WLVO. Good records (surveys at 500 and 1000 m) have f_{peak} from $(H/V)_{MT}$ lower than f_{peak} from $(H/V)_{EQ}$ (12.6 Hz) by 0.4 log units.

Curriculum Vitae

Name: Sebastian Braganza

Post-secondary   The University of Western Ontario
Education and   London, Ontario, Canada
Degrees: 2009-2015 B.Sc.

                     The University of Western Ontario
                     London, Ontario, Canada
                     2015-2017 M.Sc.

Related Work   Teaching Assistant
Experience   The University of Western Ontario
                     2015-2017

Publications:
Braganza, S., Atkinson, G.M., Ghofrani, H., Hassani, B., Chouinard, L., Rosset, P.,
Motazedian, D., and Hunter, J. (2016). Modeling Site Amplification in Eastern Canada
on a Regional Scale. *Seismological Research Lett*ers, **81**, no. 4, 1008-1021.